AN OPTICAL STUDY OF SOOT FORMATION FROM SHOCK-INDUCED BENZENE PYROLYSIS

by

GREG NELSON

B.S., Kansas State University, 1979

A MASTER'S THESIS

submitted in partial fulfillment of the

requirements for the degree

MASTER OF SCIENCE

Department of Nuclear Engineering

KANSAS STATE UNIVERSITY
Manhattan, Kansas

1981

Approved by:

Thomas W. Lester
Major Professor

THIS BOOK
CONTAINS
NUMEROUS PAGES
WITH THE ORIGINAL
PRINTING BEING
SKEWED
DIFFERENTLY FROM
THE TOP OF THE
PAGE TO THE
BOTTOM.

THIS IS AS RECEIVED
FROM THE
CUSTOMER.

ABSTRACT

Soot formation from benzene pyrolysis in a single pulse shock tube has been studied in real time optically and after the fact with electron microscopy. Reaction conditions were varied over a temperature range of 1450-2400 K, with initial benzene concentrations from 0.12 to 1.3 mole percent in argon, and reaction dwell times of < 0.1 to 2.5 msec, at an average pressure of 845 ± 144 kPa. The beam from a He-Ne laser was passed through windows bounding the reaction zone, and its transmitted intensity over time measured. From this transmission trace, which was displayed on an oscilloscope, the intensity at t = 2.5 msec, the induction time, and the rate of increase in extinction were measured. From the transmitted intensity at 2.5 msec, soot yields were determined, as a mass fraction of the initial benzene concentration, over the temperature range. At carbon atom concentrations less than 5×10^{17} ml^{-1} (behind the reflected shock wave), yields increased from below detectable limits at 1500 K to near 50% at 1800 K, and then decreased to zero at temperatures above 2100 K. At a higher concentration (2.31×10^{18} ml^{-1}), the soot yield increased continuously with temperature. Soot yields from a similar aromatic compound, toluene, were compared to those from benzene. Overall trends with temperature were similar, but the peak yield from toluene was higher with a fractional conversion of about 70%. From the induction time and rate of increase in extinction data, activation energies for soot nucleation and particle growth were calculated as ∿ 27.0 and 21.8 kcal/mole, respectively. Nucleation was concluded to be a low order kinetic process ($n \leq \frac{1}{2}$) whose rate increased continuously with temperature despite increasing

aromatic ring fragmentation. On the other hand, the particle growth rate increased continuously up to a temperature of 1800 K, and thereafter decreased. It is concluded, therefore, that the primary impact of ring fragmentation is not on the nucleation of soot, but rather on the surface growth. Surface growth was estimated to be a first order kinetic process with respect to benzene concentration, with much of the growth occurring during the quench, especially at temperatures greater than 1800 K. Soot particles were removed from product gases by filtration and measured under a transmission electron microscope. Particle diameter was found to be relatively insensitive to changes of temperature, dwell time, and initial reactant concentration.

ACKNOWLEDGEMENTS

As one might expect, the completion of this report was due to not only my own efforts, but those of others also. Steve Vaughn tutored me through the weeks of learning to operate the shock tube, and always seemed to have solutions to even the most puzzling problems. Sharon Szydlowski and Galen King were there for helpful discussions and advice, and Sharon was also indispensably helpful in data collection. Avelina Paulsen operated the electron microscope and took some fine micrographs. Mildred Buchman accomplished the arduous task of typing this report, and Barbara Wieliczka drafted the many fine figures. My wholehearted thanks is given to each of these individuals.

Special recognition should be given to Dr. Fred Merklin and Dr. Chris Sorenson for their key instruction and intellectual support in times of crisis. Finally, let it be stated that without the guidance of professor Tom Lester, this research could not have been as successful and enjoyable as it was. I am totally indebted to him for his insight and encouragement which resulted in the completion of my degree.

For Debra and Christopher.

TABLE OF CONTENTS

LIST OF FIGURES

LIST OF TABLES

1.0 PROBLEM OVERVIEW

1.1 Engineering Significance

Recently, a great deal of attention has been given by users of liquid fuels to alternate fuels as an energy source to help lessen their dependence on the often insecure, increasingly expensive, and diminishingly availabile petroleum-based fuels. The most promising potential alternate fuels include those liquids processed from coals, oil shales, and tar sands. Aside from production uncertainties, however, these fuels present a number of problems to their potential users, one of which is their higher soot forming tendency relative to many petroleum derived fuels.

Soot formation produces at least three major problems: 1) The environmental hazard posed by the emitted particles and absorbed polycyclic organic compounds; 2) the materials engineering difficulties caused by increased radiative heat transfer from soot particles to the combustor walls; and 3) the mechanical and heat transfer hindrances caused by deposition of the solid material upon critical surfaces within a mechanical device.[32] Additionally, in industrial gas turbine combustors, soot formation limits operating conditions by causing overheating of the combustion chamber from enhanced flame radiation and by the formation of carbonaceous deposits that cause fuel spray distortion and turbine dammage when they break loose.[1]

Aromatic hydrocarbons, known to constitute a significant fraction of liquid synthetic fuels, are particularly well suited to form soot upon combustion or pyrolysis. In fact, Street and Thomas[28] observed the following ranking of hydrocarbons on the basis of mixture strength

at which soot appeared in the flame (in order of increasing sooting tendency): acetylene < isoalkanes < alkanes < benzene and alkyl benzenes < alkyl naphthalenes. Although a solution to this sooting problem would be to further refine alternate fuels to reduce the aromatic content, this action could be economically unfeasable. Longwell[19] contends that a 20% increase in fuel costs will result from reducing aromatic content to present-day petroleum levels through extra processing.

To understand the chemistry involved in alternate fuel combustion, the investigator must first understand the general mechanisms of oxidation and pyrolysis of aromatic compounds. Under fuel rich conditions, pyrolysis may compete with oxidation during combustion and yield soot, among other molecules, as a reaction product.[12] Thus, pyrolytic experimentation on alternate fuel moieties, especially aromatics, could be helpful in further characterization of the combustion process as a whole.

Such an experiment has been conducted at Kansas State University by Vaughn, who studied the chemical mechanisms of soot and large hydrocarbon formation from benzene pyrolysis by using a single pulse shock tube (described in Section 2). He coupled solid and liquid recovery of reaction products with isotopic labeling of the benzene to infer reaction mechanisms leading to the formation of soot. This technique, while very useful, is limited only to the examination of stable reaction products. Optical studies can provide real time analysis of the behavior of certain molecular and radical species as well as the solid soot suspension. Neither technique alone is totally adequate, but together they can provide a more complete picture of what

occurs during the chemical and physical transformation of hydrocarbons to soot. This study seeks to augment Vaughn's work and that of others with an interpretation of optical and election microscopy data to better characterize the soot formation process.

1.2 Benzene -- Decomposition and Soot Formation

The discussion which follows is not intended to be a detailed or comprehensive review of the soot formation process (the reader is referred to excellent reviews by Palmer and Cullis,[21] Bittner and Howard,[1] and others[12,24]). Rather a brief summary of the pertinent facts, as we know them, about soot formation from aromatic hydrocarbons (using benzene as the typical aromatic) is presented.

The hydrocarbon known today as benzene was first isolated by Michael Faraday in 1825 from an oily condensate that deposited from an illuminating gas.[29] By vapor density measurements several years later, the formula was established to be C_6H_6--the formula for an unsaturated or somehow ringed compound. It was puzzling to Nineteenth Century chemists that the benzene formula suggested a polyene (multiply-double bonded) structure, but it did not behave like polyenes. Kekule' proposed a cyclic triene structure, but it was only with the advent of modern wave mechanics that the actual resonating double bond construction of benzene was correctly suggested as a valid structure.
The C-C bond distance in benzene is 1.40 Å, intermediate between single and double bond carbon distances. All bond angles are 120°, and the benzene structure is today represented as,

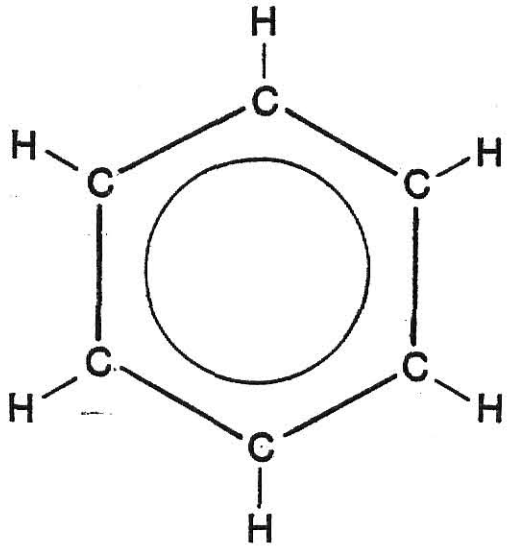

The most frequently stated link between the structure of some hydrocarbons and the propensity to form soot is a low hydrogen to carbon ratio. Benzene, the most fundamental aromatic hydrocarbon, has a H/C molar ratio of unity. When compared to petroleum fuels (H/C≈2.0), coal, tar sands and oil shale have a significantly lower H/C ratio (Vaughn[32]).† The increased soot forming tendency of these fuels is, in fact, due to a higher aromatic content than that which is found in petroleum-based fuels.

The mechanism by which soot is formed from the combustion or pyrolysis of aromatics is not well established. Several theories have been postulated that seem to describe satisfactorally the behavior of data extracted from one or more apparatus, but a unifying theory (if there is one) has yet to be supplied. The solid material called soot consists mostly of carbon and hydrogen where the C/H ratio increases from 1 to 8 as the particles mature in a flame.[1] Wersberg[34] divides the sequence of soot formation into 1) nucleation; 2) formation of small

†Although the H/C ratio seems to be a good general parameter linking structure to soot-forming tendency, care should be taken in extrapolation of the parameter to be descriptive of this tendency for all hydrocarbons.

2.5 nm crystallites, 3) formation of 25.0 nm spherical particles containing approximately 10^3 crystallites; and 4) chaining of the spherical units. He defines the first step, nucleation, as the formation of the first solid particles from gases. These gases undergo more or less simultaneous polymerization and dehydrogenation, aided perhaps by radicals or oxidation, yielding carbon as the end product. The important species participating in nucleation is the point of difference when comparing most mechanistic theories.

The Acetylene Theory, revived mainly by Porter,[22] proposes that any given hydrocarbon is first decomposed into smaller acetylenic subunits which subsequently polymerize to form larger species, and eventually condensing to form soot. Another theory is the C_2 Polymerization Theory, where an important intermediate in the soot formation pathway is the C_2 fragment (see Smith[27] or Ferguson[7]). Thirdly, the general Polymerization Theory (Gaydon,[9] Lahaye, et al.,[17] and others) conceives the original hydrocarbon as undergoing a series of polymerization reactions yielding large molecules which dehydrogenate to form the graphitic soot particle. A hybridization of these theories, proposed by Graham, et al.,[13] is shown below. To explain their results from laser attenuation studies of soot formation behind incident shock waves, two separate mechanisms were postulated to exist.

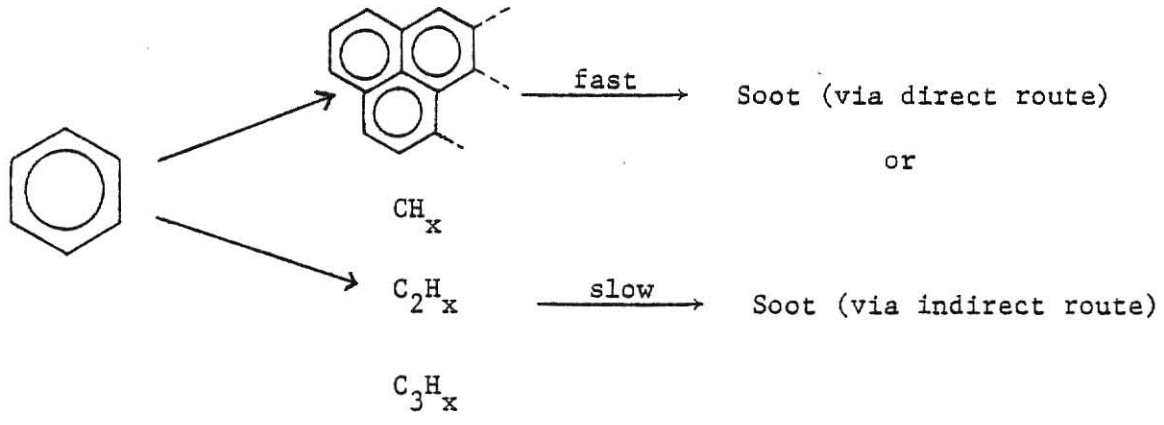

This mechanism logically suggests (if a free radical mechanism predominates) that at lower temperatures, dehydrogenation is the pre-eminent free radical producing step, and as temperature increases, actual ring fragmentation is promoted. These fragments reunite to form soot more slowly than do the larger phenyl radicals of the low temperature mechanism.

For a total carbon concentration of 2×10^{17} atoms/ml, Graham showed that soot yields determined optically from aromatic/argon mixtures decreased with temperature monotonically from 100 percent at 1800 K to zero at 2200 K (see Fig. 1-1). He further postulated that, if the essential features of the above mechanism are correct, soot conversion from acetylene (C_2H_2)/argon mixtures must be less than that for any aromatic under the same conditions. Subsequent shock heating of acetylene/argon mixtures at the same concentration showed yields to be low throughout the entire temperature range, suggesting that at low concentration, aromatic fragmentation appears to yield acetylene-like free radicals which tend to suppress the fractional conversion to soot. When high carbon atom concentrations were used ($[C]_5 > 7 \times 10^{17}$ atoms/ml), the soot yield from acetylene increased dramatically, indicating that the low yields at $[C]_5 = 2 \times 10^{17}$ atoms/ml are kinetically rather than thermodynamically controlled. In subsequent tests with aromatics, Graham showed that the variation in soot yields via the direct mechanism (for $T < 1800$ K) was very insensitive to total carbon atom concentration, quite unlike the results from experimentation in the temperature range $T > 1800$ K (fragmentation mechanism).

Wang, et al.,[33] measured laser transmission from toluene/argon mixtures heated behind a reflected shock wave. Using carbon atom

THIS BOOK CONTAINS NUMEROUS PAGES WITH DIAGRAMS THAT ARE CROOKED COMPARED TO THE REST OF THE INFORMATION ON THE PAGE.

THIS IS AS RECEIVED FROM CUSTOMER.

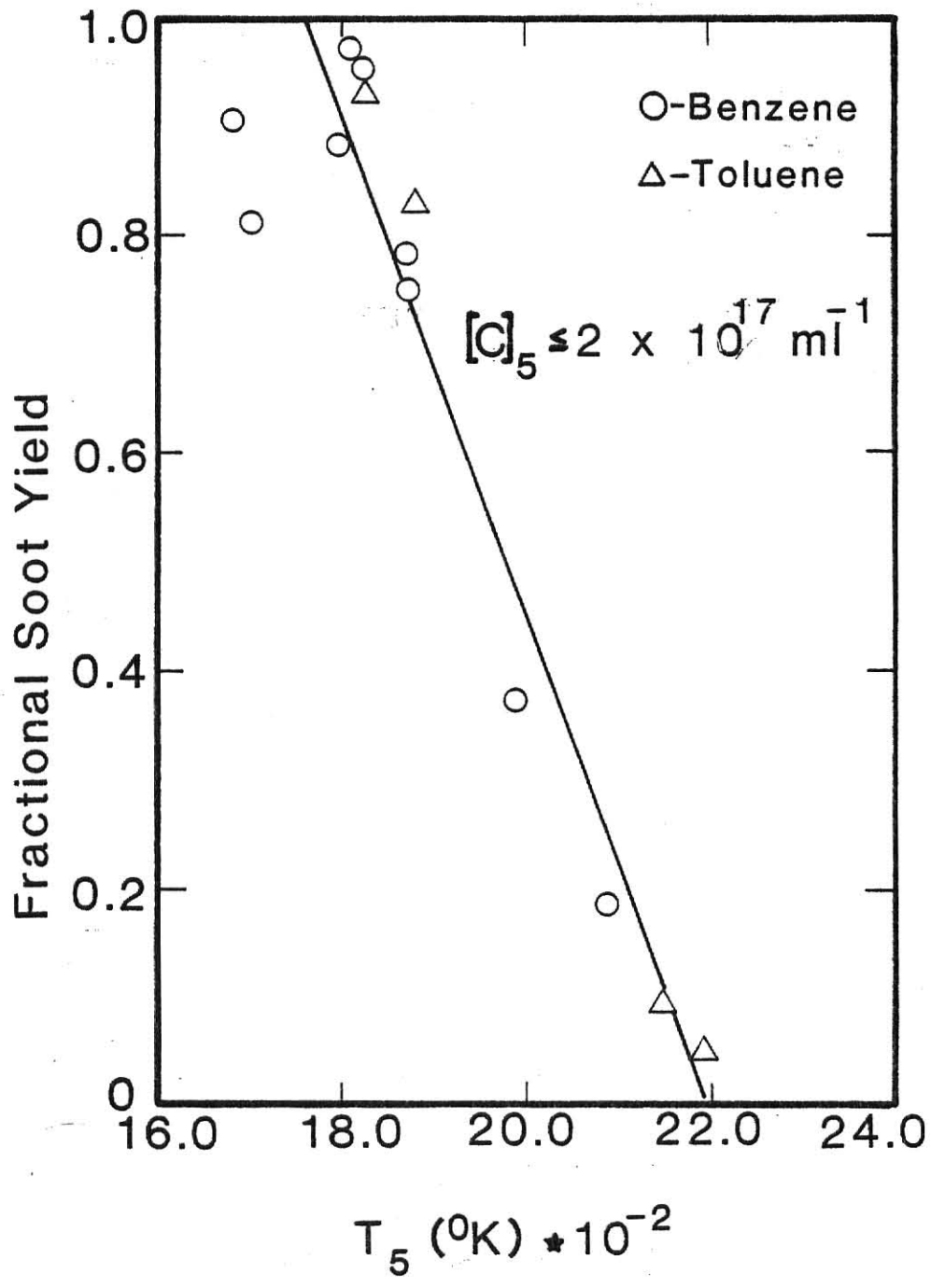

Fig. 1-1. Fractional soot yield as a function of temperature (Graham, et al.[13]).

concentrations similar to those of Graham, soot yield (2.5 msec after passage of the reflected shock wave) versus temperature curves were obtained over a wide temperature range (1400-2400 K, see Fig. 1-2). From further analysis of the transmission trace, rate equations for the soot formation process were formulated. They concluded, as Graham had, that two mechanisms (condensation and fragmentation) ultimately lead to soot formation, but that the intact ring is essential to high sooting rates, i.e. fragmentation is an unimportant route for aromatic fuels. Following this analysis, oxygen was added to the toluene/argon mixture and its effect on soot production quantified. Significant decreases in fractional soot conversion were observed over the entire temperature range (see Fig. 1-2). Corresponding rate equations were obtained with the O_2 concentration as an additional dependency.

From his aforementioned post-shock collection of pyrolysis products from benzene/argon mixtures, Vaughn[32] identified gaseous products and constructed a soot yield versus temperature curve very different from those above. Using gas chromatography and mass spectographic analysis, he identified several reaction product gases, including acetylene and styrene. Their Kekule´ structures are shown below, and in Fig. 1-3, their occurrences as a function of reaction temperature is plotted.

Acetylene Styrene

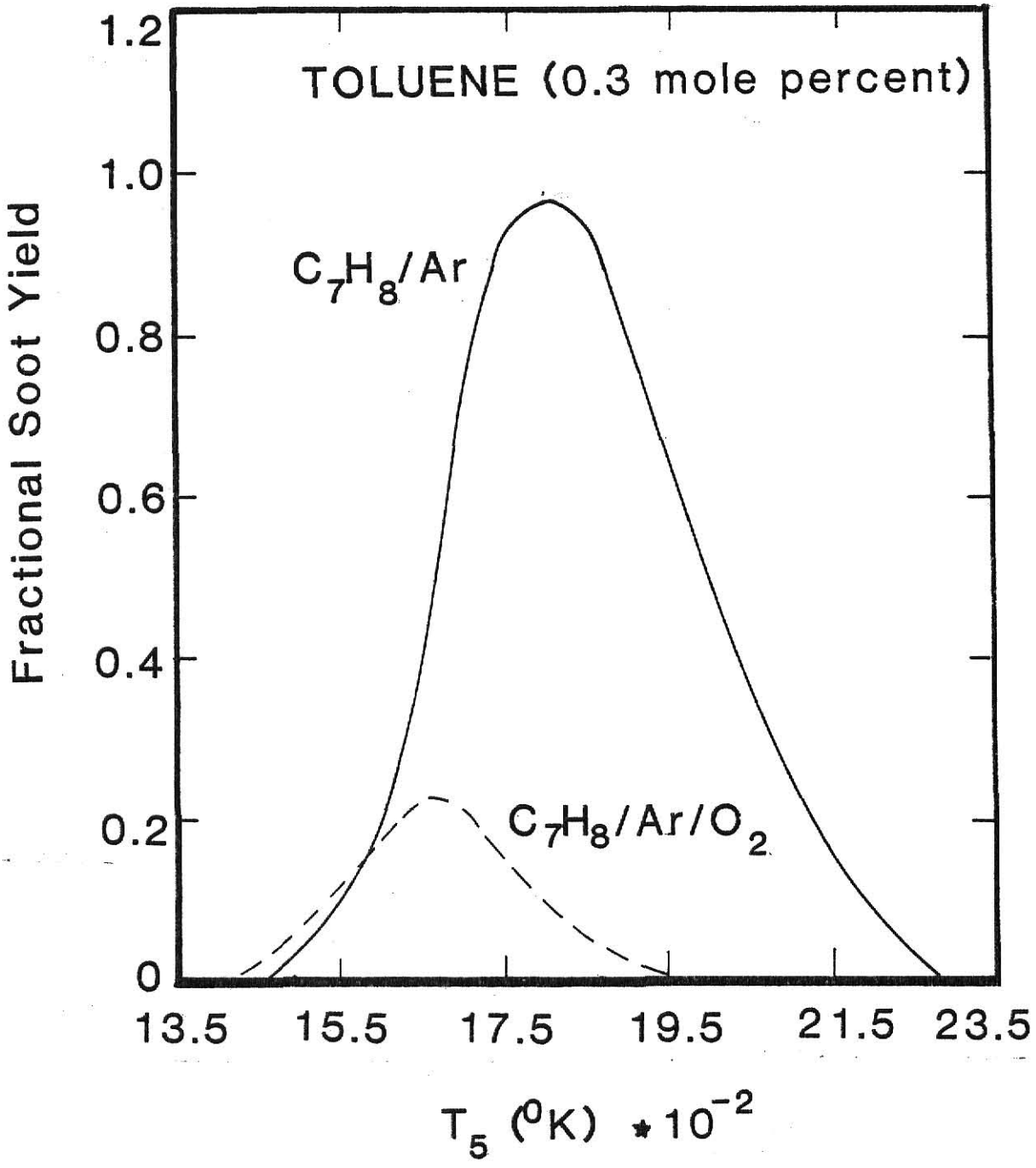

Fig. 1-2. Fractional soot yield as a function of temperature (Wang, et al.[33]).

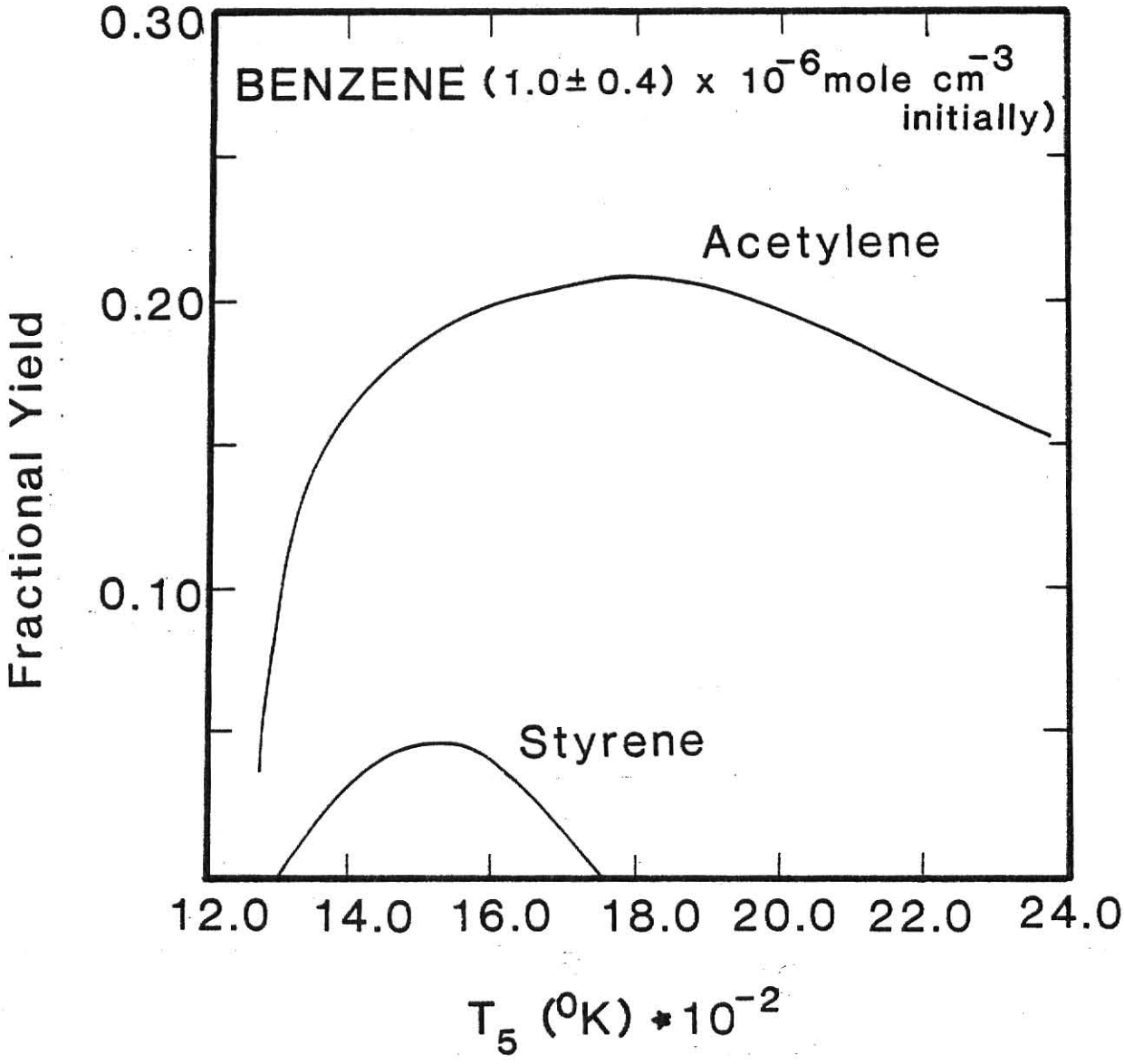

Fig. 1-3. Yields of acetylene and styrene as a function of temperature (Vaughn[32]).

Trace amounts of ethylene, diacetylene, and vinylacetylene were also detected.[†] Vaughn proceeds to postulate that addition of acetylene radicals to dehydrogenated aromatic rings accounts for most of the presence of styrene at low temperatures. By collecting and weighing soot generated by the shock heating of benzene (at a slightly higher carbon concentration than Graham, $[C]_5 \approx 4 \times 10^{17}$ atoms/ml), Vaughn constructed the temperature dependent soot yield curve shown in Fig. 1-4. The trend displayed is remarkably different from that observed by Graham and Wang, but Vaughn explains his results by pointing out that soot yields were evaluated within 2.5 msec after passage of the shock wave in the above optical studies, whereas in Vaughn's work, soot yields were measured long after reactant mixtures had been cooled to room temperature. It was observed, in fact, that by weighing the liners upon which the soot had settled after an insufficient elapsed time, the trend similar to that in the optical studies was obtained. In essence, Vaughn suggests that much of the soot finally produced appears after a relatively long period of time following the high temperature shocks. This result is consistent with the belief that a free radical mechanism persists after ring fragmentation, since this process, once initiated, requires little energy to proceed. In further analysis, Vaughn showed that the overall disappearance rate of benzene was best described by a second order rate expression with an experimental activation energy of 38.2 kcal/mole. Vaughn also measured individual soot particle diameters from micrographs taken through a transmission electron microscope, and found a remarkably narrow size distribution about 21 ± 1 nm.

[†]It is interesting to note that the presence of one-, three-, and five-carbon species was less than the minimum detectable amount in the experiments.

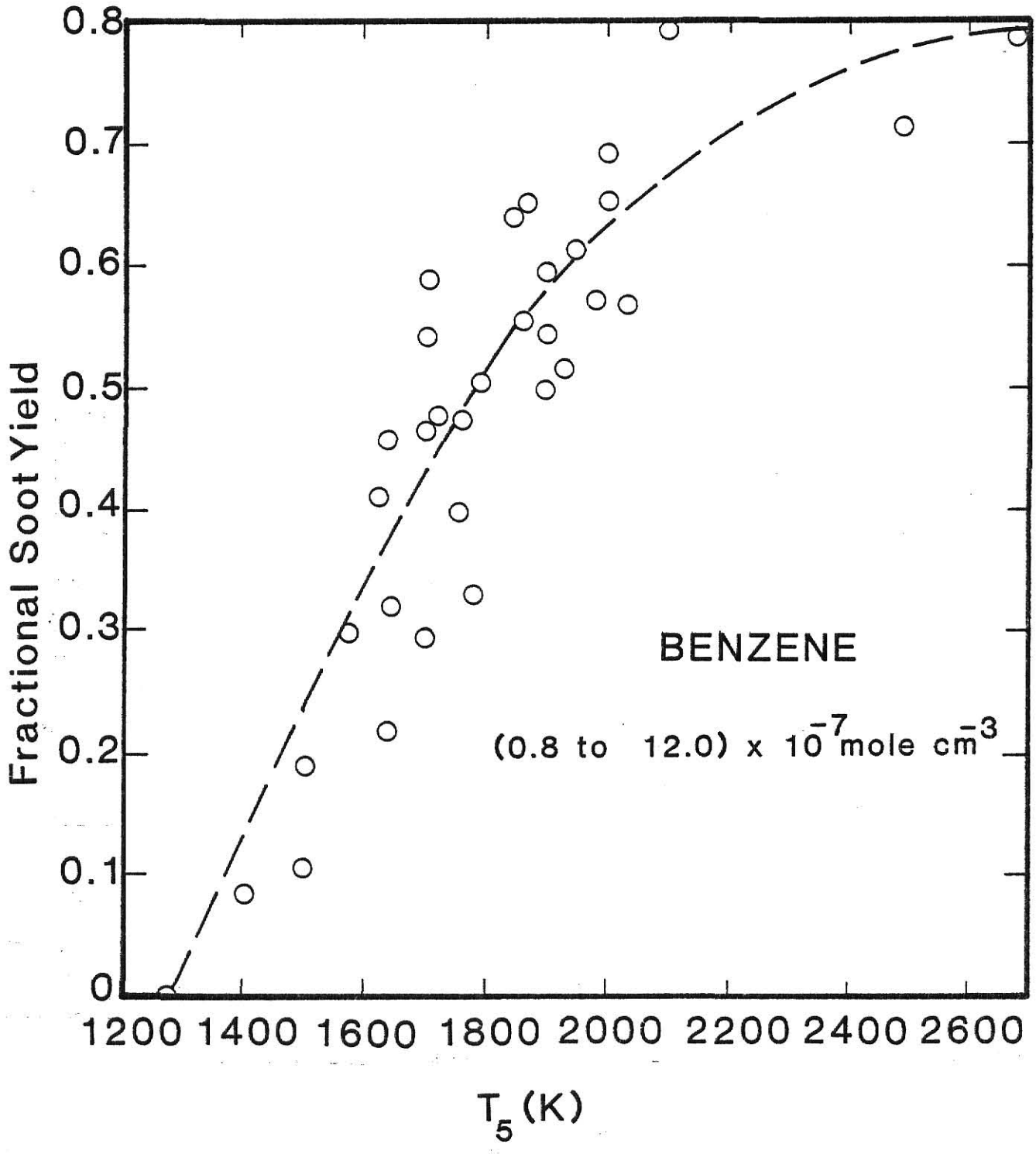

Fig. 1-4. Fractional soot yield as a function of temperature (Vaughn[32]).

From some of the more recent research on soot formation, we can conclude that there is no general agreement on whether, during soot formation from the pyrolysis and combustion of aromatic hydrocarbons, these aromatic molecules undergo condensation reactions directly without losing their aromatic character, whether they break up into small fragments which then form soot via polyacetylene, or whether both mechanisms occur. It is from this position in the soot formation dilemma that the present investigation begins.

2.0 EXPERIMENTAL

2.1 Introduction

Shock tubes have been used to study soot formation from the pyrolysis of a number of organic compounds. In recent work at this laboratory, Vaughn[32] studied the mechanisms of benzene pyrolysis and soot formation. Isotopic labeling was used in conjunction with mass spectrometry to infer mechanisms from the stable products. Solid and liquid recovery techniques were also developed to permit both gravimetric determination of soot yields and mass balances. Graham, et al.[13] presented results from an extensive optical study of the soot formation from shock-heated benzene and alkyl benzenes. From laser extinction traces, they proposed a reaction mechanism consisting of two different temperature dependent pathways, and provided data which supported this mechanism. Laser extinction measurements have been used also by Wang, et al.[33] to study the soot formation from shock-heated toluene. Arrhenius equations were developed for the soot induction times and the rate of soot formation as a function of temperature and the concentrations of toluene, hydrogen, oxygen, and argon.

The purpose of the research reported in this thesis is to augment the chemical and gravimetric analyses of Vaughn with optical techniques to more completely cover the time and reactant concentration ranges of importance to the problem of soot formation in a high intensity combustor.

2.2 The Single Pulse Shock Tube

A shock tube is a device in which a plane shock wave is generated

by the bursting of a diaphragm separating high and low pressure gases. The passage of this wave at supersonic speed compresses the initially low pressure gas. If the shock wave is allowed to reflect off the end wall, the gas is compressed further. Additionally, molecules accelerated by the incident shock are decelerated to a nearly stagnant condition behind this reflected wave. Accompanying this sudden compression is a transient temperature rise proportional to the change in pressure. The quiescent, high pressure, high temperature gas persists behind the reflected shock until the rarefaction fan arrives to cool the hot gas isentropically within several milliseconds. If hydrocarbons are among the components of the low pressure gas mixture, their reactions subsequent to shock heating may be observed optically by following either the emission or absorption of light by reaction participants. Following a run, stable gas, liquid, or solid reaction products may be collected and analyzed by gas chromatography, mass spectrometry, or some other analytical technique. The reader should consult Seeker[26] and Gaydon & Hurle[10] for additional information on the shock tube.

2.2.1 Basic Design and Operation

The Kansas State University single pulse shock tube (SPST) was designed and built, after the original design of Glick, et al.,[11] by Seeker. Specific information regarding its construction or operation may be obtained from his M.S. thesis[25] or from a series of recent papers.[4,31,32] The tube has been modified to collect solid and gaseous products[32] (see Fig. 2-1).

The tube is constructed of 5.08 cm i.d., type 304 stainless steel seamless tube, and is divided primarily into two sections which are

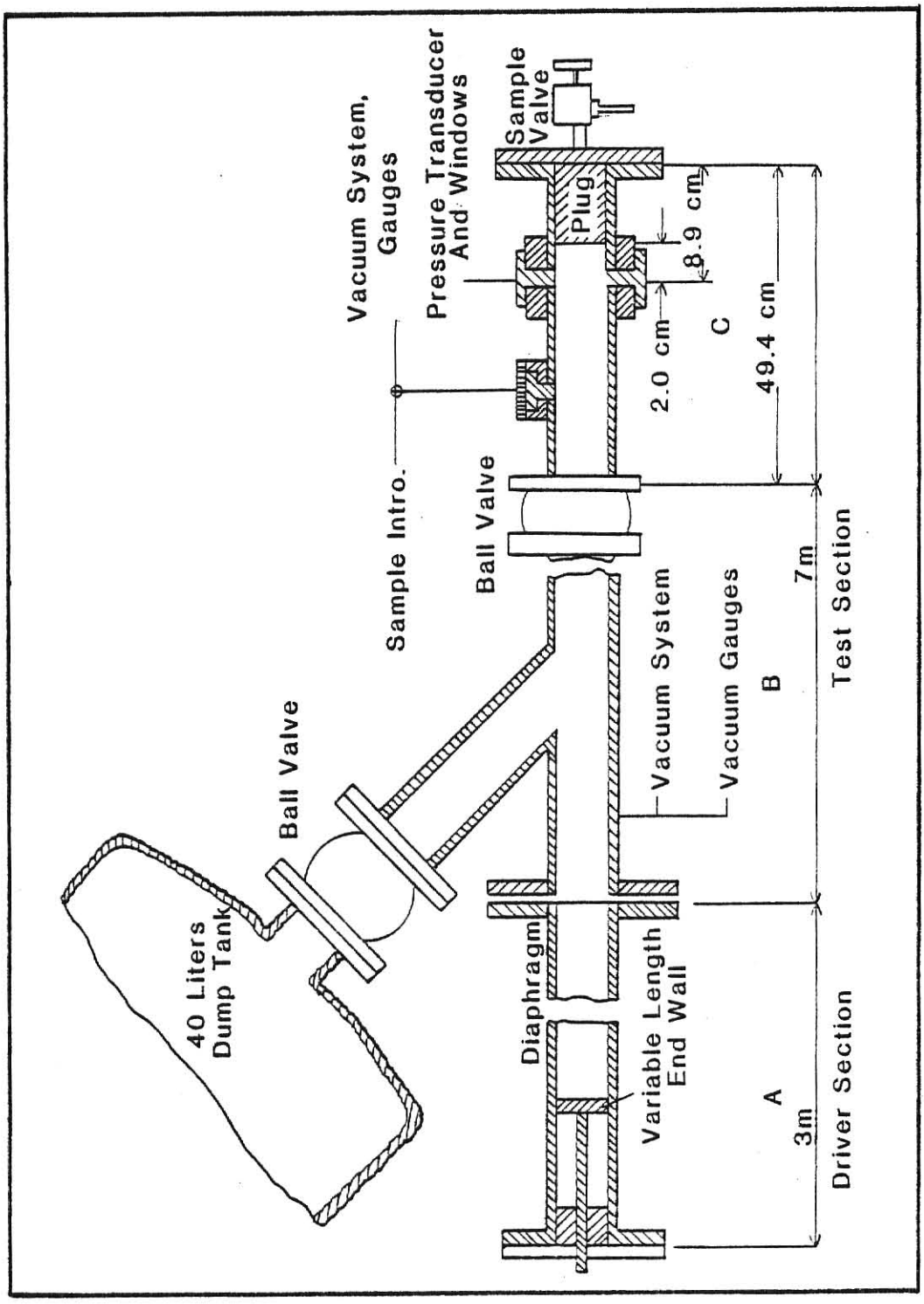

Fig. 2-1. Schematic of the KSU shock tube.

separated by a flanged diaphragm assembly. Shock waves are initiated by mechanically rupturing mylar diaphragms of chosen thickness. The driver section is of continuously variable length (1-3m), and holds the high pressure ($\leq 4.1 \times 10^3$ kPa) gas which expands through the ruptured diaphragm to generate the shock wave. Helium is used as the driver gas because its low molecular weight permits rapid acceleration and yields the strongest shock of any gas other than H_2, due to its high speed of sound.

The low pressure, or driven section, is seven meters long. The last 49.4 cm of this section can be isolated from the remainder of the low pressure section by a full port, in-line valve. This end section, which will be elaborated on shortly, is the experimental region to which the chemical and physical processing of the reactant gas is confined. The 6.51 meters of the driven section upstream (with respect to the incident shock) of the ball valve, termed the test section, contains taps for vacuum systems, gauges, and gas introduction. Connected to the test section near the diaphragm assembly at an obtuse angle to the incident shock wave is a 40 liter dump tank (see Fig. 2-1). Initially evacuated and filled to the same pressure as the rest of the test section, this volume is exposed to weak shock waves as the incident shock front passes the intersection, and so its pressure remains lower than the static pressure still present in the high pressure end. This represents a preferred pathway for the reflected shock wave, and once in the tank, the shock wave is trapped, preventing further processing of the sample gases. While the shock wave is traversing the low pressure section, a rarefaction fan is propagated into the high pressure section and rebounds from the end plate.

These waves travel downstream to quench the reactions taking place in the shock heated test gas. Thus, this gas experiences the high temperature behind the reflected shock until the cooling rarefaction fan arrives. Discussion of this controllable time period may be found in Section 2.2.3.

The experimental section contains optical windows and taps for vacuum systems, sample introduction, and post-shock gas sampling (see Fig. 2-2). The centerline of the circular quartz windows (1.27 cm diameter, 1.27 cm thick) is situated 2.0 cm from an end plug which terminates the section. The 7.0 cm plug was added after a series of experiments showed that the optical monitoring of soot formation should be conducted within one or two centimeters of the end of the experimental section (see Appendix A for details).

Prior to an experiment, argon gas is introduced into the entire low pressure section that was previously evacuated to less than 0.1 mtorr. The leak rate was about 1.33×10^{-5} torr/sec. Argon, a monoatomic, noble gas, was chosen because its specific heat does not vary with temperature. After this step, the ball valve is shut and the experimental section is evacuated while the driver section is filled with helium to the desired pressure. The test gas mixture (aromatic hydrocarbon dilute in argon) is added to the isolated experimental section until it is within two torr of being isobaric with the rest of the driven section. Just prior to diaphragm rupture, the ball valve is swung inline. Immediately following the shock it is shut manually so that reaction products are trapped in a known volume. A more detailed procedure for operation of the SPST may be found in Vaughn[32], Breipohl[4], or Szydlowski.[31]

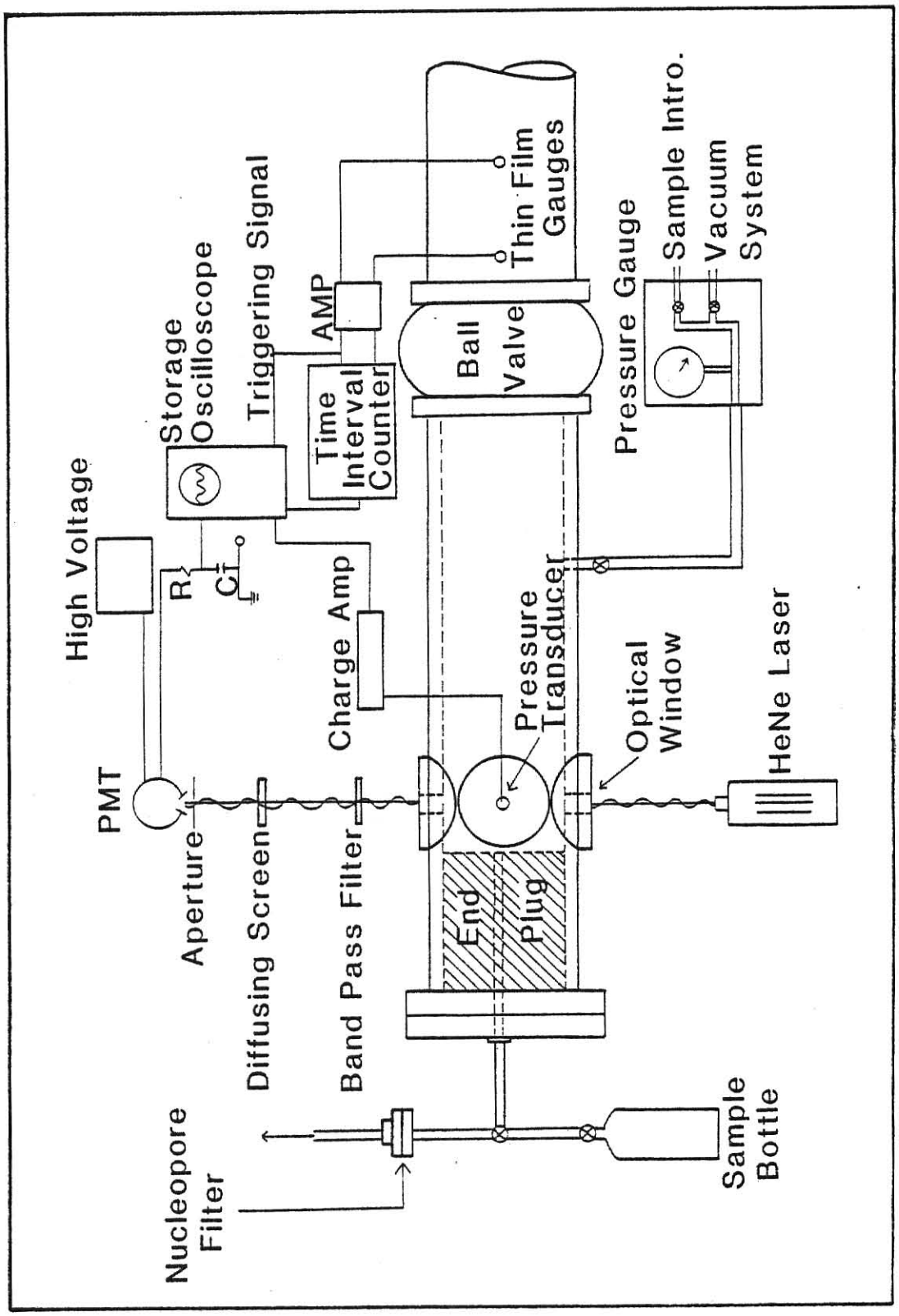

Fig. 2-2. Experimental section with optical arrangement.

Fig. 2-3. The experimental section.

THIS BOOK CONTAINS SEVERAL DOCUMENTS THAT ARE OF POOR QUALITY DUE TO BEING A PHOTOCOPY OF A PHOTO.

THIS IS AS RECEIVED FROM CUSTOMER.

THIS BOOK CONTAINS NUMEROUS PICTURES THAT ARE ATTACHED TO DOCUMENTS CROOKED.

THIS IS AS RECEIVED FROM CUSTOMER.

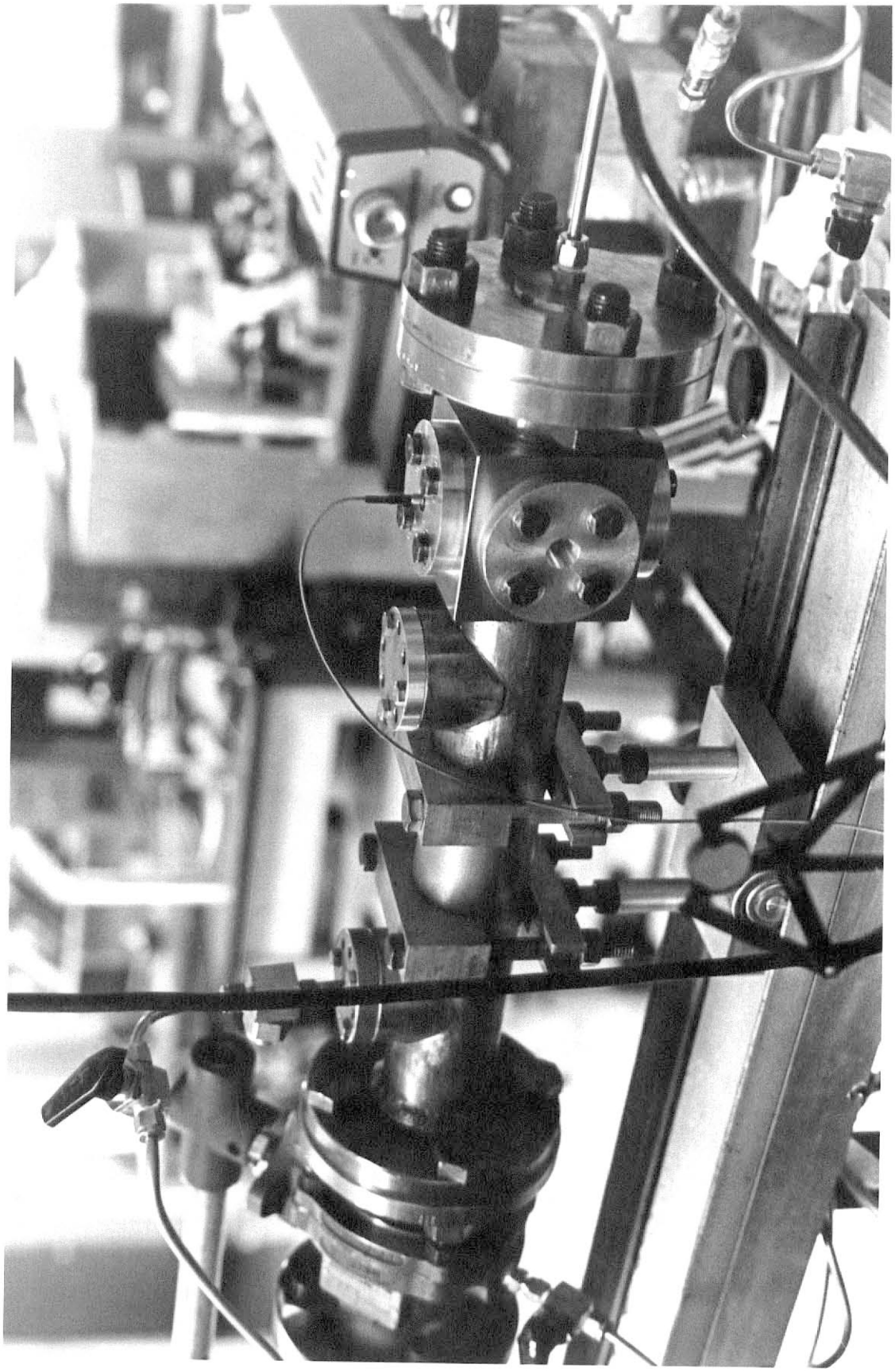

2.2.2 Gaseous Mixtures

The two reactants used in this experiment, benzene and toluene (Fisher, Certified Grade > 99% pure), were used without further purification. Mixtures were made by injecting one of the above liquid components with a syringe into an evacuated stainless steel bottle (Whitey, 500 cm^3) and then adding argon (Matheson, 0.99999 minimum purity) as a diluent to a pressure of 9.67×10^2 kPa (9.57 atm). After allowing at least 12 hours for proper mixing, the mixture concentrations were determined by gas chromatographic analysis. Reactant (aromatic) concentrations in these experiments ranged from 0.13 to 1.23 mole percent in argon. Gaseous solutions were kept dilute so that properties (i.e., speed of sound, specific heat) of a pure argon medium could be used in calculation of shock wave parameters to a good approximation.

2.2.3 Determination of Reaction Conditions

Due to the transient nature of wave phenomena, thermodynamic conditions behind both the incident and the reflected shock wave must be determined by instrumentation with very fast dynamic response. A piezoelectric pressure transducer (Kistler, Model 603A1) with charge amplifier is located in the same axial plane as the optical windows. From its output, displayed on the screen of a Tektronix (Model 7623) storage oscilloscope, the reaction time behind the reflected shock is determined. The incident shock velocity is measured by two platinum thin-film gauges installed 20.3 cm apart, nearly flush with the inside wall, just upstream of the ball valve. Each platinum strip of approximately 50 Ω resistance is heated by the passage of the shock front. The resulting resistance change produces a voltage pulse which

is amplified and fed to a Fluke (Model 1952B) time interval counter that measures the elapsed time between the two pulses to within ± 0.1 μsec. From the time and the separation distance, a shock wave velocity can be calculated. This velocity divided by the sonic velocity in argon yields the Mach number for the wave. From this Mach number one can calculate, with proper assumptions, the temperature and pressure behind the reflected shock. Typical Mach numbers for this experiment are approximately three.

Once the Mach number of the incident shock wave is known, T_5 and P_5, the temperature and pressure behind the reflected wave respectively, may be calculated from relations given by Gaydon and Hurle,[27]

$$T_5 = T_1 \frac{[2(\gamma-1)M^2+(3-\gamma)][(3\gamma-1)M^2-2(\gamma-1)]}{(\gamma+1)^2M^2} \qquad (2\text{-}1)$$

and

$$P_5 = P_1 \frac{[2\gamma M^2-(\gamma-1)]\ [(3\gamma-1)M^2-2(\gamma-1)]}{(\gamma+1)[(\gamma-1)M^2+2]} \quad , \qquad (2\text{-}2)$$

where M is the Mach number of the incident shock wave, γ is the specific heat ratio of the test gas, and T_1 and P_1 are the temperature and pressure of the undisturbed test gas. These equations are derived under the assumption that the gas properties do not change with temperature and that there are no non-ideal losses over the interval considered (i.e., heat transfer, frictional losses, and non-ideal reflections are

neglected).[32] It should also be noted that the derivation assumes that the test gas velocity is brought to zero behind the reflected shock.

It has been determined by Vaughn[32] and Seeker[26] that shock deceleration occurs, and that the reflection of the shock off the end wall does not bring the test gas completely to rest. Additionally, had a diatomic test gas been used in the driven section, specific heat ratio variances with temperature could be expected. Therefore, empirical relations determined by Vaughn[32] were used to modify the temperature as calculated from eqn. (2-1). Measuring both the incident and reflected shock velocities and solving the conservation equations, Vaughn corrected reflected shock gas temperatures. He obtained the following correlation for tests in argon:

$$T'_5 = (0.866\ T_5 + 10)K \quad , \qquad r^2 = 0.9983 \quad . \qquad (2\text{-}3)$$

A further correction is often needed to obtain an accurate reflected shock temperature in these experiments. As can be seen from the sample oscillogram in Fig. 2-4a, the pressure increases above its initial value behind the reflected shock wave during the 2.5 msec reaction time. The equations so far do not account for the corresponding temperature rise which must also occur. If it is assumed that this compression is isentropic, then the temperature rise may be related to the pressure via

$$\frac{T'_5}{T_5} = \left(\frac{P'_5}{P_5}\right)^{\frac{\gamma-1}{\gamma}} \quad , \qquad (2\text{-}4)$$

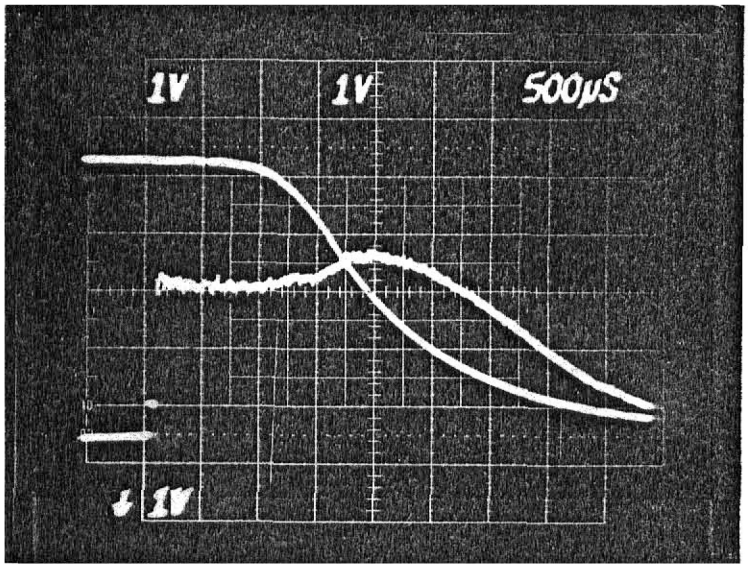

(a)

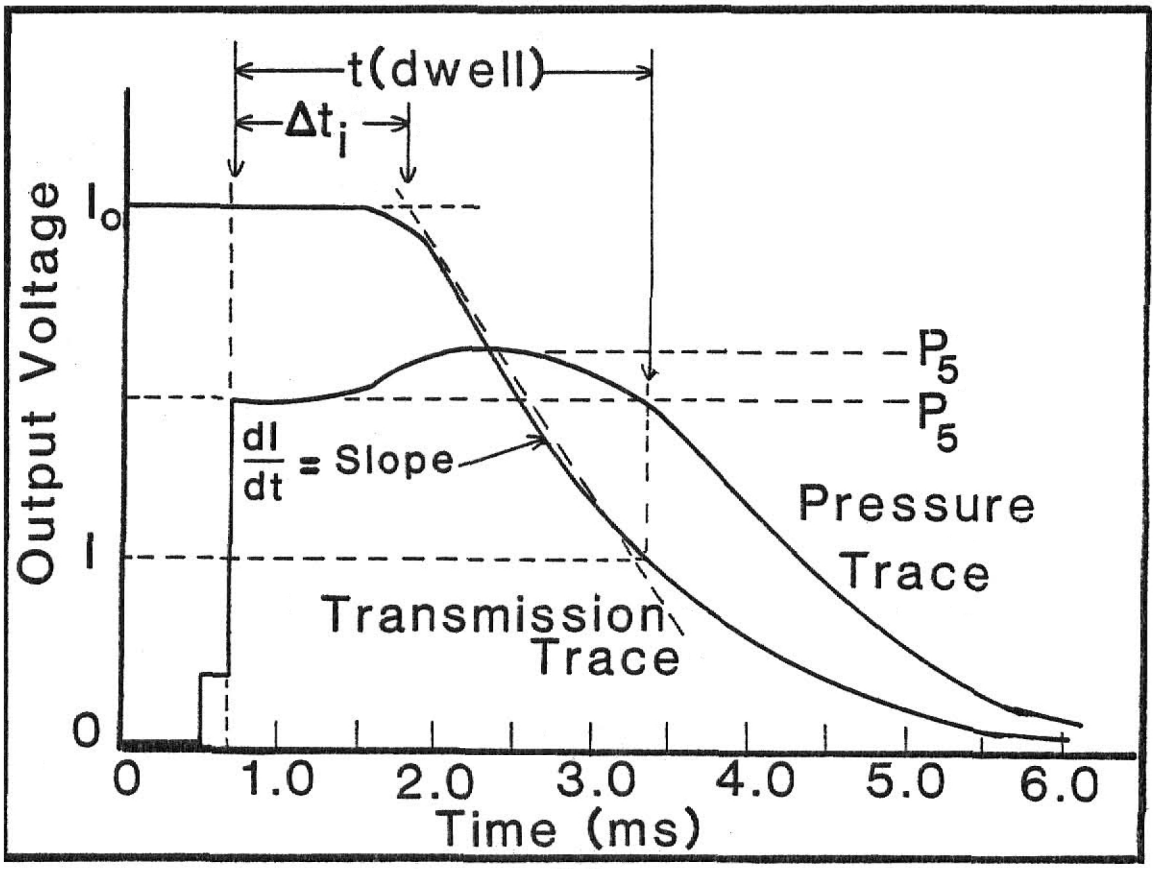

(b)

Fig. 2-4. (a)Sample oscillogram, and (b)Methodology for determining characteristic shock parameters.

where T_5' is the corrected shock gas temperature and P_5'/P_5 is the ratio of peak to initial pressure, determined from the oscillogram. Use of eqn. (2-4) yields the maximum temperature, which exists, of course, for only a fraction of the reaction time. A temperature that better reflects the temperature existing during the reaction is obtained by averaging the maximum temperature with the initial reflected shock temperature. It has been determined by graphical integration that an average occurs at approximately 40 percent of the difference between the maximum and minimum temperatures behind the reflected shock wave. Thus, combining eqn. (2-4) and this new factor, an equation for the average temperature may be written as

$$\overline{T}_5 = 0.4\ T_5' \left[\left(\frac{P_5'}{P_5} \right)^{\frac{\gamma-1}{\gamma}} - T_5 \right] + T'_5 \quad ,$$

which simplifies, using (2-3), to

$$\overline{T}_5 = 10 + .866 T_5 \left[0.6 + 0.4 \left(\frac{P_5'}{P_5} \right)^{\frac{\gamma-1}{\gamma}} \right] \quad , \qquad (2\text{-}5)$$

where T_5 is given by eqn. (2-1) and P_5'/P_5 typically varies from 1.0 to 1.5 over the temperature range. Similarly, an average pressure can also be calculated:

$$\overline{P}_5 = 0.4P_5' + 0.6P_5 \quad . \qquad (2\text{-}6)$$

All data and resulting conclusions in this experiment are based on temperatures and pressures calculated from these expressions. For simplicity, $\overline{T}_5$ and $\overline{P}_5$ will be written henceforth as T_5, and P_5 with the above corrections implicit in their evaluation.

Because the length of the driver section is variable, the dwell time, defined to be that time period between passage of the reflected shock wave and arrival of the rarefaction fan (at the plane of observation), may be varied. This dwell time is also the length of time the test gas mixture is allowed to react at high temperatures. Most data in this experiment were taken during a dwell time of 2.5 msec, which corresponds to a driver section length of 2.35 meters.

Reaction temperature in a shock tube may be varied by increasing or decreasing the pressure of the driver gas relative to that of the test gas. A helium pressure of 1.8×10^3 kPa (18 atm) and a test gas pressure of 120 torr will produce a temperature of about 2200 K behind the reflected shock wave. If the pressure were changed to 1.6×10^3 kPa (16 atm) and 150 torr respectively, a temperature near 1650 K could be expected. It has been observed experimentally that if, over a range of temperatures, the pressures of these two gases are changed stepwise by an equal percentage (i.e., a 5% decrease in one gas with a 5% increase in the other), the pressure behind the reflected shock wave will remain nearly constant. Thus, at a fixed dwell time, the reaction temperature may be varied over a wide range (1400-2200 K) while the reaction pressure does not change (8.2 ± 1.4 atm). The reader should consult Seeker[26] for information regarding how experimental prediction of reaction conditions differs from theoretical predictions.

In addition to the dwell time and the temperature, the reactant concentration may also be varied. This is accomplished simply by adjusting the volume of aromatic added to the sample container before argon dilution during mixture preparation. A list of reaction conditions for this experiment is presented in Table 3-2.

2.3 Optical Study of Soot Formation

Optical Measurements have been used extensively to follow soot formation in a number of apparatus. A review of the merits of various approaches has been presented by Bonczyk.[3] The techniques described are aimed at measuring at least two properties of a particulate suspension, principally mean particle size and number density. The approach used in this study is to monitor only the volume fraction, and from this data, estimate the fractional yield of soot as a function of the variable shock parameters described in Section 2.2 above. This technique has been used, with some variations, by Graham, et al.,[13] Wang, et al.,[33] and Pagni and Bard.[20]

2.3.1 Optical Theory

When a beam of monochromatic light passes through a length, L, of a polydisperse, homogeneous aerosol, the transmitted intensity, I, is related to the unattenuated intensity, I_o, by

$$I = I_o \exp(-\tau L) \ , \qquad (2\text{-}7)$$

where τ is the extinction coefficient given by

$$\tau = \int_o^\infty N(r) Q_{ext}(m,r,\lambda) \pi r^2 \, dr \ , \qquad (2\text{-}8)$$

at given λ and refractive index m. $N(r)dr$ is the concentration of particles whose radii are in the range dr about r, and $Q_{ext}(m,r,\lambda)$ is the extinction efficiency factor for those particles. In general, this extinction efficiency may be given by a sum of the scattered and absorbed components:

$$Q_{ext} = Q_{sca} + Q_{abs} \quad .$$

Each of these components is related directly to the particle diameter by

$$Q_{sca} = \frac{8}{3} \alpha^4 F_s(m,\lambda) \qquad (2\text{-}9)$$

$$Q_{abs} = 24\alpha F_a(m,\lambda) \qquad (2\text{-}10)$$

where $\alpha = 2\pi r/\lambda$. These equations assume spherical particles with the upper limit for particle radii generally set at $r/\lambda \leq 0.05$.[15] $F_s(m,\lambda)$ and $F_a(m,\lambda)$ are factors defined in terms of the refractive index (from Pagni and Bard):

$$F_s(m,\lambda) = \frac{\{[n^2-(nk)^2-1][n^2-(nk)^2+2]+4n^4k^2\}^2+36n^4k^2}{[(n^2-(nk)^2+2)^2+4n^4k^2]^2} \qquad (2\text{-}11)$$

$$F_a(m,\lambda) = \frac{n^2k}{(n^2-(nk)^2+2)^2+4n^4k^2} \quad , \qquad (2\text{-}12)$$

where n and k combine as real and imaginary parts of the complex refractive index, $m = n(1-ik)$.

If the attenuating particles are small, $\alpha << 1$ and the scattering efficiency factor, proportional to α^4, is negligible compared to the absorption term. Then the extinction efficiency factor may be approximated by

$$Q_{ext} \simeq 24\alpha F_a(m,\lambda) \quad .^{\dagger} \tag{2-13}$$

According to the small particle limit of the Lorentz-Mie theory for the scattering and absorption of light from spherical particles, it can be shown, for fixed wavelength λ and refractive index m of the particle material, that the extinction coefficient (above as τ) is proportional to the volume fraction occupied by the particles.[20] Thus by defining

$$f_v = \frac{\text{volume occupied by particulate}}{\text{total volume}}$$

$$\equiv \frac{4}{3}\pi \int_0^\infty N(r) r^3 dr \quad , \tag{2-14}$$

and assuming spherical particles of small diameter compared to the wavelength, then from eqns. (2-8), (2-13) and (2-14):

$$\tau = 36\pi F_a(m,\lambda) f_v/\lambda \quad . \tag{2-15}$$

$^{\dagger}F_a(m,\lambda)$ is related to the quantity E{m}, found in publications by Graham, et al.,[13] and Wang, et al.,[33] by $F_a(m,\lambda) = \frac{1}{6}E\{m\}$.

By combining eqn. (2-15) with (2-7), an expression for the particulate volume fraction results:

$$f_v = -\lambda \ln\left(\frac{I}{I_o}\right) \Big/ 36\pi L F_a(m,\lambda) \quad , \qquad (2\text{-}16)$$

where I_o, I, and L are measurable quantities and λ and m are known.

Assurance that the small particle limit approximation can be used is gained by directly calculating Q_{abs} and Q_{sca} for a range of particle sizes using eqns. (2-9)-(2-12). Soot particles produced from aromatic hydrocarbons are reported in the literature[3,32] to range in diameter from 3 to 50 nanometers. Table 2-1 presents absorption and scattering efficiency factor values encompassing this range of particle sizes for λ = 632.8nm (the laser wavelength used in this study) and the refractive index (discussed below). From this table it can be seen that the ratio of absorption to extinction efficiency is greater than 0.95 for particle diameters less than about 70 nm. It will be shown in Chapter 3 that particle sizes encountered in this experiment are well below this limit.

Since the volume fraction, and thus the soot yield, are functions of the refractive index, an accurate expression for such must necessarily be known. Using a dispersion model based on rigorous consideration of the electronic band structure and dispersion constants, Lee and Tien[18] predicted the spectral refractive index as a function of temperature for soot in hydrocarbon flames.

Table 2-1 Variation of Attenuation Efficiency Coefficients with Particle Diameter at λ = 632.8 nm.

D(nm)	α	Q_{sca}	Q_{abs}	$\left(Q_{abs}/Q_{ext}\right)*10^2$
0.2	10^{-3}	$7.31(10^{-13})$	$6.74(10^{-4})$	100.0
2.0	10^{-2}	$7.31(10^{-9})$	$6.74(10^{-3})$	100.0
20.0	10^{-1}	$7.31(10^{-5})$	$6.74(10^{-2})$	99.9
40.0	0.2	$1.17(10^{-3})$	0.135	99.1
60.0	0.3	$5.92(10^{-3})$	0.202	97.2
80.0	0.4	0.0187	0.270	93.5
120.	0.6	0.0947	0.404	81.0
160.	0.8	0.299	0.539	64.3
200.	1.0	0.731	0.674	48.0

They also found that optical constants are rather insensitive to temperature changes in the range of typical flame temperatures. From their analysis at 1600 K and 632.8 nm, the authors report a refractive index for soot as

$$m = 1.9[1.0-i(0.25)] \quad , \qquad (2\text{-}17)$$

whereby from eqn. (2-12),

$$F_a(632.8nm) = 0.028 \ .$$

Although differing refractive indices (usually with respect to the imaginary part) are reported by Stull and Plass,[30] Dalzell and Sarofim,[5] and others, and in contrast to Graham's[13] adjustment of the refractive index to better suit his data, the refractive index used in this experiment is taken from this most recent estimate. The effect of absorption, which is related to the imaginary term in the refractive index, is shown in Figures 2-5, 2-6, & 2-7 where the efficiency factors are plotted against α. In the example chosen, the real part stays nearly the same ($n \approx 1.29$) while the imaginary part increased from zero to 1.37 (from Kerker[15]). In an additional figure (Fig. 2-8) is plotted the variance of calculated soot yield with changing k. The yields are normalized to $k = 0.25$, the value selected in this study.

2.3.2 Optical Measurements

To measure the volume fraction of soot generated during an experiment, extinction measurements were made of a light beam directed

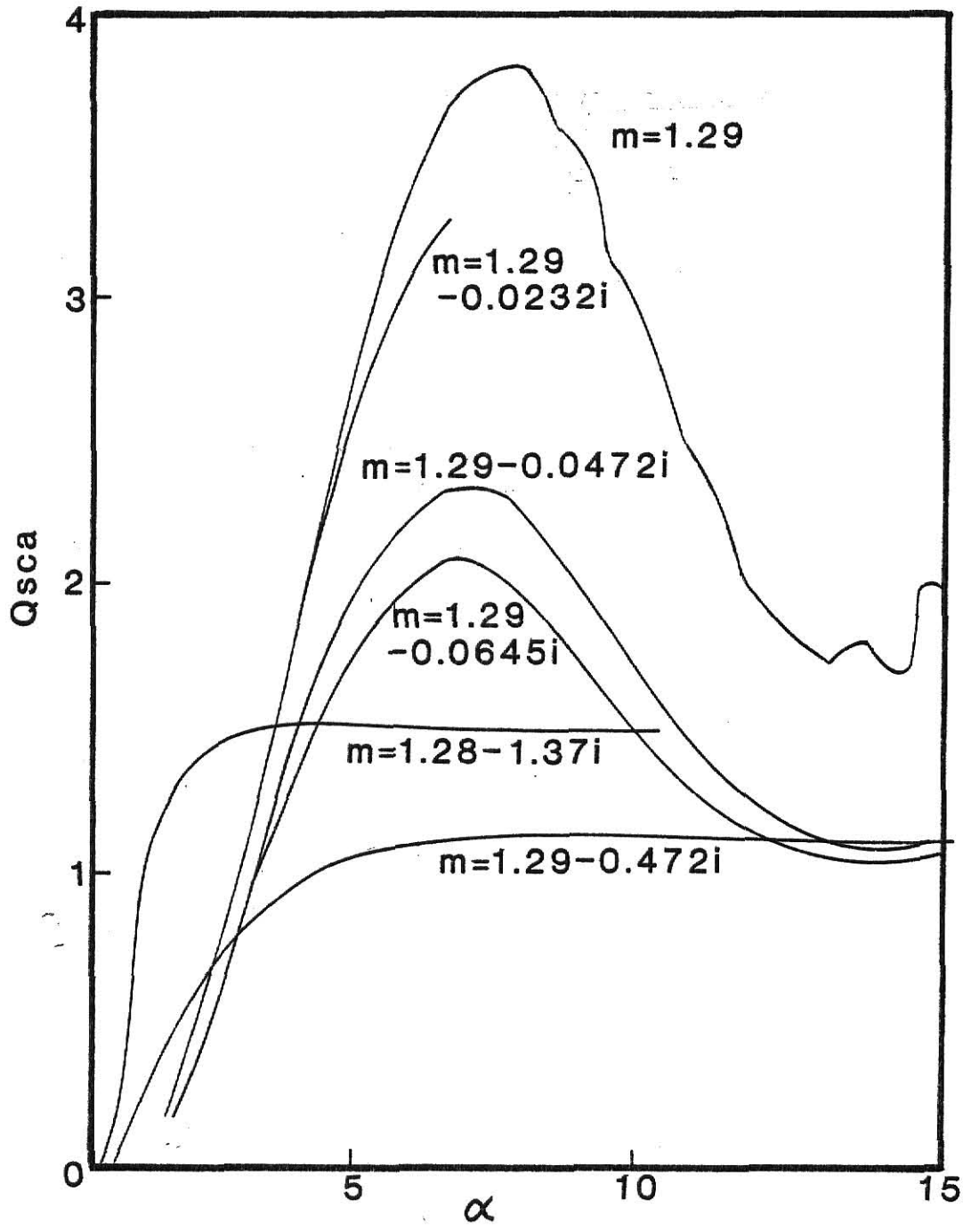

Fig. 2-5. Scattering efficiency factor as a function of particle size parameter, α.

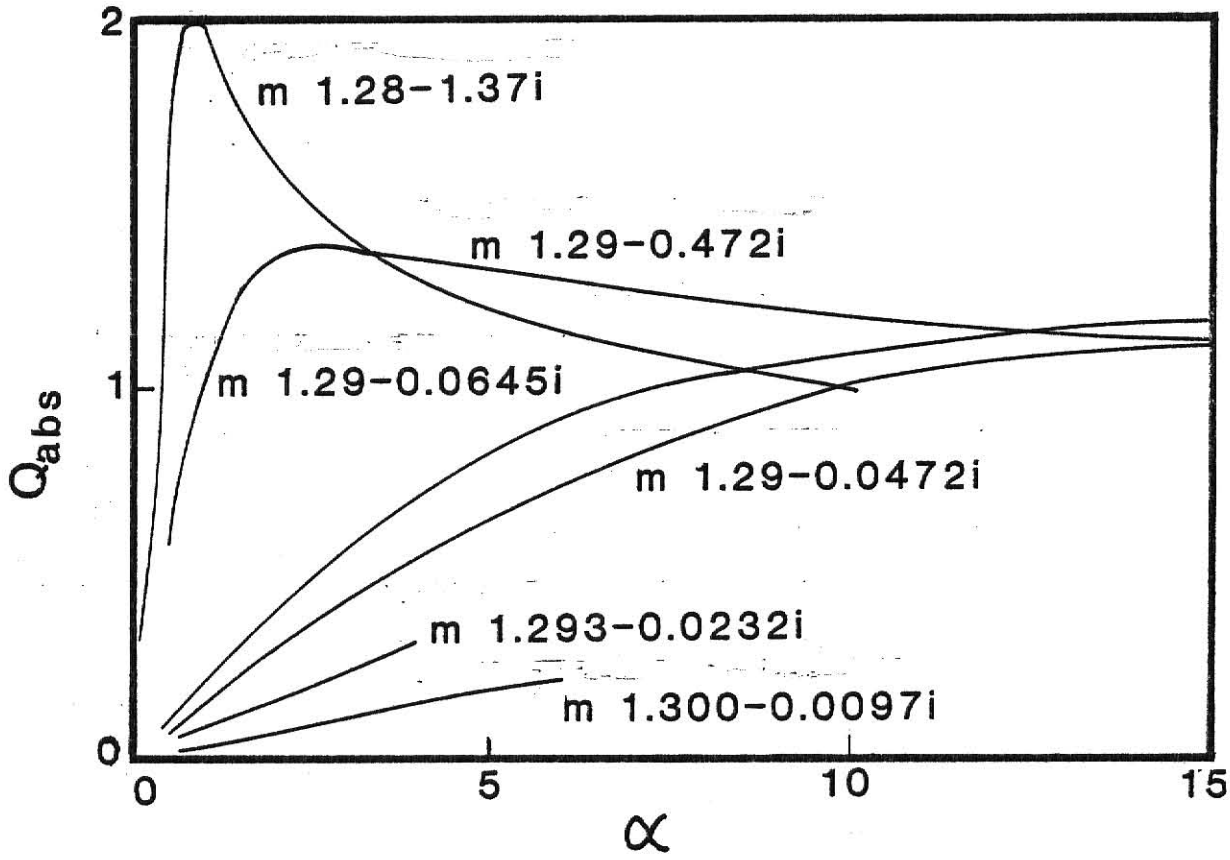

Fig. 2-6. Absorption efficiency factor as a function of α.

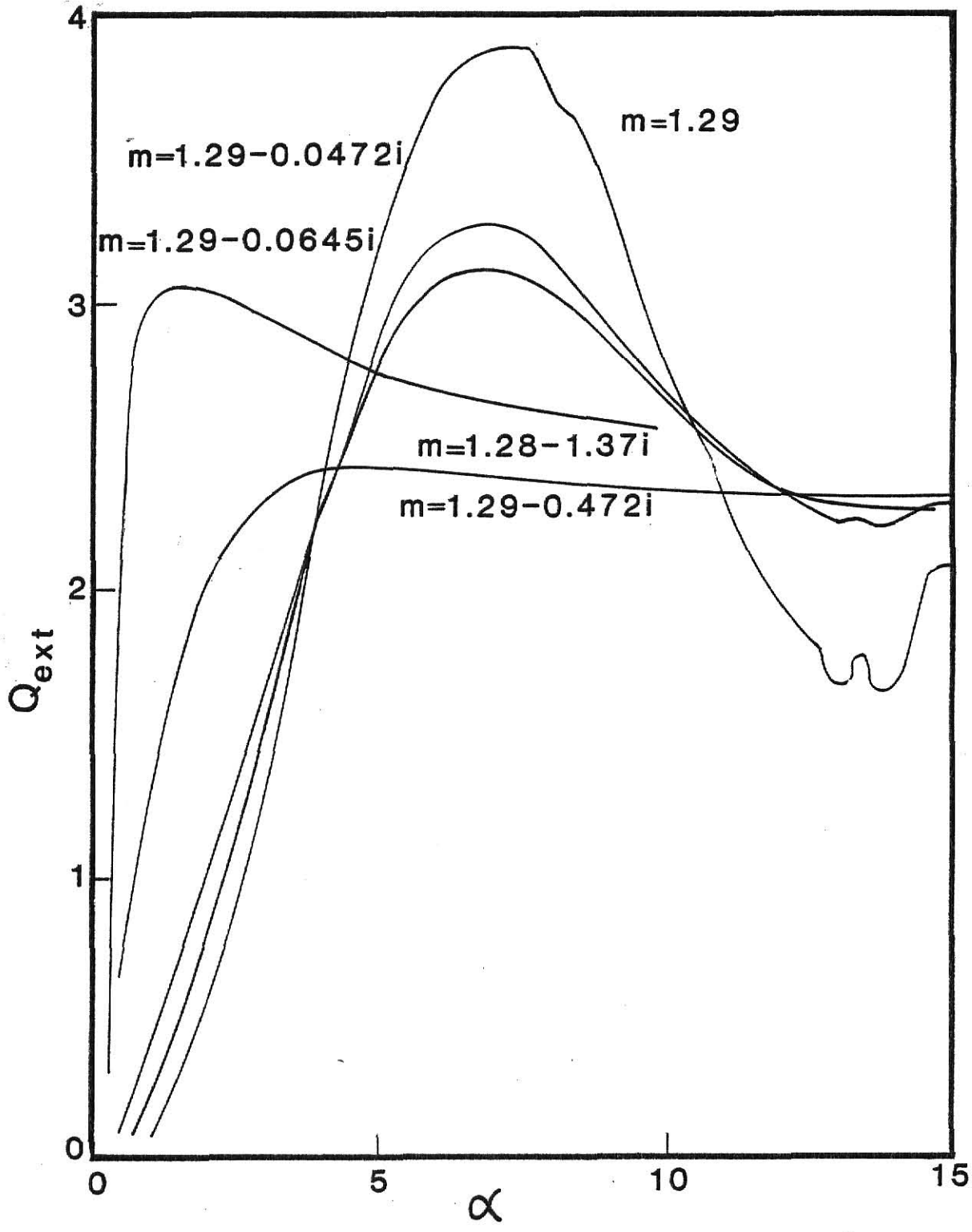

Fig. 2-7. Extinction efficiency factor as a function of α.

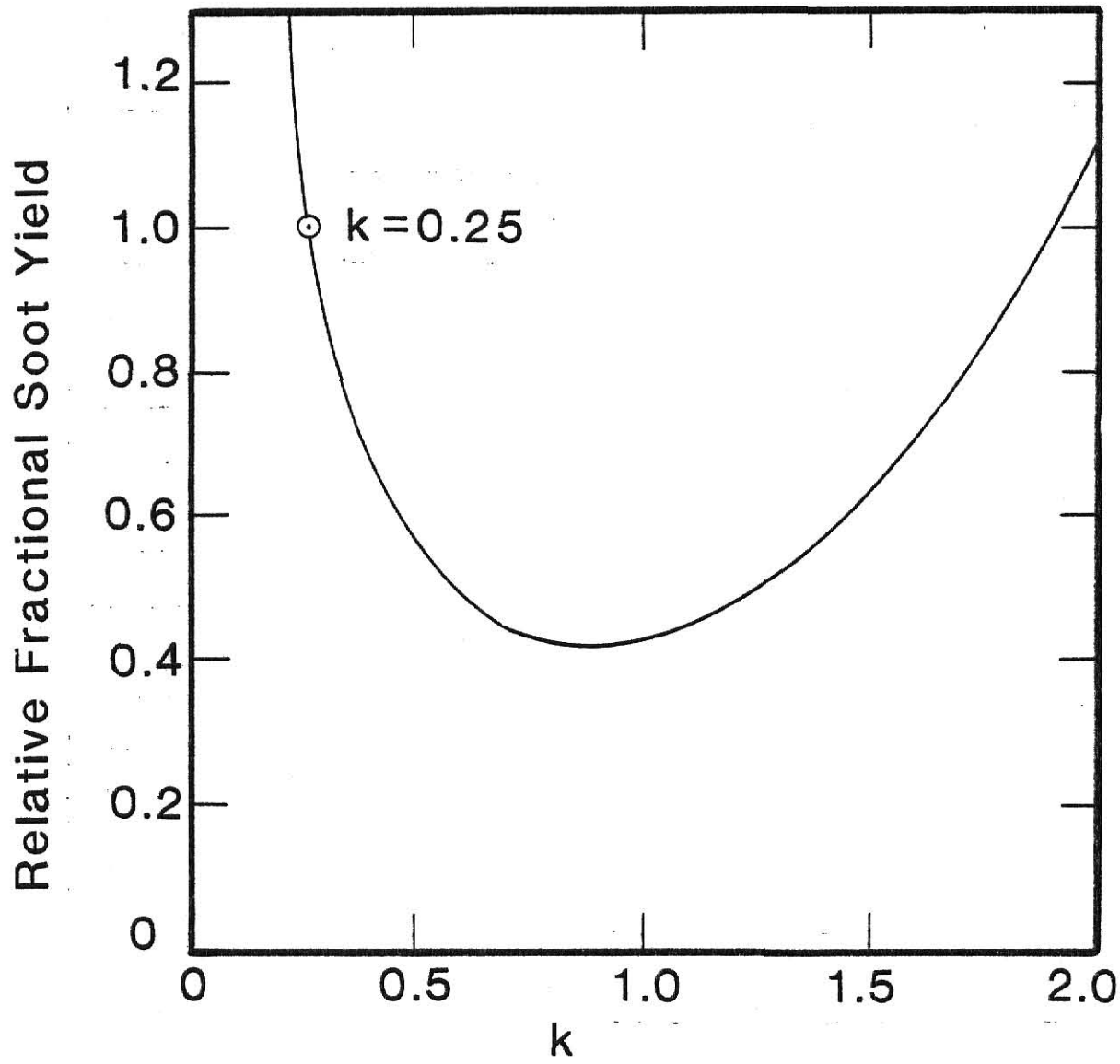

Fig. 2-8. Soot yield as a function of the imaginary part of the refractive index, k, with the real part equal to 1.9.

horizontally across the reaction zone. A laser beam from a Jodon (Model HN5) 5mW HeNe laser is directed through the quartz windows bounding the tube as shown before in Fig. 2-2. After exiting the tube, the beam passes through a narrow-band pass filter, which has a full width at half maximum of 10.0 nm about 632.8 nm. A mylar diffusing screen decreases the beam's intensity before it passes through an aperture (10mm) attached to the detector housing. The diffuse light then strikes the photocathode of an RCA IP28 photomultiplier tube, the output of which is amplified and displayed on the storage oscilloscope (see Appendix 3 for PM tube response data). Electrical noise was a problem, and the amplified signal had to be filtered through a low-pass RC circuit ($\tau = 6.8 \times 10^{-5}$ sec). Experiments performed with and without the filter demonstrated that the frequency response of the system was adequate to track satisfactorally the change in beam transmission with time (see Appendix B).

During the reaction time, products have been observed that both absorb and emit visible radiation. In this experiment, only the laser beam transmission was measured. Emission from the shock heated gases was negligible at the point of detection due to the high selectivity of the band pass filter and the physical distance between the shock tube and the detector. To ascertain this, tests were conducted where emission from the hot gases and incandescent particles was passed through the optical train in the absence of the laser beam. No emission was detected. A decrease in transmitted intensity is related quantitatively to extinction by soot or large gas phase hydrocarbons. In fact, Graham, et al.[13] showed from light scattering measurements that

absorbing gas phase molecules are only present in substantial concentrations early in soot growth, and soot particles themselves are the predominant absorber from t = 0.90 msec until the end of the shock flow.

Oscillograms showing traces from laser transmission and pressure transducer output were shown in Fig. 2-4a. The rarefaction fan arrives to quench the reaction, shown as the sudden decrease in pressure. The laser transmission may be read off the oscillogram at this instant, and this value is recorded along with the initial intensity, I_o. If simplifying assumptions are made, the volume fraction of soot can be related to these two intensities by eqn. 2-16, repeated here:

$$f_v = -\lambda \ell n\left(\frac{I}{I_o}\right) / 36\pi L F_a(m,\lambda) \ ,$$

where $F_a(\lambda)$ is a function of the complex refractive index, m.

The soot formation delay time, Δt_i, is defined to be the time lapse between passage of the reflected shock wave and the initial detection of beam extinction. The tangent to the transmission trace at the point of greatest extinction rate increase is extrapolated back to intersect the extended I_o line, and the delay time is recorded at this point (see Fig. 2-4b). These times may be plotted as a function of temperature and an equation describing the reaction rate may be written (see chapter 3).

2.4 Post-Shock Analysis

The stable reaction products are collected after selected shocks for analysis by venting the high pressure (ca. 2 atm) mixture contained in the experimental section through a filter or into a gas sample

bottle. Suspended soot particles are filtered from the gaseous stream by a Nucleopore (0.015 μm, nominal opening) polycarbonate membrane held in place by a metal housing (Nucleopore, 25mm). Venting takes place for several minutes until the pressure in the experimental section is reduced to nearly atmospheric. The filters are removed and attached to a scanning electron microscope (SEM) sample pedestal by double-sticky cellophane tape. After special preparation by a technician, the affixed soot samples are examined under an ETEC Auto Scan Ul SEM at magnifications up to 70,000 X. Micrographs from a transmission electron microscope were also taken for sizing of the individual spherical soot particles. Micrographs produced by the TEM (Philips, Model 201) were more useful in size determination than those of the SEM because of vibration difficulties experienced in using that latter instrument at high magnifications. Sample collection for the TEM is similar to that employed for SEM analysis except that copper sample grids (300 mesh) are placed in front of the Nucleopore filter. The grids are previously coated with a thin layer of 30% Formvar solution which traps the comparatively tiny soot particles. The soot covered copper grids served as the viewing medium for the TEM. The Nucleopore filter, in this arrangement, was useful only to restrict the gas flow and to supply a surface upon which the grids could rest. Particle size was determined by measuring at least twenty image diameters on the micrograph negatives with a graduated scaled magnifying glass, averaging, and then dividing by the corresponding magnification.

Collection of gaseous products is accomplished by simply venting the gases isolated in the experimental section into a previously

evacuated stainless steel bottle (Whitey, 150 ml). Because the reactants were confined to an axial zone of 12.1 cm after compression behind the reflected shock front, it was necessary to wait approximately one hour after each run for the products to diffuse sufficiently throughout the isolated test section in order for the mixture to become homogeneous. This waiting period was determined by Vaughn[32] to be of sufficient duration. The filled sample bottles are checked for positive pressure with respect to atmospheric pressure (esential for subequent gas analysis), and then analyzed by gas chromatography using a Tracor (Model 560) gas chromatograph, equipped with dual flame ionization detectors.

3.0 RESULTS

The pyrolysis of benzene and toluene was studied over a temperature range of 1400 to 2450 K. Although laser extinction analysis was conducted for each, only data collected from the benzene runs have been analyzed to yield results regarding reaction kinetics and soot particle sizes. The reader is referred to Appendix D, where the toluene data are tabulated. Tabular data for the benzene pyrolysis experiments may be found at the end of this chapter (Table 3-2). Results presented here pertain to the following: 1) fractional soot yield as it is affected by temperature, carbon atom concentration, and dwell time; 2) post-shock gas analysis; 3) reaction kinetics of soot particle formation and growth; and 4) soot particle size as it is influenced by temperature, dwell time, and carbon atom concentration.

3.1 The Formation of Soot

Soot production was measured optically during the pyrolysis of benzene at different temperatures, dwell times, and reactant concentrations. To determine soot yields, defined to be the ratio of the mass of soot produced per unit volume to the mass of benzene per unit volume initially present, pyrolysis of benzene was conducted at a constant dwell time, 2.5 msec. These fractional yields were calculated using the approach outlined in Secion 2.3. The influence of temperature on the soot yields at 2.5 msec dwell time is displayed in Figs. 3-1 and 3-2 for three different benzene concentrations. Photomultiplier tube output was read off oscillograms to the nearest 0.1 V. This resulted in an instrumental uncertainty of ± 0.05 to ± 0.08 in fractional soot yields shown in the figures. The curve drawn through each data set results from a

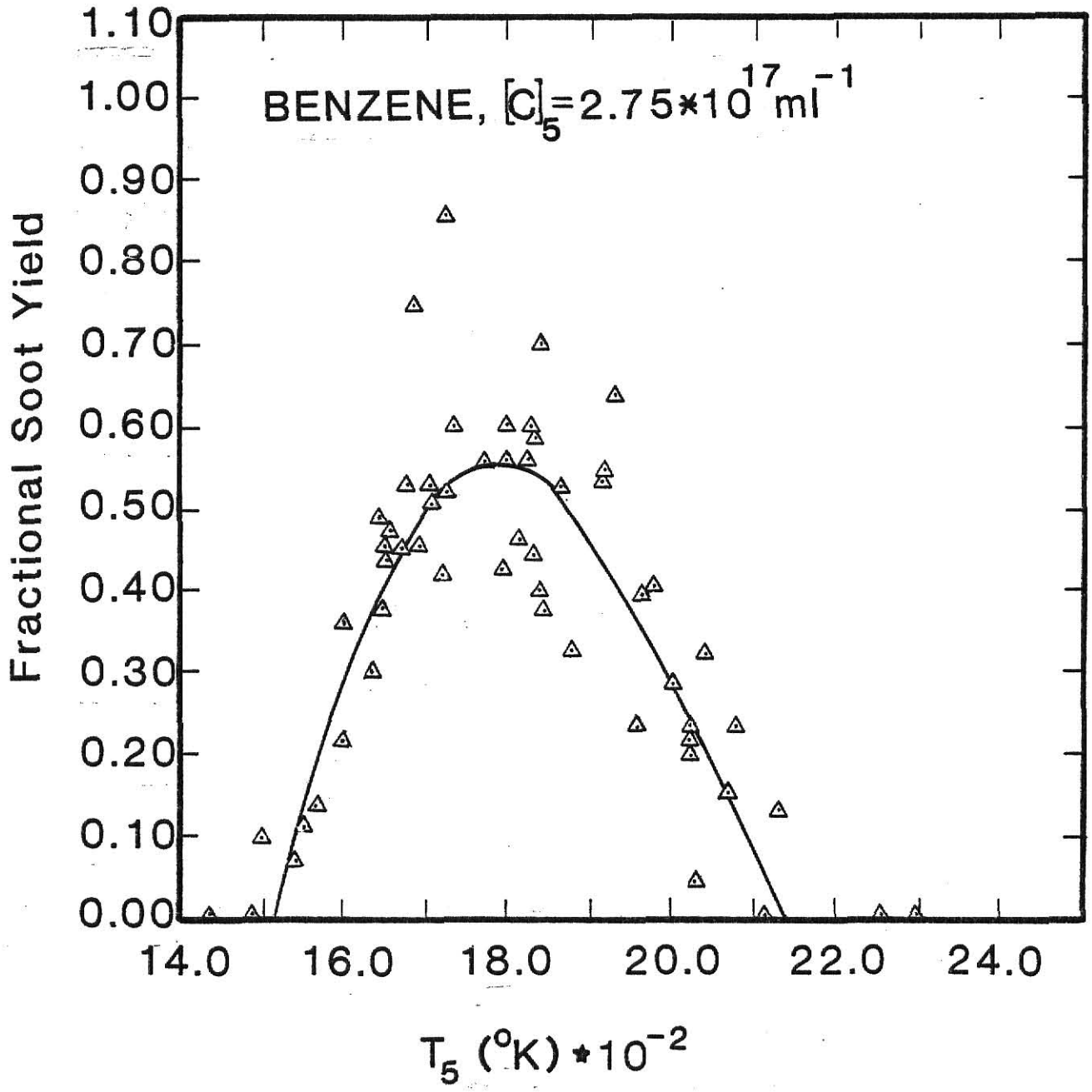

Fig. 3-1. Fractional soot yield as a function of reaction temperature for benzene at the lowest concentration studied.

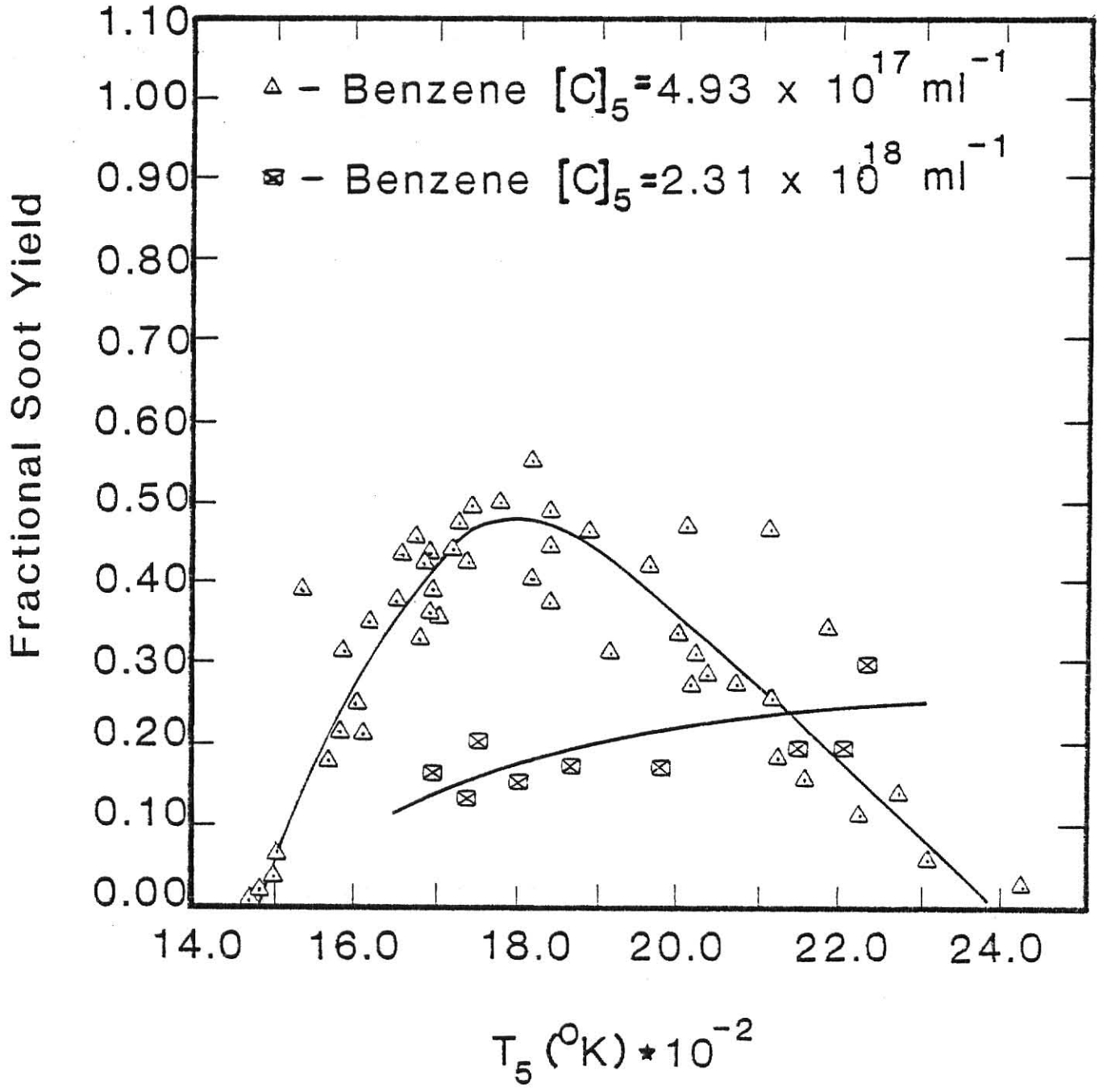

Fig. 3-2. Fractional soot yield as a function of reaction temperature for benzene at intermediate and highest concentration studied.

At the two lowest carbon atom concentrations, $[C]_5 = 2.75 \times 10^{17}$ and 4.93×10^{17} ml^{-1} (behind the reflected shock waves), the maximum fractional soot yields are approximately 0.55 and 0.48 respectively, and both maxima occur at a temperature of about 1800 K. Both curves are qualitatively similar, except at temperatures above 2100 K where soot yields for a carbon atom concentration of 4.93×10^{17} ml^{-1} persist to much higher temperatures than do those from a carbon atom concentration of 2.75×10^{17} ml^{-1}. Below 2100 K, the yields for these concentrations are roughly equivalent (to within experimental uncertainty).

The soot yield at the highest concentration, $[C]_5 = 2.31 \times 10^{18}$ ml^{-1} is qualitatively much different in that it increased monotonically with temperature over the temperature range studied. A curve through these data was drawn from a fourth-order fit assuming that the first measurable soot yields occur at about 1500 K, the temperature at which soot was first observed at the lower concentrations.

A similar analysis was also performed for toluene. The soot yields as a function of temperature are shown in Figs. 3-3 and 3-4 ($[C]_5 = 4.06 \times 10^{17}$ and 7.90×10^{17} ml^{-1}). The curves are qualitatively similar in shape to those of benzene, but there are several quantitative differences. Nearly 70 percent of the carbon atoms from toluene were converted to soot for both concentrations[†], and both maxima appear to occur at temperatures between 1800 and 1900 K. Perceptible soot yields occurred at about 1450 K -- slightly cooler than with benzene. At temperatures greater than 2100 K the soot yields from both benzene and toluene increase with increasing carbon atom concentrations.

[†]Care should be taken when assessing maximum yields. Because optical data usually display wide fluxuations at this point, these numbers are useful primarily for comparison.

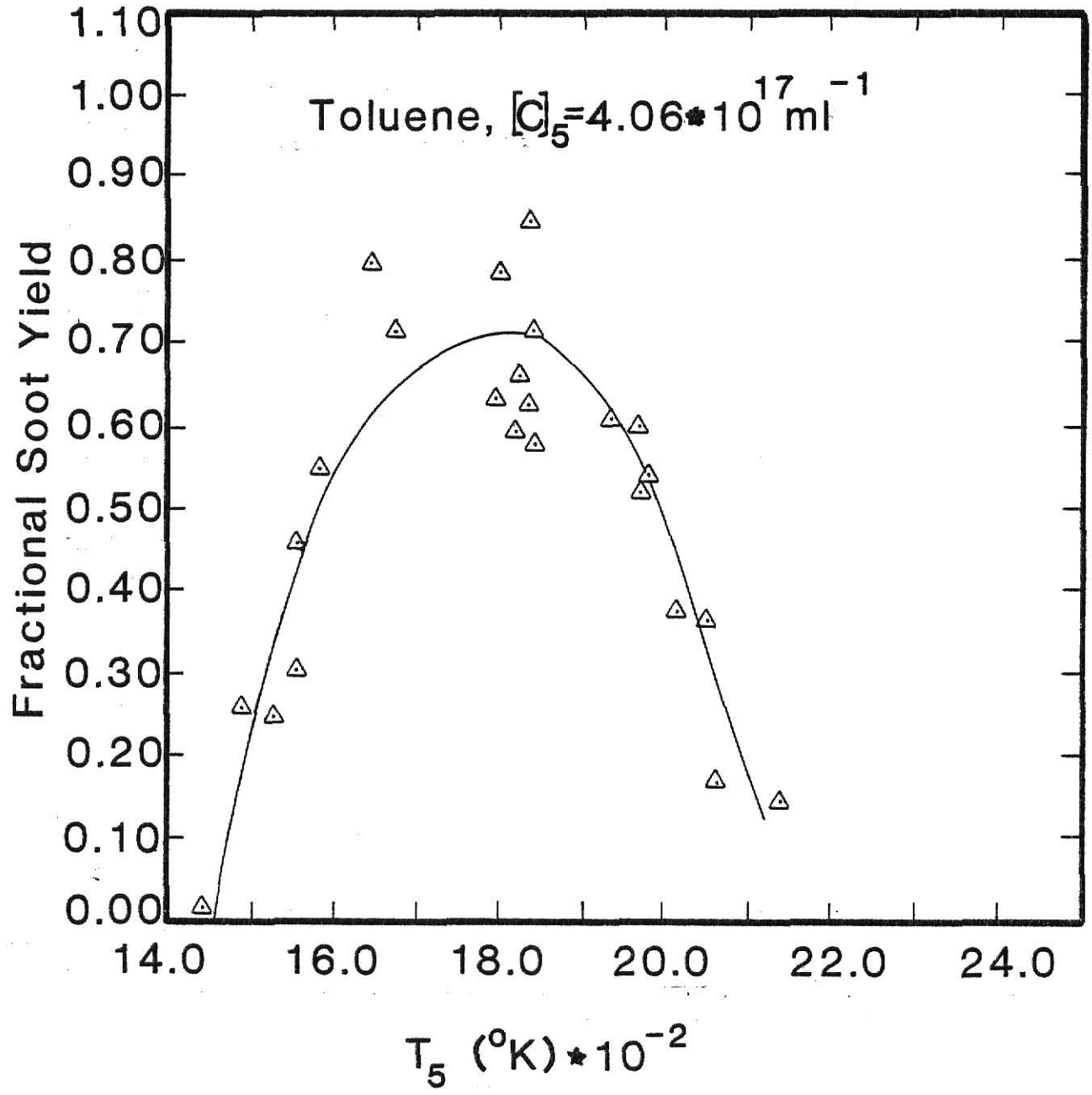

Fig. 3-3. Fractional soot yield as a function of reaction temperature for toluene at lowest concentration studied.

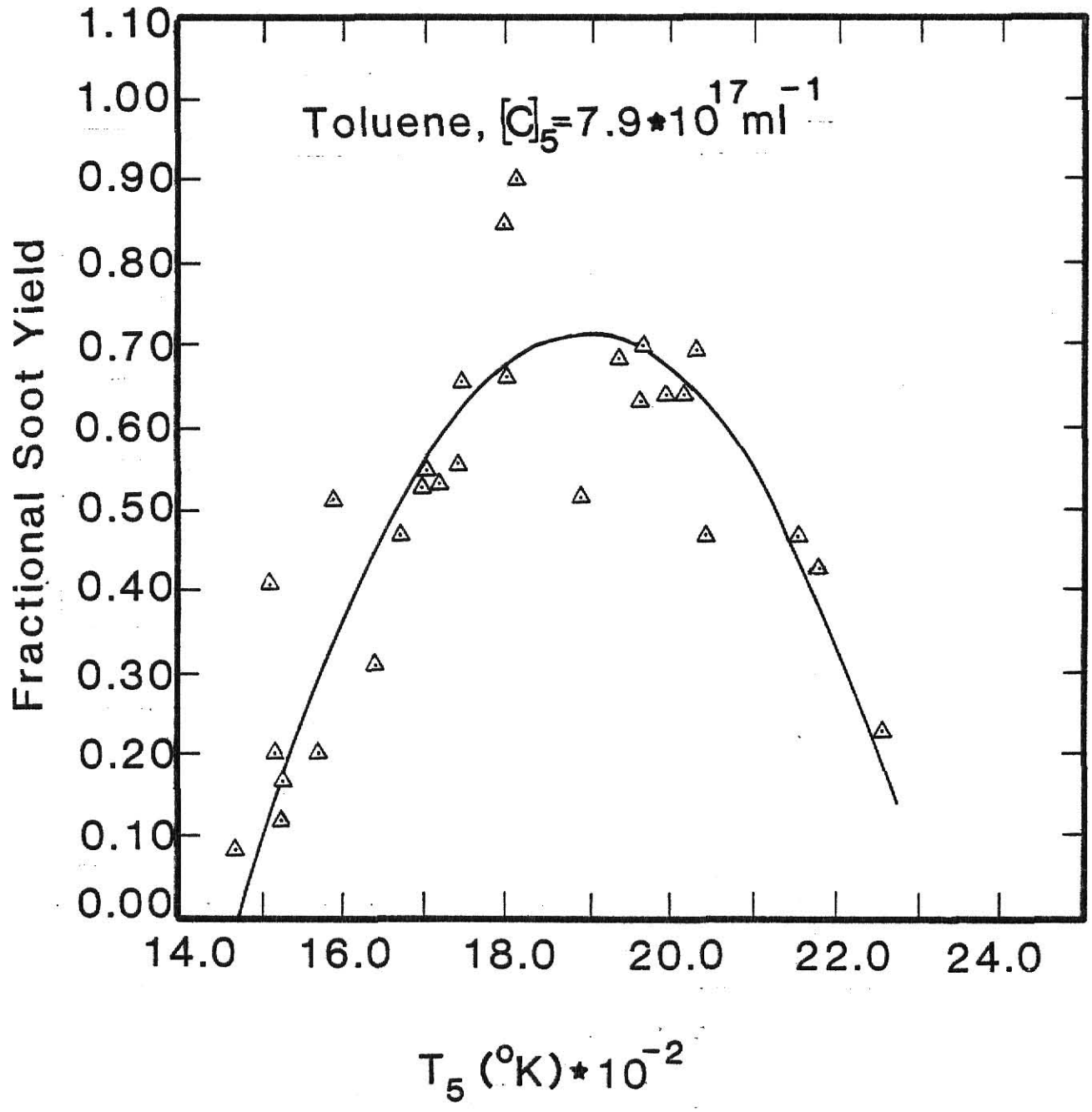

Fig. 3-4. Fractional soot yield as a function of reaction temperature for toluene at the highest concentration studied.

The effect of dwell time (length of reaction time at the reflected shock temperature) on soot production from benzene pyrolysis was investigated by incrementally decreasing the length of the driver section (see Chapter 2). This caused the rarefaction fan to arrive at the test section sooner; thus the reactions were quenched sooner. Dwell times were varied from <0.1 msec to 2.5 msec at a constant temperature for two reactant concentrations ($[C]_5 = 4.93 \times 10^{17}$ and 2.31×10^{18} ml^{-1}). Increases in yields with dwell time were observed in both cases as can be seen from results presented in Fig. 3-5.

3.2 Gaseous product Analysis

The sampling of product gases was accomplished by venting the isolated experimental section into a previously evacuated stainless steel bottle (see Chapter 2). Gas chromatographic analysis was performed on the contents and the production of acetylene, as well as the concentration of unreacted benzene, were measured. In Fig. 3-6 is plotted moles of product gas per mole of benzene initially present versus temperatures. Acetylene yields increase from below detectable limits between 1400 and 1500 K to about 45 percent near 1900 K where they appear to level off. Because of the uncertainty beyond this point, the curve through this data was hand drawn. The amount of unreacted benzene continuously decreases over the experimental temperature, and the curve results from an exponential fit to the data.

3.3 Reaction Kinetics

The rate of soot particle growth can be calculated by directly analyzing the laser transmission traces. It may be noted from the

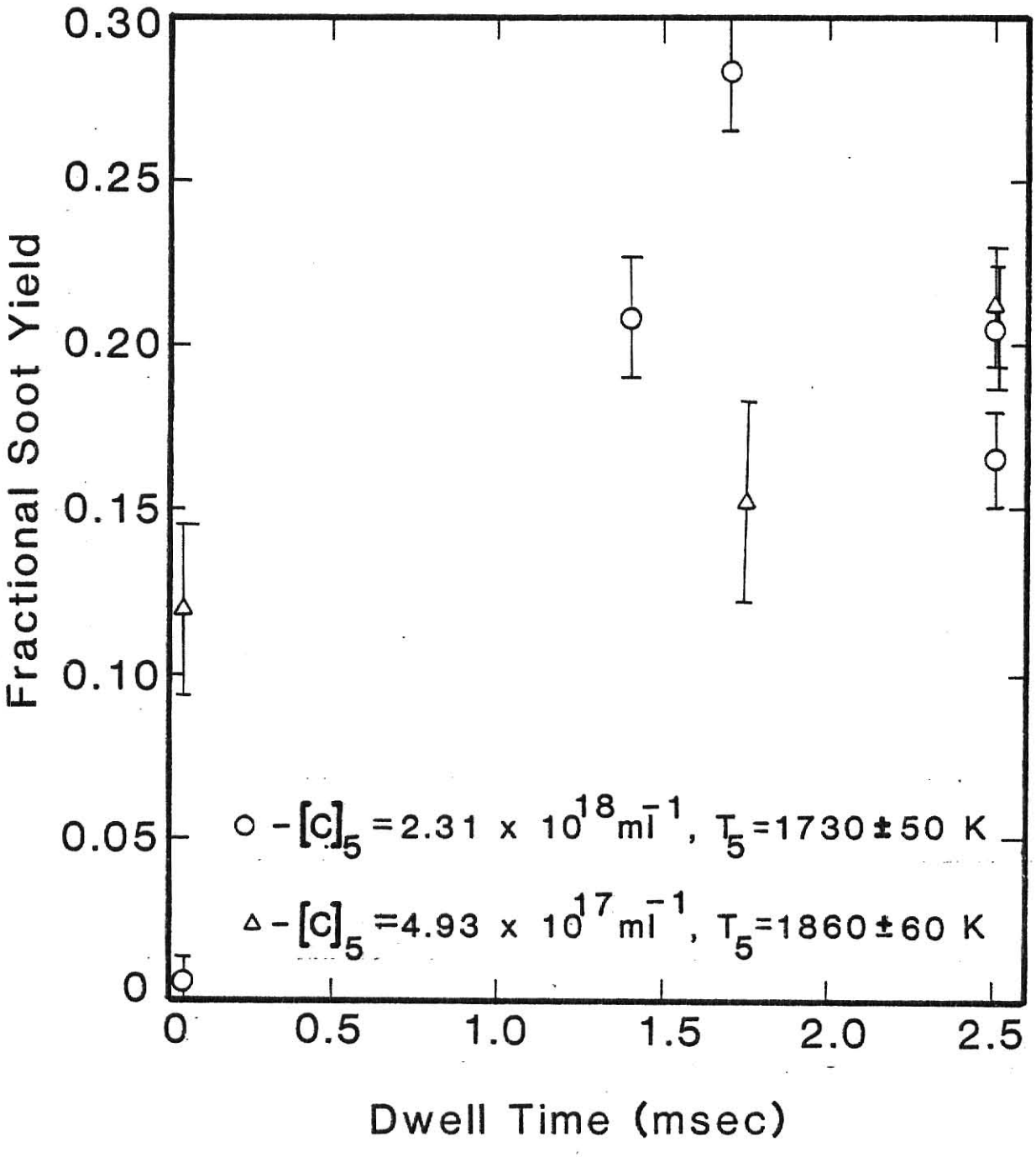

Fig. 3-5. Effect of time at reflected shock condition on the soot yields as determined by laser extinction measurements at 2.5 msec.

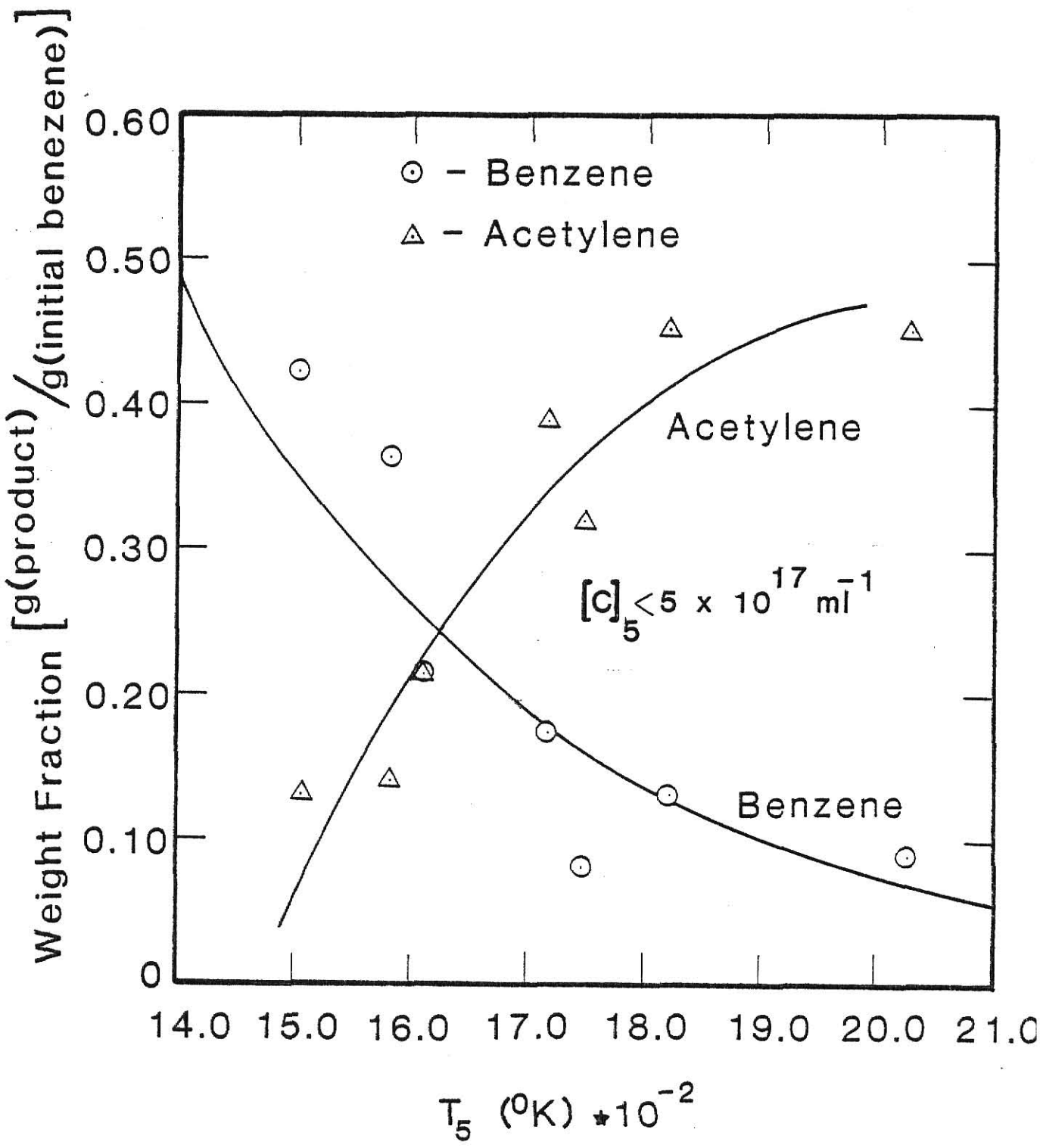

Fig. 3-6. Yields of acetylene and benzene as a function of reaction temperature.

oscillogram in Fig. 2-4a that once beam transmission begins to decrease, its decrease is nearly linear with time. By measuring the change in transmitted intensity over a time interval, a rate of soot volume growth may be estimated.

By multiplying eqn. (2-16) by the density of carbon (1.86 g/ml)[†], one obtains an expression for the soot density as a function of transmitted light intensity. Differentiating with respect to time yields

$$\frac{d\rho_s}{dt} = \frac{-1.86\lambda}{36\pi LF_a(m,\lambda)} \cdot \frac{1}{I(t)} \cdot \frac{dI}{dt} \quad , \qquad (3\text{-}1)$$

where dI/dt is the slope of the transmission curve at the time when extinction is first detected. Thus I(t) is I(0) which is equal to unity. If it is assumed that the rate of change of the soot particulate volume depends on the benzene concentraion to the n^{th} power, than a rate equation of the following form may be used:

$$\frac{d\rho_s}{dt} = A[p(C_6H_6)]^n \exp(-E_a/RT) \quad , \qquad (3\text{-}2)$$

where E_a is the activation energy in kcal/mole, R is the molar gas constant in kcal/mole-K, $p(C_6H_6)$ is the partial pressure of benzene

---

[†]This value of carbon density may vary with temperature, but it is assumed to be constant over the temperature range studied because of the lack of accurate knowledge of its relationship to temperature.

behind the reflected shock wave, T is the reflected shock gas temperature in ^{o}K, and A is a constant. .Equating eqns. (3-1) and (3-2):

$$\frac{-1.86\lambda}{36\pi LF_a(m,\lambda)} \cdot \frac{1}{I(0)} \cdot \frac{dI}{dt} = -k\frac{dI}{dt} = A[p(C_6H_6)]^n \exp(-E_a/RT) \quad , \qquad (3\text{-}3)$$

where $k = (1.86\lambda)/36\pi LF_a(m,\lambda)$ and $\frac{1}{I(0)} = 1$. Taking the logarithum of both sides, eqn. (3-3) may be rearranged to the form

$$\ell nk + \ell n\{-\frac{dI}{dt}[p(C_6H_6)]^{-n}\} = \ell nA - E_a/RT \quad . \qquad (3\text{-}4)$$

If k is assumed to be constant over the range of temperatures (non-varying refractive index), then differentiation of eqn. (3-4) with respect to 1/T and solving for E_a gives:

$$E_a = -Rd\left\{ \ell n\{-[p(C_6H_6)]^{-n}\frac{dI}{dt}\}\right\} / d(1/T) \quad . \qquad (3\text{-}5)$$

The term

$$A_n \equiv -\ell n\{-[p(C_6H_6)]^{-n}\frac{dI}{dt}\}$$

may be plotted against 1/T for differing values of n. The partial pressure of benzene behind the reflected shock is obtained by multiplying the total pressure, P_5, by the molar fraction of benzene in argon. In Figs. 3-7 and 3-8, A_n is plotted against the inverse temperature for reaction oders n = 1 and 2 respectively. The slope of

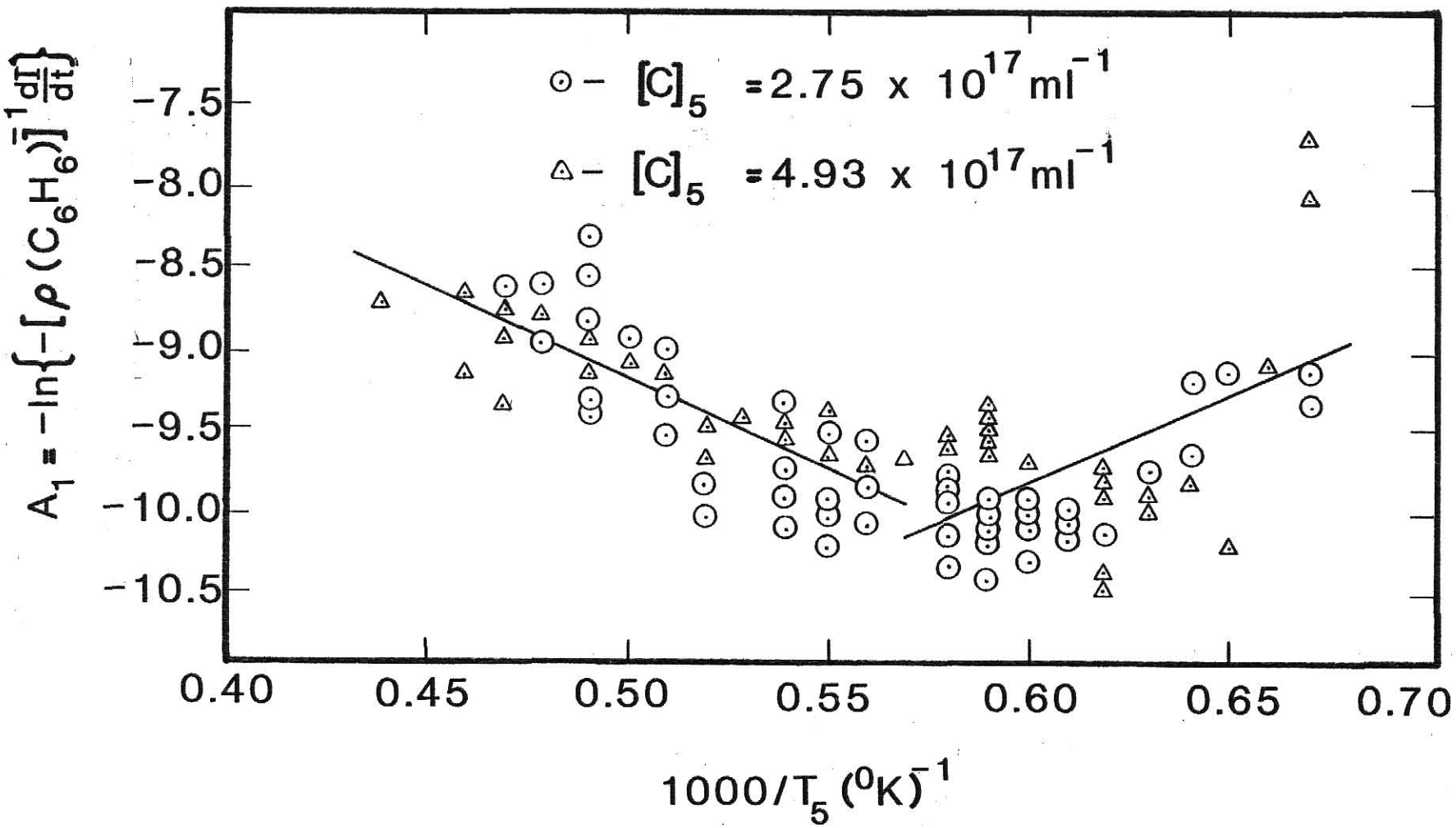

Fig. 3-7. Rate of increase of laser beam extinction as a function of temperature; first order dependence on benzene concentration.

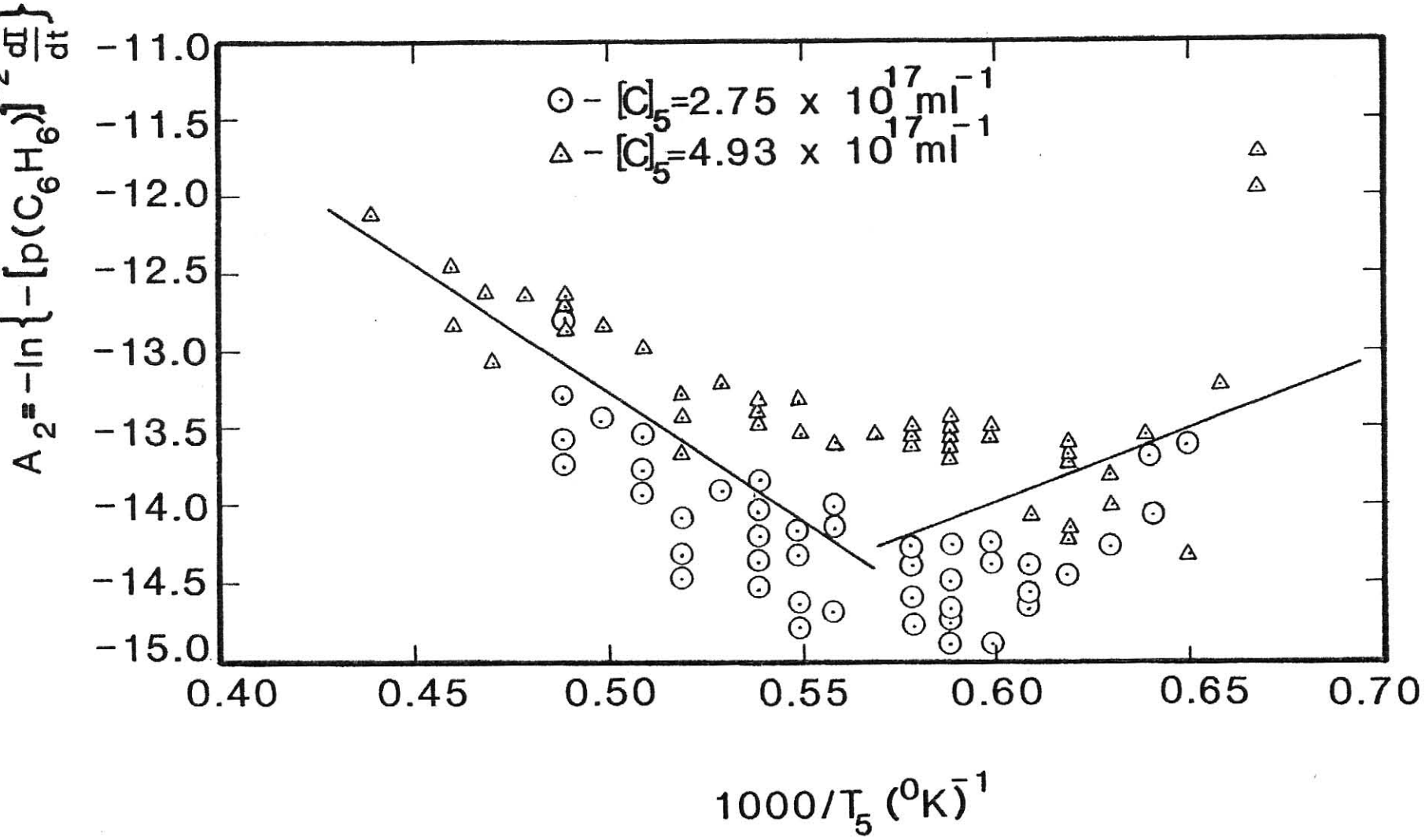

Fig. 3-8. Rate of increase of laser beam attenuation as a function of temperature; second order dependence on benzene concentration.

the best fit line through the points will equal E_a/R. Because soot yields do not increase monotonically with temperature in the concentration range $[C]_5 < 5 \times 10^{17}$ ml^{-1}, only those data below $T_5 \simeq 1750$ K ($1000/T_5 \geq 0.57$) can be used in this calculation. When comparing data, a first order reaction assumption (n=1) provides a slightly better fit ($r^2=0.18$) than assuming a reaction of second order ($r^2=0.073$). The activation energy for this concentration range was found to be 21.8 kcal/mole for a first order reaction and 17.0 kcal/mole for one of second order.

Plotted in Fig. 3-9 is A_n versus 1/T for the pyrolysis experiments in which the carbon atom concentration was greater than 5×10^{17} ml^{-1}. Because soot yield increases monotonically with temperature at these carbon atom concentrations, all data points could be used in the slope determination, and the activation energy was calculated to be 0.450 kcal/mole and -0.134 kcal/mole for first and second order reactions respectively. Note that both plots yield very nearly horizontal lines.

The induction time, defined to be the length of time between passage of the reflected shock wave and the onset of beam extinction, may be conceptually related to the average time for small nucleating species to condense from the gas phase into a large enough particle to result in detectable laser beam attenuation. An effective energy of activation for reactions leading to this important event may be estimiated from these data. If one assumes that, at the onset of extinction, the minimum detectable amount of extinction corresponds to equal amounts of carbon being formed for all conditions of temperature

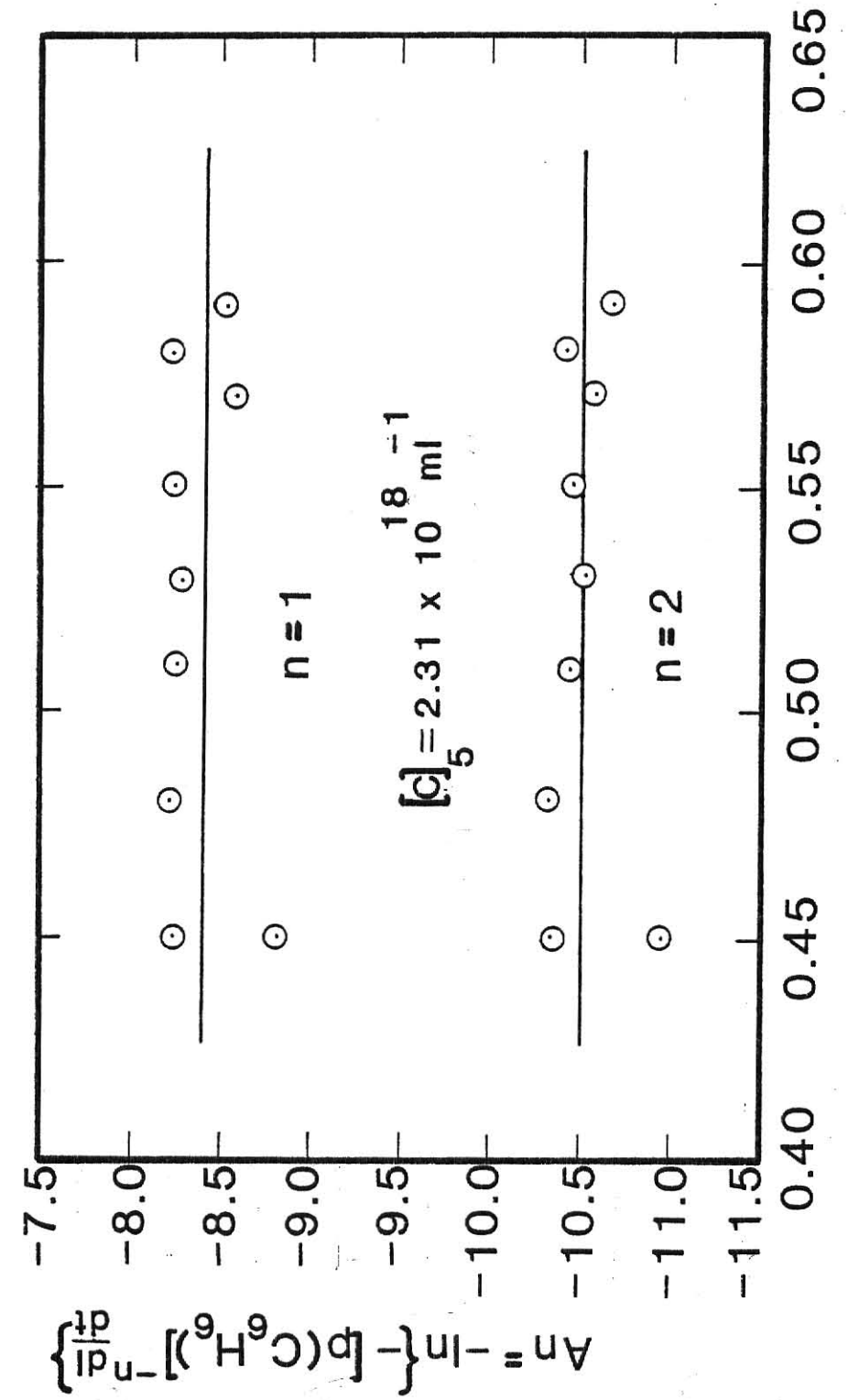

Fig. 3-9. Rate of increase of laser beam extinction as a function of temperature; first and second order dependence on benzene concentration.

and pressure in the reaction zone,[14] then from eqn. (3-2)

$$(\Delta\rho_s)_{initial} = A[p(C_6H_6)]^n \exp(-E_a/RT)\Delta t_i \quad , \qquad (3\text{-}6)$$

where E_a is the activation energy for soot nucleation and Δt_i is the measured induction time in seconds. Using a similar development which led to eqn. (3-5), eqn. (3-6) may be solved for the activation energy to give

$$E_a = Rd\left(\ell n\{[p(C_6H_6)]^n \Delta t_i\}\right) \quad d(1/T) \quad . \qquad (3\text{-}7)$$

Now if

$$B_n \equiv \ell n\ \{[p(C_6H_6)]^n \Delta t_i\}$$

is plotted against inverse temperature for different reaction orders, the activation energy for soot nucleation from benzene pyrolysis may be calculated from the slope of the best fit line via eqn. (3-7).

The induction time was found to vary only slightly with reactant concentration at a given temperature over the concentration range studied. Because of this behavior, a reaction order less than n=1.0 could be expected. Figures 3-10 through 3-12 plot B_n versus inverse temperature for the three concentrations studied. The data were not extended to temperatures greater than 2100 K because the induction times became very short. At low temperatures (T_5< 1500 K), negligible carbon formation posed another limitation. For an assumed reaction order of

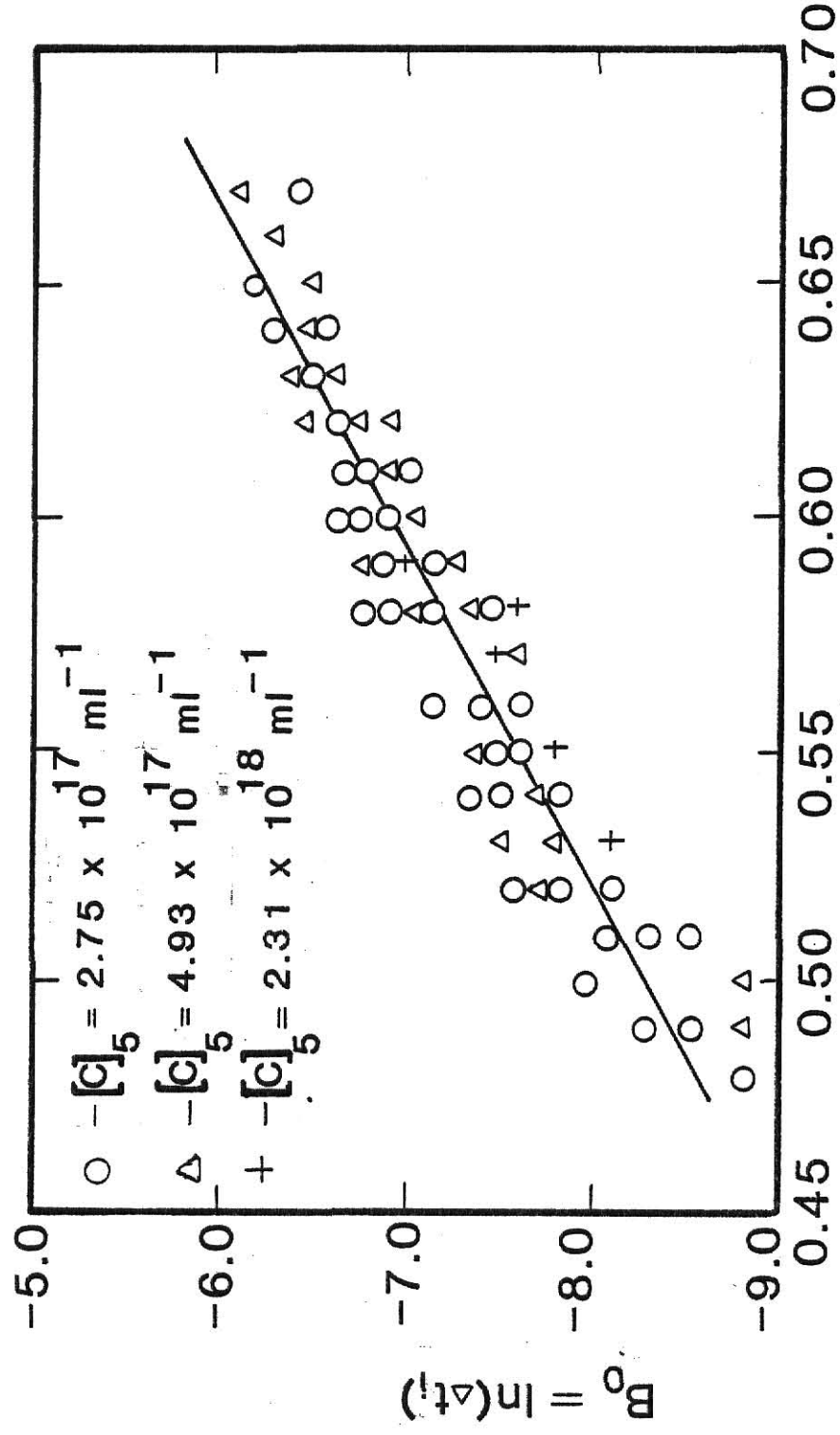

Fig. 3-10. Induction time till soot formation as a function of temperature; zeroth order dependence on benzene concentration.

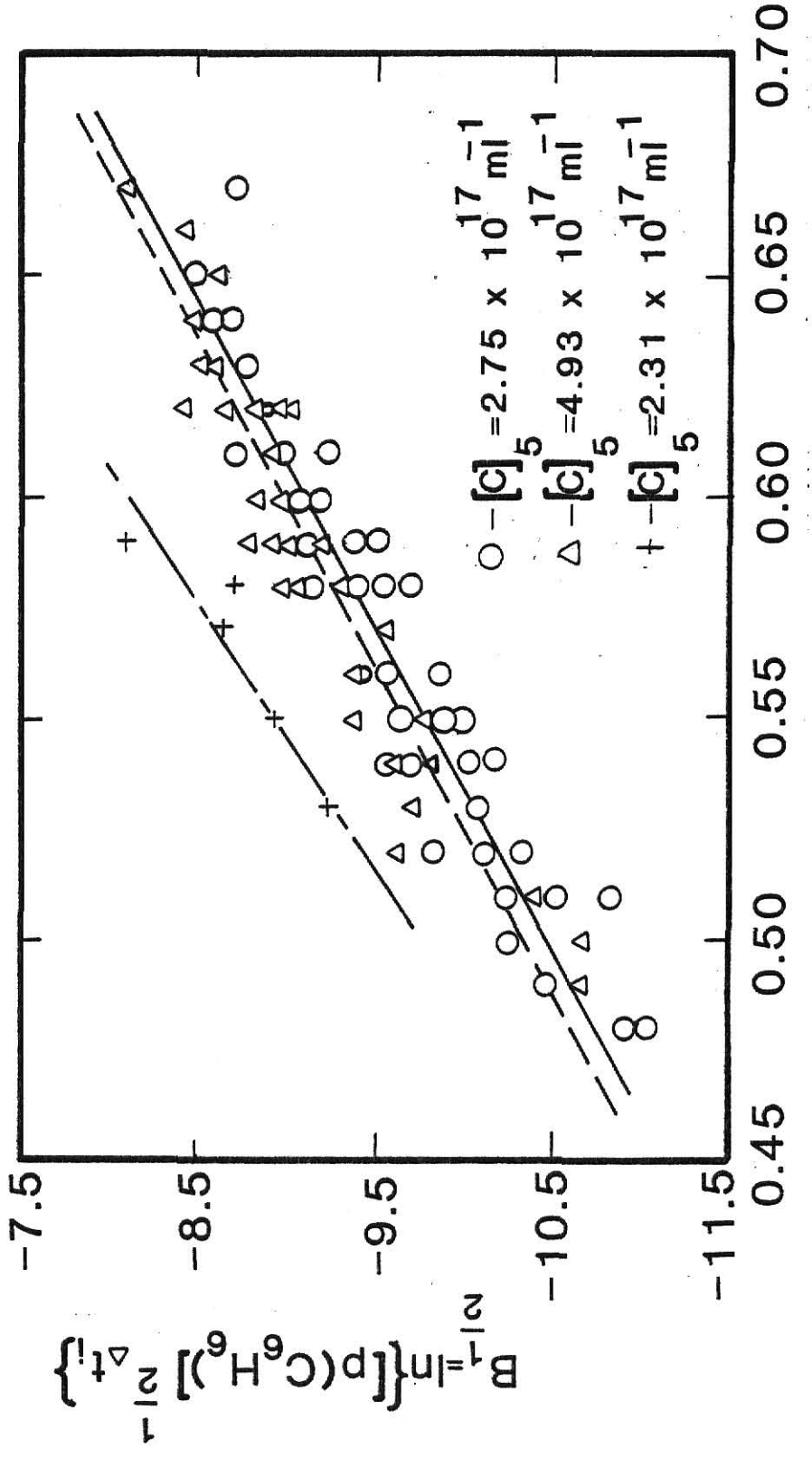

Fig. 3-11. Induction time till soot formation as a function of temperature; one-half order dependence on benzene concentration.

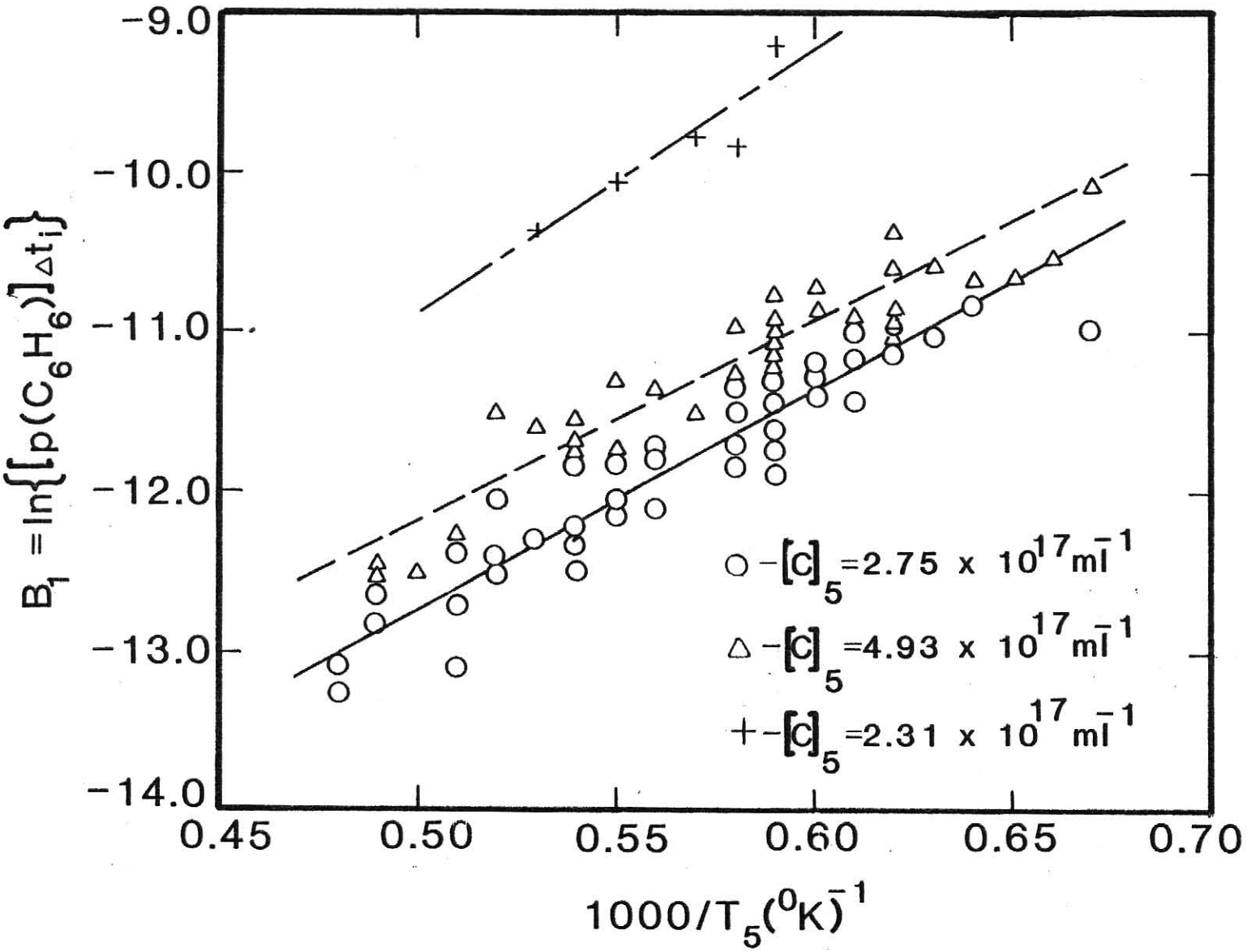

Fig. 3-12. Induction time till soot formation as a function of temperature; first order on benzene concentration.

zero, a single line was fitted through these data (r^2=0.912), and an activation energy of 27.6 kcal/mole was calculated. For reaction orders of 0.5 and 1.0, the data sets for each concentration had to be analyzed separately. For concentrations of 2.75 x 10^{17}, 4.93 x 10^{17}, and 2.31 x 10^{17} ml^{-1}, activation energies for a one-half order reaction were found to be 26.9, 26.9, and 32.1 kcal/mole respectively with correlation coefficients r^2 = 0.912, 0.916 and 0.856 respectively. Similarly for a reaction order of 1.0, activation energies were calculated as 27.8, 24.9, and 32.7 kcal/mole (r^2 = 0.856, 0.897, and 0.850) respectively. It is evident that the data best fit by a straight line are those from a reaction orders of zero and one-half because of the higher correlation coefficients.

3.4 TEM Sizing of Soot Particulates

Within five minutes after completing an experiment, a gases from the experimental section were vented into lines through a nucleopore filter which trapped much of the particulate suspended in the product stream. Photographs were taken of the soot agglomerates thus collected as they appeared under a transmission electron microscope at high magnification. From their image on the negatives, measurements were made to determine the size of the particles.

Soot produced from benzene pyrolysis is shown in Figs. 3-13 through 3-15 as it appeared at the indicated magnification. Individual particles in the agglomerates or chains are seen to be nearly spherical, and the size distribution is found to be very narrow. For instance, in Fig. 3-13, the average particle diameter is 16.2 nm with a standard

Fig. 3-13. Soot agglomerates from transmission electron microscopy at 81100 X.

T_5= 1656 K
Δt_i= 0.5 msec
P_5= 7.1 atm
$[C]_5$= 4.93 x 10^{17} ml^{-1}

Fig. 3-14. Soot agglomerates from transmission electron microscopy at 112,500 X.

T_5= 1755 K
Δt_i= 2.5 msec
P_5= 8.0 atm
$[C]_5$= 2.31 x 10^{18} ml^{-1}

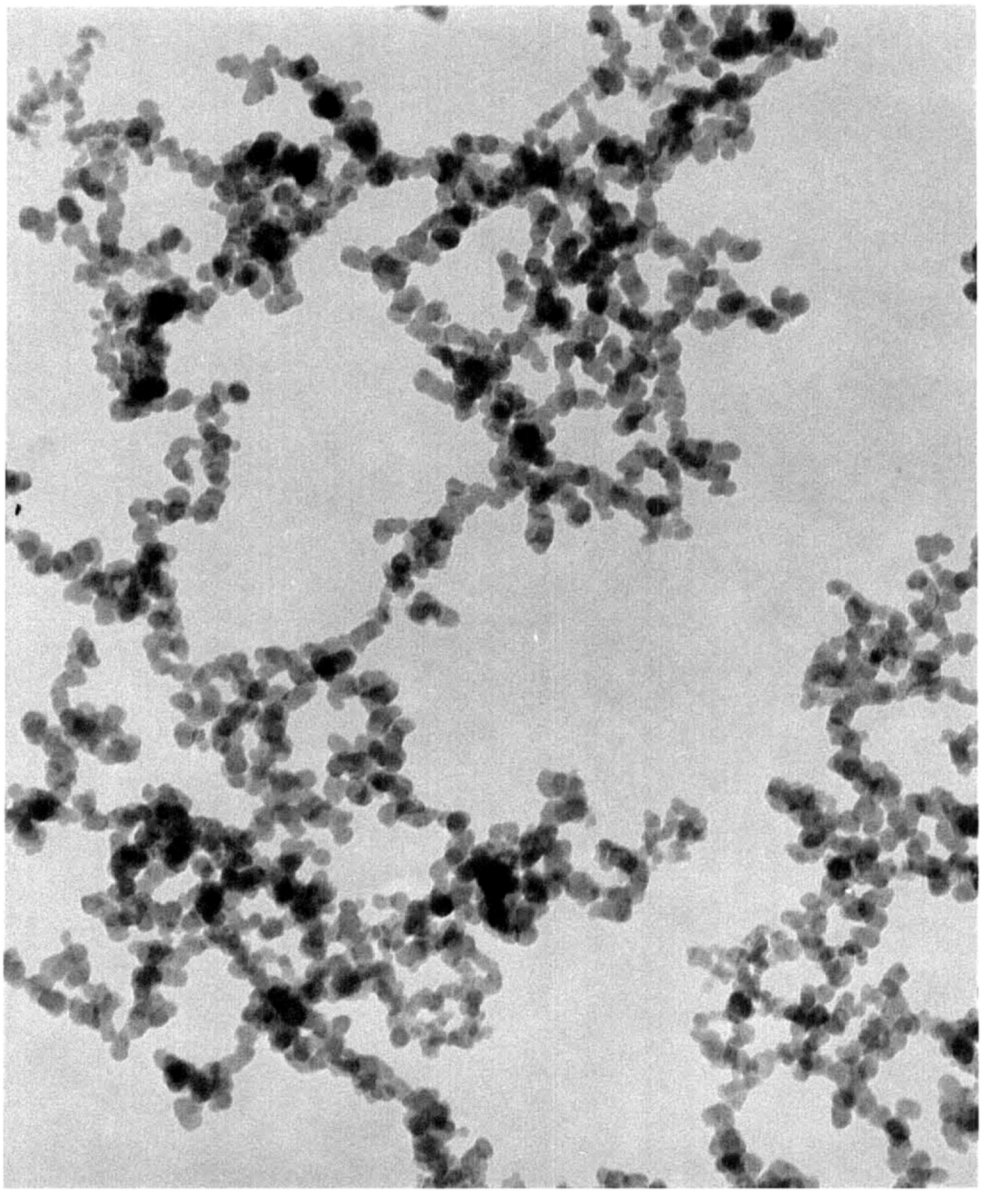

Fig. 3-15. Soot agglomerates from transmission electron microscopy at 254,000 X.

T_5= 1755 K
Δt_i= 2.5 msec
P_5= 8.0 atm
$[C]_5$= 2.31 x 10^{18} ml^{-1}

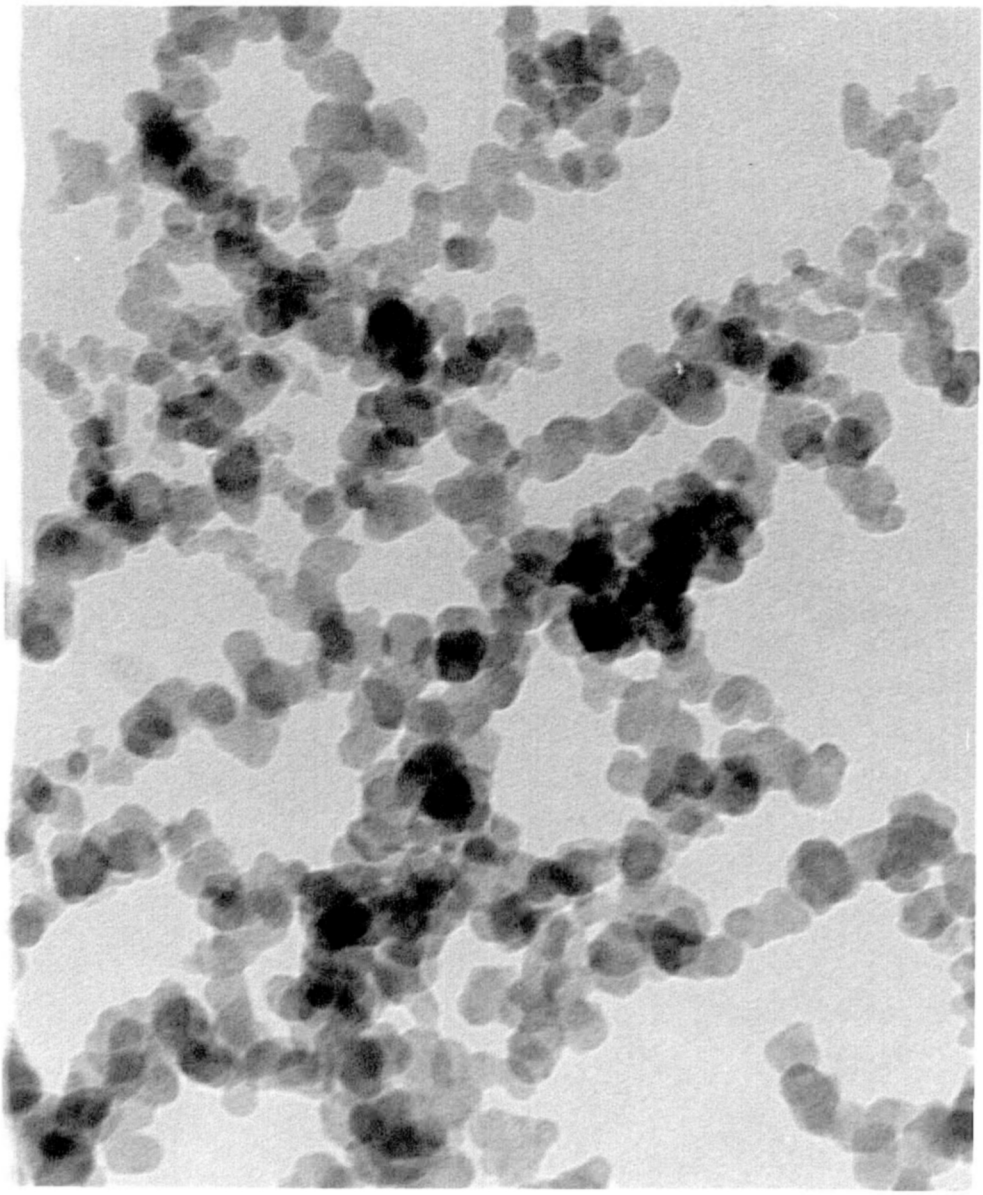

deviation of 2.6 nm. Results from other particle size determinations are given in Table 3-1.

In Fig. 3-16, the structure of the soot agglomerate is seen to be quite different from the usual "pearl necklace" appearance. Individual particles are not clearly distiguishable, and no attempt was made to determine sizes. This type of soot appeared rarely and unexpectedly, and so the reason for its occurrence could not be ascertained. The last photograph (Fig. 3-17) was taken with a scanning electron microscope at comparatively low magnification (3100X). This three-dimensional view shows the fluffy appearance of soot as it rests upon the filtering membrane.

To study the influence of temperature, dwell time, and reactant concentration on the final particle size, a limited number of shocks were conducted with a systematic variation of these parameters. In the following plots, error bars represent standard deviations in measurement. The response of the particle size to temperature is shown in Fig. 3-18 for a dwell time of 2.5 msec and a carbon atom concentration of 4.93×10^{17} ml^{-1}. The diameters varied from 18.1 to 25.0 nm over a temperature range of 800 K. The effect of dwell time on particle size for temperatures from 1690 to 1860 K at $[C]_5 = 4.93$ and 23.1×10^{17} ml^{-1} is shown in Fig. 3-19. Within the range of the experimental uncertainty, it appears that soot particles have reached their limiting size even at vanishingly small residence times behind the reflected shock wave. Finally, the particle size variation with concentration is shown in Fig. 3-20 for carbon atom concentrations of 4.93×10^{17} and

Table 3-1 Soot Particle Size Data

RUN	T_5 (deg K)	t_{dwell}(msec)	D(nm) ±σ(nm)	Benzene mole fraction
225	1662	2.5	21.0 ±2.5	0.0025
227	1500	2.5	19.0 ±2.5	"
281	2300	2.5	25.0 ±3.4	"
282	1850	2.5	19.4 ±2.5	"
283	1850	2.5	18.1 ±3.0	"
304	1837	1.8	15.4 ±2.7	"
305	1934	2.5	15.6 ±2.3	"
306	1834	<0.1	13.7 ±1.6	"
307	1837	~0.1	13.8 ±1.9	"
309	1780	2.7	13.2 ±1.7	"
310	1604	1.5	a	"
311	1641	1.2	16.4 ±2.4	"
312	1656	0.5	16.2 ±2.6	"
313	1765	<0.1	a	"
314	1775	2.5	18.6 ±4.4	0.0130
315	1778	1.6	22.2 ±2.8	"
316	1666	<0.1	25.5 ±4.0	"
317	1702	1.4	24.8 ±3.4	"

[a] Diameter was undetermined because of indistinct particles.

Fig. 3-16. Soot agglomerates from transmission electron microscopy at 112,000 X.

T_5= 1765 K
Δt_i= <0.1 msec
P_5= 7.8 atm
$[C]_5$= 4.93 x 10^{17} ml^{-1}

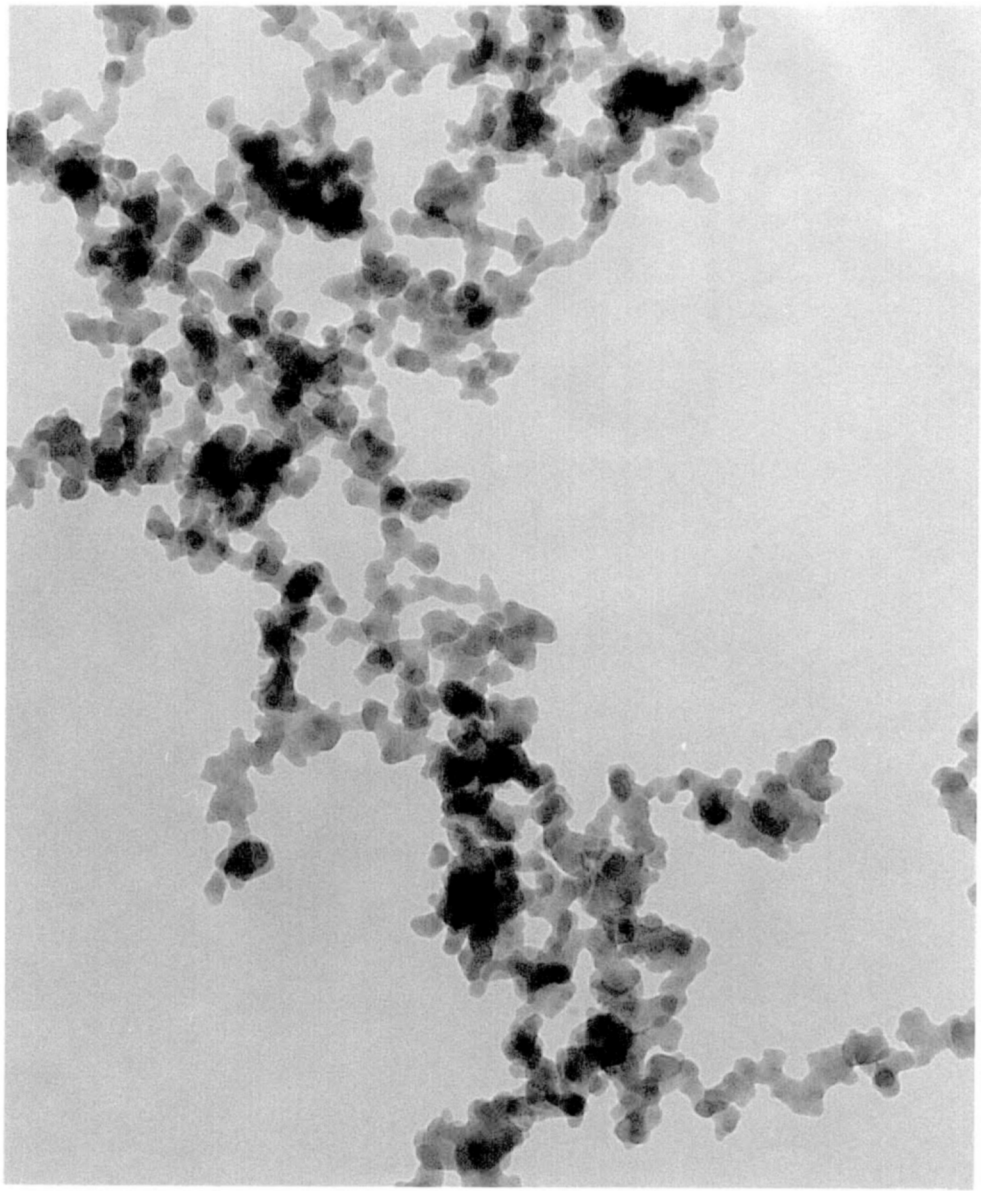

Fig. 3-17. Soot agglomerates from scanning electron microscopy at 3100 X.

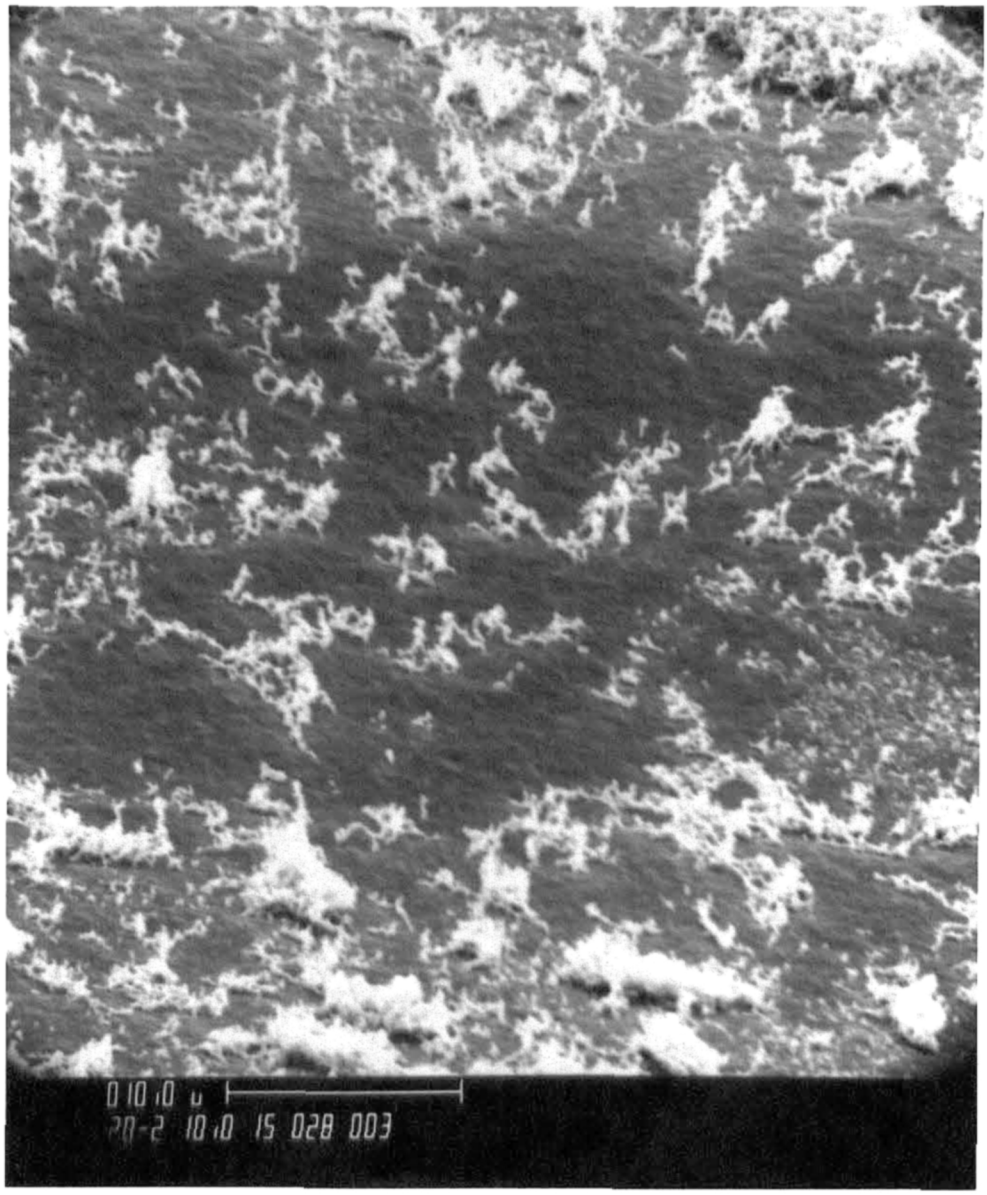
0 10.0 u
20-2 10.0 15 028 003

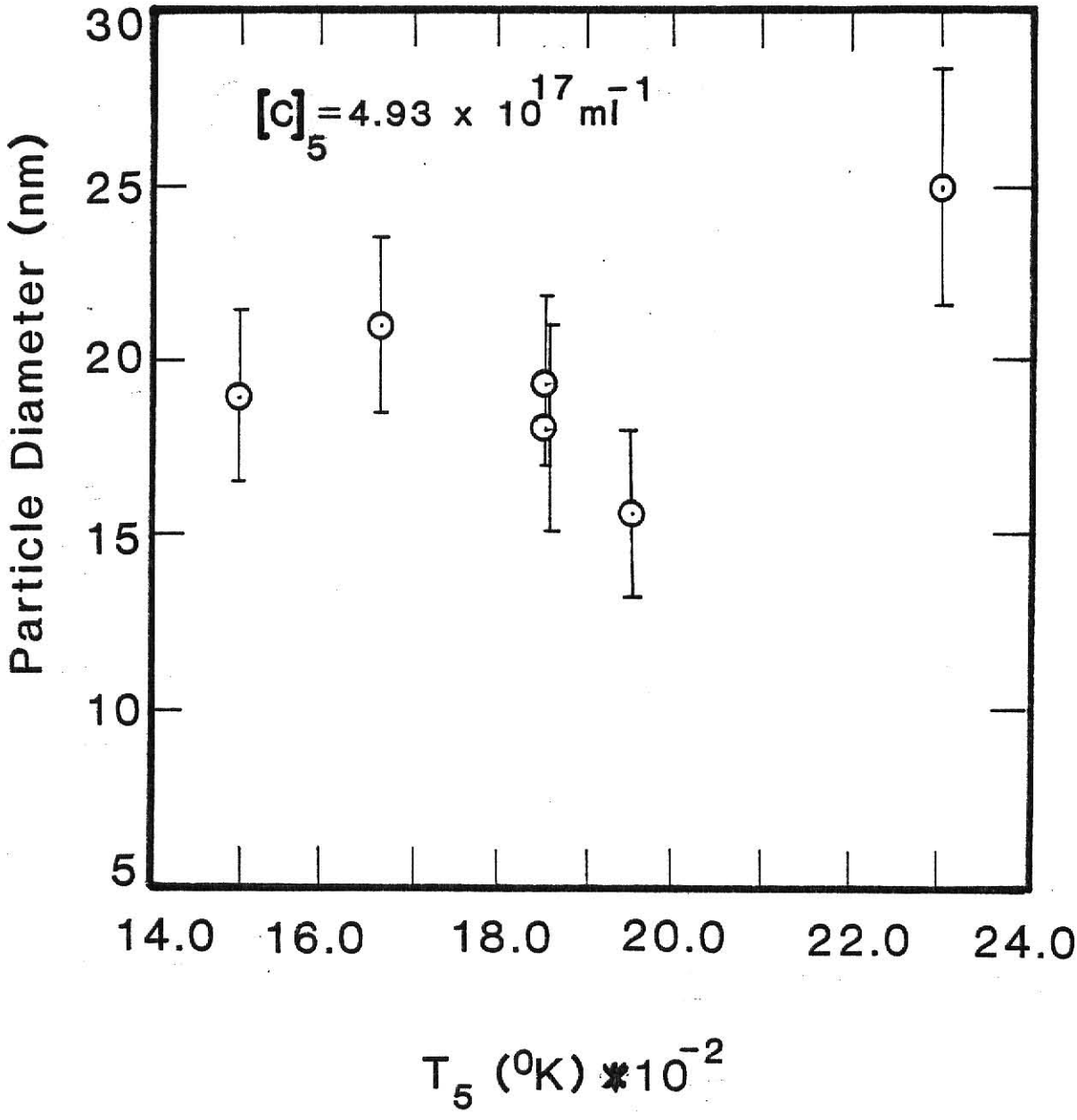

Fig. 3-18. Particle diameter as a function of reaction temperature; dwell time of 2.5 msec.

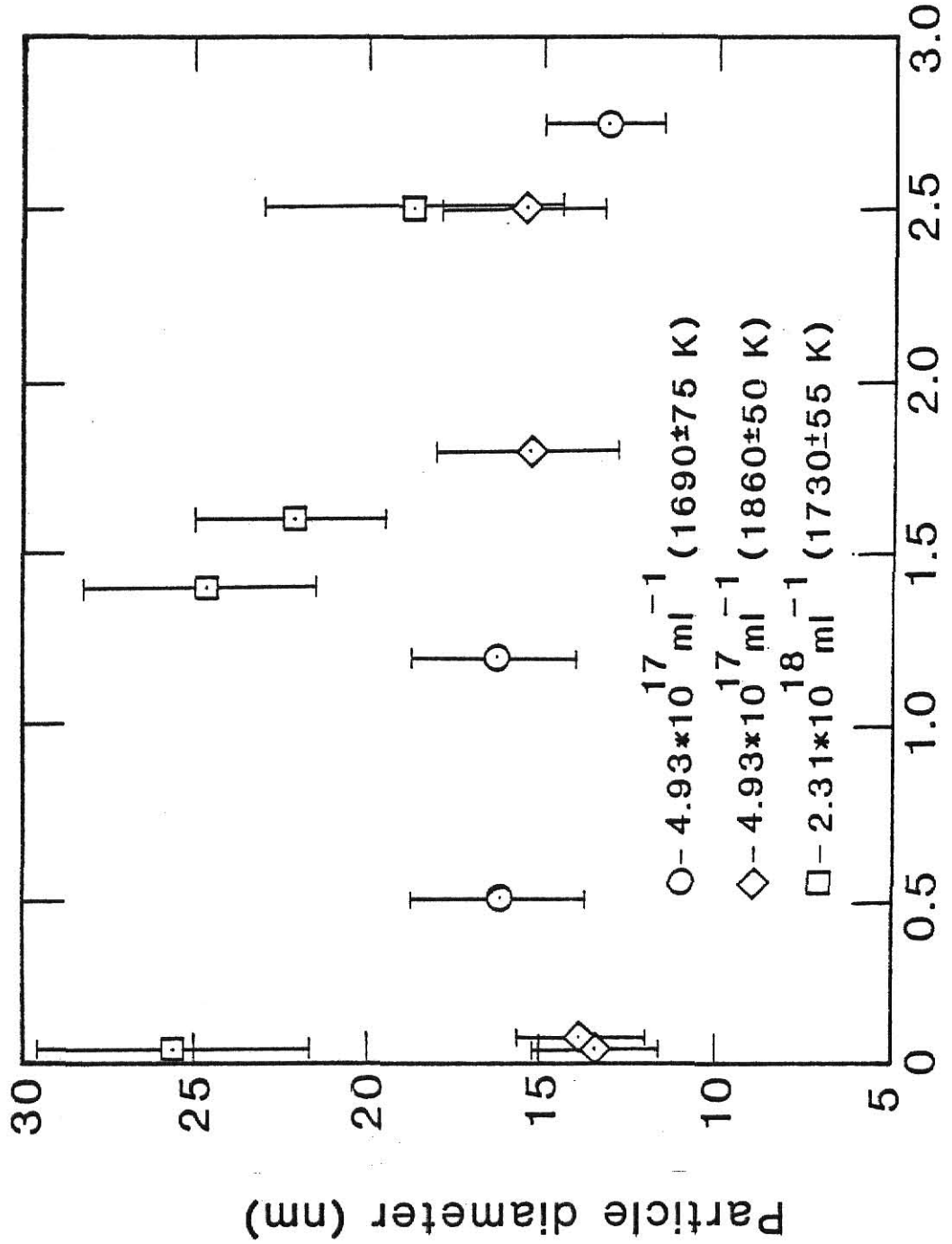

Fig. 3-19. Particle diameter as a function of reaction dwell time.

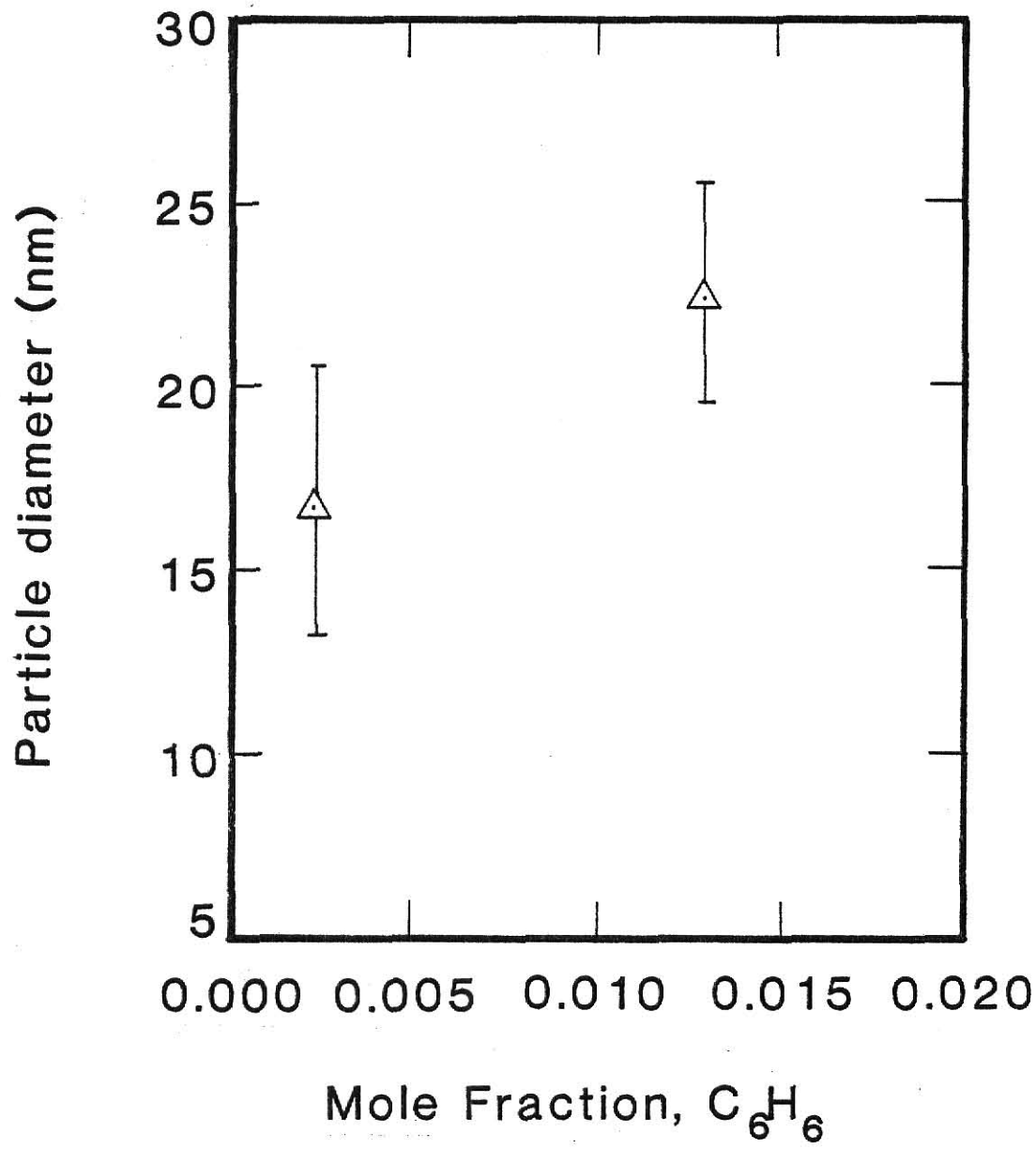

Fig. 3-20. Particle diameter averaged over all dwell times and temperatures as a function of initial benzene concentration.

2.31×10^{18} ml^{-1}(0.0024 and 0.0130 moles benzene per mole argon initially, respectively). The two points on this plot represent averages of diameters over the range of dwell times at which these constant temperature shocks were run.

Table 3-2 Individual Benzene Shock Data

RUN	T_5(K)	$p(C_6H_6)$(atm)[a]	Soot Yield(%)	Δt_i(msec)	$-dI/dt(msec^{-1})$	$f_m\left(\frac{\text{moles benzene}}{\text{mole argon}}\right)$
157	1490	0.0111	0.0	∞	0.0	0.0016
158	1539	0.0114	6.9	2.0	0.10	"
159	1655	0.0129	44.0	1.0	0.25	"
160	1417	0.0100	0.0	∞	0.0	"
161	1500	0.0109	9.5	1.6	0.10	"
162	1599	0.0113	21.5	1.5	0.20	"
163	1656	0.0124	45.6	1.1	0.25	"
164	1683	0.0127	45.1	1.0	0.25	"
165	1653	0.0123	47.6	1.1	0.25	"
166	1566	0.0112	13.9	1.8	0.16	"
167	1646	0.0117	38.0	1.2	0.26	"
168	1721	0.0127	56.9	0.6	0.25	"
169	1676	0.0095	52.9	1.2	0.26	0.0012
170	1720	0.0096	41.8	0.9	0.20	"
171	1721	0.0093	52.4	0.8	0.23	"
172	1775	0.0098	55.6	0.8	0.22	"
173	1706	0.0091	51.5	0.9	0.20	"
174	1708	0.0089	53.0	0.8	0.20	"
175	1804	0.0097	56.0	0.6	0.19	"
176	1826	0.0098	56.1	0.6	0.21	"
177	1865	0.0097	52.8	0.4	0.16	"

Table 3-2 Individual Benzene Shock Data (cont.)

RUN	T_5(K)	$p(C_6H_6)$(atm)[a]	Soot Yield(%)	Δt_i(msec)	$-dI/dt$(msec^{-1})	f_m (moles benzene / mole argon)
178	1916	0.0103	53.7	0.4	0.18	0.0012
179	2003	0.0106	28.1	0.35	0.075	"
180	1975	0.0104	40.2	0.2	0.11	"
181	2028	0.0108	20.7	0.1	0.067	"
198	2034	0.0127	7.1	0.1	0.056	0.0014
199	2028	0.0131	21.9	0.2	0.13	"
200	1917	0.0119	54.1	0.5	0.18	"
204	2044	0.0133	32.6	0.25	0.14	"
205	2070	0.0129	15.8	0.15	0.18	"
206	1842	0.0125	69.9	0.40	0.30	"
207	1688	0.0113	75.1	0.8	0.35	"
208	1931	0.0126	64.0	0.3	0.26	"
209	2131	0.0129	13.1	<0.1	0.078	"
210	1554	0.0115	11.2	1.8	0.11	0.0016
211	1432	0.0108	0.2	∞	0.00	"
212	1721	0.0137	86.0	0.8	0.41	"
213	1643	0.0122	49.3	0.9	0.29	"
214	1603	0.0118	36.1	1.3	0.26	"
215	1634	0.0120	29.9	1.5	0.26	"
216	2076	0.0142	23.4	0.15	0.11	"

Table 3-2 Individual Benzene Shock Data (cont.)

RUN	T_5(K)	$p(C_6H_6)$(atm)[a]	Soot Yield(%)	Δt_i(msec)	$-dI/dt$(msec^{-1})	$f_m\left(\frac{\text{moles benzene}}{\text{mole argon}}\right)$
217	1823	0.0137	60.1	0.55	0.27	0.0016
218	1796	0.0134	60.0	0.6	0.25	"
219	1835	0.0137	59.5	0.55	0.26	"
220	1734	0.0120	60.7	1.0	0.25	"
221	1968	0.0142	39.6	0.3	0.19	"
222	2028	0.0132	22.6	0.2	0.10	"
261	1819	0.0110	46.8	0.5	0.16	0.0013
262	1843	0.0111	37.4	0.4	0.13	"
263	1875	0.0114	33.1	0.4	0.14	"
264	1839	0.0118	39.9	0.65	0.16	"
265	1690	0.0104	40.8	1.1	0.21	"
266	1954	0.0123	22.0	0.25	0.11	"
267	2295	0.0129	0.0	∞	0.0	"
268	2255	0.0124	0.0	∞	0.0	"
269	1794	0.0111	43.1	0.5	0.15	"
270	1831	0.0115	44.4	0.5	0.17	"
271	2110	0.0118	0.0	∞	0.0	"
182	1487	0.0159	1.9	2.0	0.03	0.0023
183	1650	0.0184	77.2	1.0	0.43	"
184	1612	0.0181	71.3	1.0	0.47	"
185	1582	0.0164	23.0	1.6	0.32	"

Table 3-2 Individual Benzene Shock Data (cont.)

RUN	T_5(K)	$p(C_6H_6)$(atm)[a]	Soot Yield(%)	Δt_i(msec)	$-dI/dt(msec^{-1})$	$f_m\left(\frac{\text{moles benzene}}{\text{mole argon}}\right)$
186	1603	0.0163	69.9	1.0	0.47	0.0023
187	1508	0.0153	6.9	1.8	0.13	"
188	1540	0.0158	39.4	1.5	0.40	"
223	1588	0.0193	31.8	1.4	0.36	"
224	1683	0.0220	45.5	0.7	0.36	"
225	1662	0.0217	44.3	0.9	0.35	"
226	1658	0.0223	38.0	1.0	0.36	"
227	1501	0.0194	3.6	2.2	0.058	"
228	1570	0.0204	18.5	1.5	0.32	"
229	1614	0.0205	21.4	1.25	0.36	"
230	1605	0.0202	25.3	1.6	0.34	"
231	2113	0.0237	47.2	0.1	0.27	"
232	2186	0.0238	34.2	0.0	0.21	"
233	2278	0.0255	13.6	0.0	0.12	"
234	1484	0.0171	1.4	∞	0.010	0.0024
235	1695	0.0209	43.2	0.7	0.31	"
236	1621	0.0189	35.8	1.1	0.31	"
237	1693	0.0199	42.3	0.8	0.31	"
238	1750	0.0203	49.5	0.5	0.31	"
239	1736	0.0201	47.1	0.65	0.31	"

Table 3-2 Individual Benzene Shock Data (cont.)

RUN	T_5(K)	$p(C_6H_6)$(atm)[a]	Soot Yield(%)	Δt_i(msec)	$-dI/dt$(msec^{-1})	$f_m\left(\frac{\text{moles benzene}}{\text{mole argon}}\right)$
240	1701	0.0194	39.0	1.1	0.31	0.0024
241	1701	0.0187	36.1	1.0	0.28	"
242	1784	0.0196	50.9	0.6	0.31	"
243	1847	0.0204	49.4	0.4	0.29	"
244	1824	0.0201	55.5	0.4	0.30	"
245	1890	0.0233	46.7	0.4	0.29	0.0026
246	1705	0.0197	36.0	0.9	0.29	"
247	1682	0.0189	33.5	1.0	0.30	"
248	1966	0.0139	42.4	0.2	0.25	"
249	1739	0.0204	42.7	0.85	0.31	"
250	1726	0.0194	44.7	0.9	0.31	"
251	2157	0.0235	15.4	0.1	0.14	"
252	2223	0.0244	11.1	<0.1	0.042	"
253	1918	0.0230	31.8	0.45	0.023	"
254	1847	0.0218	44.5	0.45	0.31	"
255	1847	0.0209	37.7	0.4	0.27	"
256	2123	0.0238	18.3	<0.1	0.16	"
257	2115	0.0249	25.8	0.1	0.18	"
258	2074	0.0250	27.7	0.1	0.19	"
259	2315	0.0261	5.7	0.0	0.05	"
260	2422	0.0266	2.8	0.0	<0.02	"

Table 3-2 Individual Benzene Shock Data (cont.)

RUN	T_5(K)	$p(C_6H_6)$(atm)[a]	Soot Yield(%)	Δt_i(msec)	$-dI/dt(msec^{-1})$	$f_m\left(\frac{\text{moles benzene}}{\text{mole argon}}\right)$
272	2032	0.0252	28.9	0.15	0.20	0.0027
273	1822	0.0211	40.4	0.6	0.27	"
274	2021	0.0238	27.1	0.15	0.18	"
275	2003	0.0246	33.7	0.15	0.23	"
276	2021	0.0249	31.0	0.15	0.23	"
297	1870	0.1057	17.3	0.3	0.43	0.0130
298	1979	0.1163	17.4	0.1	0.47	"
299	2149	0.1218	19.4	0.05	0.47	"
300	2198	0.1186	19.5	0.05	0.46	"
301	1805	0.1083	15.8	0.4	0.43	"
302	1738	0.1092	13.2	0.5	0.42	"
314	1755	0.1041	20.5	0.55	0.57	"
318	2236	0.1218	29.9	0.0	0.84	"
319	1700	0.1135	16.5	0.9	0.58	"

[a]Partial pressure behind the reflected shock.

4.0 DISCUSSION OF RESULTS

In the previous chapter, results from an optical study of the soot formation from benzene pyrolysis were presented as they related to soot yield, kinetics, and solid and gaseous product characteristics. These results are now compared with those of similar studies, and an interpretation is presented of how these findings help clarify the mechanism of soot formation from aromatic molecule pyrolysis.

4.1 Adoption of a Mechanism

As explained in Chapter 1, there is no general, unifying theory which outlines the process of soot formation. Many mechanisms have been proposed, but it is probable that there is no single mechanism that adequately describes soot formation under all conditions. This can, in fact, be inferred from the debate that now rages among experts in the combustion field. Recently, however, a mechanism involving free radical polymerization has been proposed which seems to satisfactorily explain qualitatively the soot yields from the pyrolysis of aromatics. Fragmentation of the aromatic compound is predicted to occur, producing a pool of free radical species which combine with the intact ring structures to form large gas phase molecules, eventually leading to soot or polycyclic organic material. In the case of the benzene ring, the simplest kind of fragmentation would produce a hydrogen atom (C-H bonding energy = 112 kcal/mole) and a phenyl radical. As the temperature increases, fragmentation of the ring occurs, and these radical fragments may combine with cyclic radicals repeatedly to form large polycyclic molecules which resemble that polybenzoid structure thought to be soot-like. The presence of styrene in post-shock gases as reported by Vaughn[32] suggests that dehydrogenation, coupled with ring

fragmentation, does indeed take place. Figure 4-1 shows a mechanism proposed by Bittner and Howard[2] involving ring fragments and cyclic radicals (the existence of any of the participating molecules was inferred from their presence as stable gaseous products). From the present experiment and those of others,[13,33] it is manifest that at extremely high temperatures (>2400 K), very little soot results, thus one might infer that extensive fragmentation is detrimental to the formation of soot.

However, it is more proper to say that, based upon the benzene decomposition work of Vaughn and Bittner and the results of this research, both intact rings and ring fragments (in proper relative quantities) are required to form large yields of soot in short residence times. This hypothesis envisions that both ring fragmentation and intact ring structure are necessary for soot formation, and not that a distinctly dual path mechanism proposed by Graham, et al.,[13] actually exists (Chapter 1). Peculiarities exhibited by the results in this study will be used to support this hypothesis. Irregularities arise, however, and they will be explained or discounted as they surface in a discussion of the results in the sections to follow.

4.2 The Formation of Soot

Well over 200 shock experiments were performed with benzene/argon and toluene/argon mixtures. Results relating dwell time, temperature, and initial aromatic concentration to the fractional soot yield from benzene pyrolysis may be found in Section 3.1. The effect of temperature on soot production from toluene pyrolysis is also presented in that section.

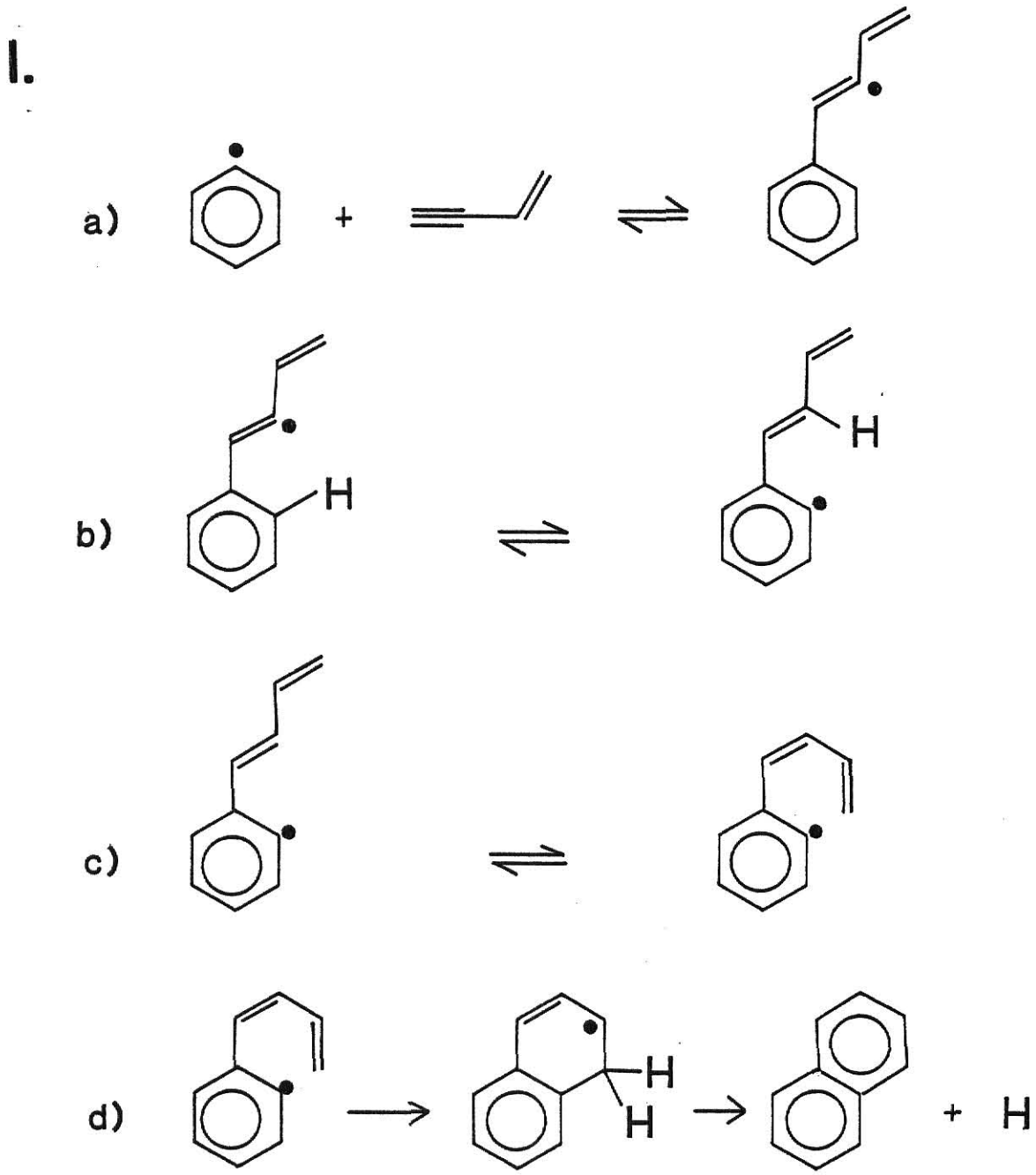

Fig. 4-1. Mechanism of benzene conversion to higher aromatics as proposed by Bittner and Howard.[2]

II.

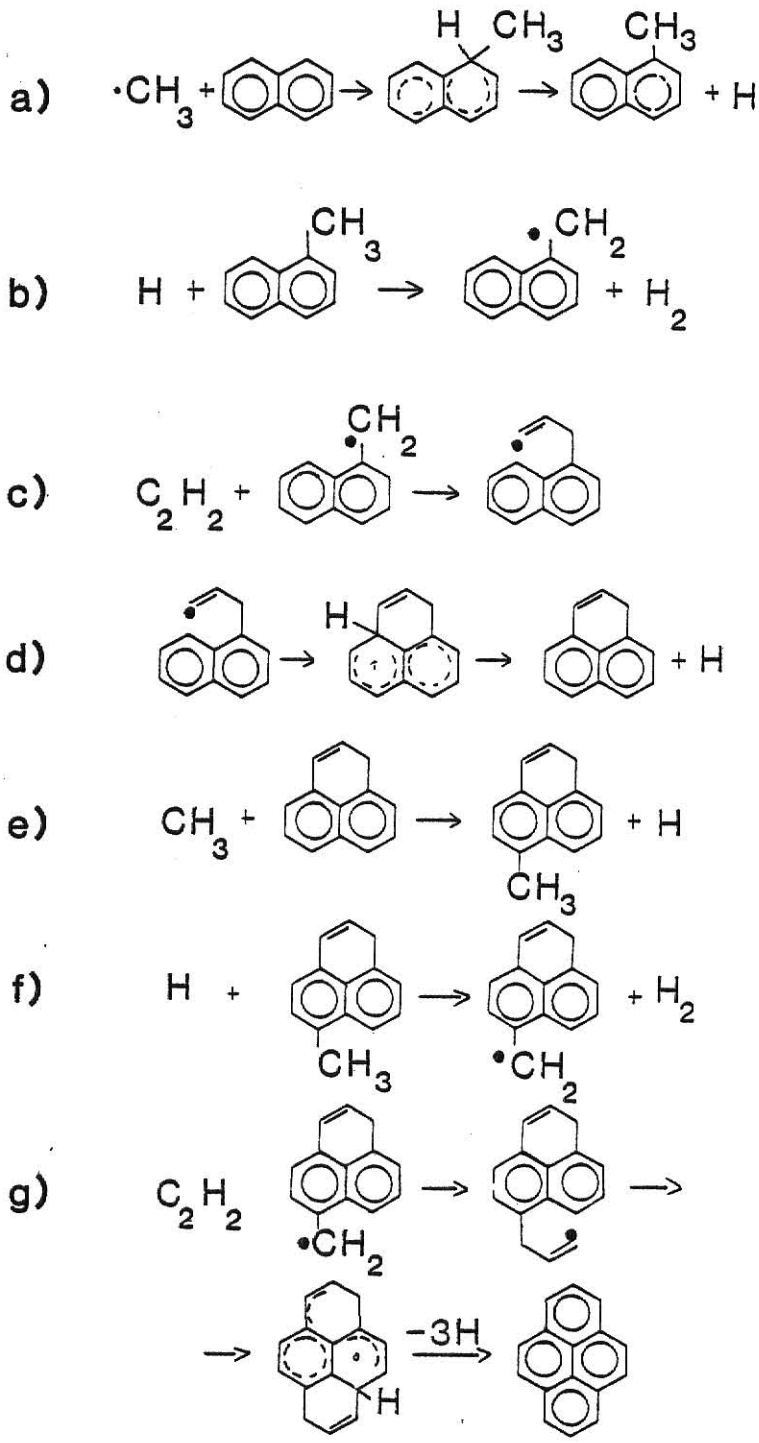

Fig. 4-1. Mechanism of conversion of benzene to higher aromatics as proposed by Bittner and Howard[2] (continued).

4.2.1 Dwell Time Effects

By incrementally decreasing the length of the driver section, the dwell, or residence time of a shock experiment was varied. Plotted in Fig 3-5 is soot yield at 2.5 msec versus dwell time at a constant temperature for two reactant concentrations ($[C]_5 = 4.93 \times 10^{17}$ and 2.31×10^{18} ml^{-1}). As can be seen from the figure, shortening of the dwell time results in smaller soot yields at both concentrations. Since it is seen from Fig. 3-19 that particle size is fairly constant over the range of dwell times, fewer, and not smaller particles must result when the dwell time is decreased. At these temperatures (1680 - 1920 K), 0.3 to 1.0 msec were required before soot was initially detected. Thus, since measureable soot was formed from dwell times less than 0.1 msec during the cooling period, reactions leading to particle nucleation and growth must not require sustained high pressure and temperature.

Vaughn[32] presented data from a similar experiment that showed significant soot formation occurring even at the shortest dwell times at similar concentrations and temperatures. Results from the present optical study appear to parallel those of Vaughn in this regard, though additional data would be helpful. Vaughn concluded that the reactions leading to soot formation are of low activation energy, as are free radical reactions. Activation energies calculated from real time analysis in the present experiment (discussed in Section 4.4) are at $[C]_5 < 5 \times 10^{17}$ ml^{-1}, much higher than those characteristic of free radical reactions. Thus, it is not likely that reactions leading to soot formation are predominately free radical in nature.

4.2.2 Temperature Effects

Soot first appeared when benzene/argon mixtures (mole fraction $f_m \leq 0.0027$, $[C]_5 \leq 5 \times 10^{17}$ ml^{-1}) were pyrolyzed at a temperature near 1500 K for 2.5 msec. At this residence time, sufficient dehydrogenation and/or fragmentation of the benzene molecule occurred producing adequate soot to be detected optically. Acetylene, which is produced by ring fragmentation, first appears at this temperature (see Section 3.2), so one can infer that some ring rupture is necessary for the efficient production of soot. Not enough data were collected at the high concentration ($[C]_5 = 2.31 \times 10^{18}$, $f_m = 0.013$) to determine the minimum temperature at which soot would first be detected.

As the temperature is increased from 1500 to 1700 K, fractional soot yields increase; more acetylene is present in the product gas, and thus more ring fragmentation is occurring. At 1800 K, maximum soot yields are attained for $[C]_5 = 5 \times 10^{17}$ ml^{-1}. It is possible that at these conditions (low concentrations, $P_5 = 8$ atm, $T_5 = 1800$ K) the ideal ratio of noncyclic fragments to cyclic radicals as reaction intermediates exists. As the temperature is further increased, the soot yield tends toward zero, at least for low concentrations. This reduction in soot must be prompted by extensive fragmentation of the ring at high temperatures.

When comparing soot yields above 2100 K for differing carbon atom concentrations, one observes that the highest concentration exhibits the highest yields. Graham, et al.[13] showed from acetylene studies that at high temperatures ($T_5 > 1850$ K), even small radicals such as C_2H can combine to form soot; however this process is concentration dependent

(an increase in concentration will increase soot yields, see Chapter 1). Similarly, if extensive ring fragmentation of benzene is occurring at high temperatures, increasing fractional soot yields should accompany an increase in carbon atom concentration. This was, in fact, observed at temperatures greater than 2100 K for the three concentrations tested. Even when comparing toluene yields, (Figs. 3-3 and 3-4), we observe results that are similar to those of benzene and those reported for acetylene.

At the highest carbon atom concentration studied ($[C]_5 = 2.31 \times 10^{18}$ ml^{-1}), soot yields continued to increase with temperature (Vaughn also reported this trend at lower concentrations). Greater yields at $T_5 > 2100$ K were seen, as mentioned above. At lower temperatures, soot yields were significantly lower than at the lower concentrations. No product gas analysis was performed for these high concentration runs to see if some stable gas phase molecule exists as a more favorable reaction product. It is possible that terminating radical reactions leading to the formation of such alternative products are prevalent under these conditions.

An experiment at $T_5 = 2236$ K using the high concentration ($[C]_5 = 2.31 \times 10^{18}$ ml^{-1}) requires special comment. The oscillogram from this shock showed that the laser beam transmission decreased so fast as to challenge the minimum response time of the RC filtering circuit (see Appendix B). Indeed, a greater amount of soot was being formed under these conditions than in any other experiment conducted. It is not clear to what extent the inadequate response time of the circuit interfered with the transmission measurement; however, it is clear that

analysis of the trace after integration by the circuit would result in a yield less than that which actually occurred. Therefore this yield (Fig. 3-2) is low by an unknown amount. Because of much smaller rates of soot formation in all other experiments, such uncertainty does not exist.

When soot yield versus temperature plots are compared to the gravimetrically-determined results of Vaughn (see Fig. 4-2), we observe obvious differences especially in the overall trend. Vaughn's analysis did not discriminate between soot and polycyclic organic material adsorbed on the particles and liners. He reasoned that decreases in soot yield observed optically could be explained by considering the fact that the optical yields were for soot formation 2.5 msec after arrival of the shock wave, whereas the gravimetric yields, which continuously increased with temperature, were determined after the reaction had been quenched by the rarefaction fan. In essence, Vaughn proposed that much of the soot at temperatures above 1800 K is formed during the cooling period. Furthermore, since soot continued to settle on the liner for up to sixteen hours after the experiment, while only a few minutes were necessary for settling after lower temperature shocks, it appears that much of the chaining to form large soot agglomerates must be occurring long after the experiments at high temperatures.

In this experiment, soot yield from aromatic pyrolysis were qualitatively similar to those reported by Graham, et al.[13] and Wang, et al.[33] at temperatures greater than about 1900 K and for carbon atom concentrations less than 5×10^{17} ml^{-1}. Cleaning the inside of the experimental section several minutes after completing each shock allowed

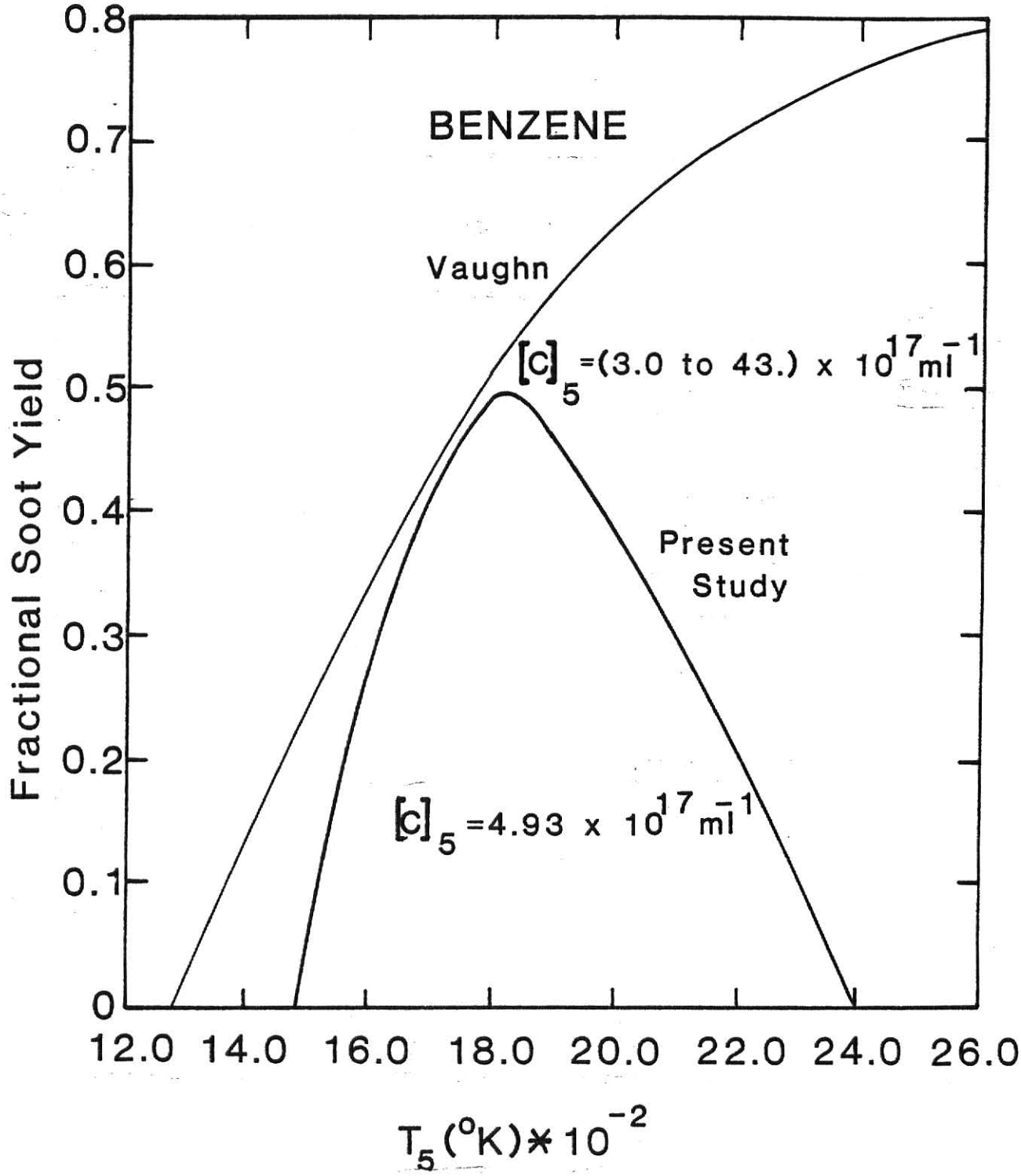

Fig. 4-2. Comparison of soot yields versus temperature from benzene, as determined optically in this study and gravimetrically by Vaughn.[32]

a subjective estimate of the amount of soot formed. These estimates seemed to agree well with the results from the optical analysis. After a high temperature run, where little soot was observed 2.5 msec after passage of the reflected shock wave, a correspondingly sparse amount of soot was wiped from the inside of the tube. Evaluation such as this depends on the tendency of the soot to coagulate into large enough aggregates to settle out quickly. Specifically, sluggish settling requires either that the particles are smaller or their character be changed so that they do not chain as readily. Thus, waiting long periods for the soot to settle (as Vaughn did) would be the only way to detect such phenomena. Unfortunately, the particle sizes determined from the microscopic examination of the soot generated in this experiment (see Section 4.5) do not show great variance with temperature, and as chaining appeared uniform, the reason for the disagreement between the soot yields of this experiment and those of Vaughn remains unsettled at this point.

Toluene shocks were completed to compare 1) soot yields with those resulting from benzene pyrolysis; and 2) with results from recent experiments by Wang, et al..[33] It may be seen by comparing Figs. 3-1, 3-2 with 3-3 and 3-4 that, while trends are similar at $[C]_5 > 8 \times 10^{17}$ ml^{-1}, toluene exhibits much higher soot yields upon pyrolysis than does benzene. Also notable is the fact that soot is detected at cooler temperatures from toluene ($T \approx 1450$ K) than from benzene. The importance of formation of a benzyl radical in soot formation from toluene pyrolysis is emphasized by Scully and Davies.[24] The bond strength of the C-H bond in $C_6H_6CH_2$-H is less than a C-H bond in benzene, and thus loss of this methyl hydrogen

is possible at lower temperatures. This probable production of benzyl radicals at cooler temperatures perhaps explains why toluene forms soot more readily at these temperatures than does benzene.

A comparative plot of the soot yields of this study with those of Wang, et al.[33] and Graham, et al.[13] is shown in Fig. 4-3. Note that the qualitative behavoir of the data sets from Wang and this study is similar, but the maximum yields observed by Wang are significantly greater. This difference is further magnified when one considers that Wang, and also Graham, used a refractive index which yielded $F_a(m,\lambda)$ values of 0.049 and 0.042 respectively, compared to 0.028 used in this study. Had Wang or Graham chosen the refractive index used here, they would have calculated peak yields far in excess of 100 percent. The amount of soot produced in this present study was evidently much less than that in these previous experiments. The dependence of soot yields on the refractive index in optical studies of this type becomes apparent when results like these are compared. A mass ballance of soot, benzene, and acetylene in this experiment indicates that closure to within ± 10% was achieved in a temperature range about 1800 K. Therefore, the soot yields could not have been higher, but may have been still lower if some hydrocarbon species are not accounted for.

4.3 Gaseous Product Analysis

Gaseous product analysis was completed chromatographically, and the resulting amounts of acetylene and remaining benzene are plotted as function of temperature for $[C]_5 > 5 \times 10^{17}$ ml^{-1} in Fig. 3-6. An increase in the post-shock acetylene concentration with temperature

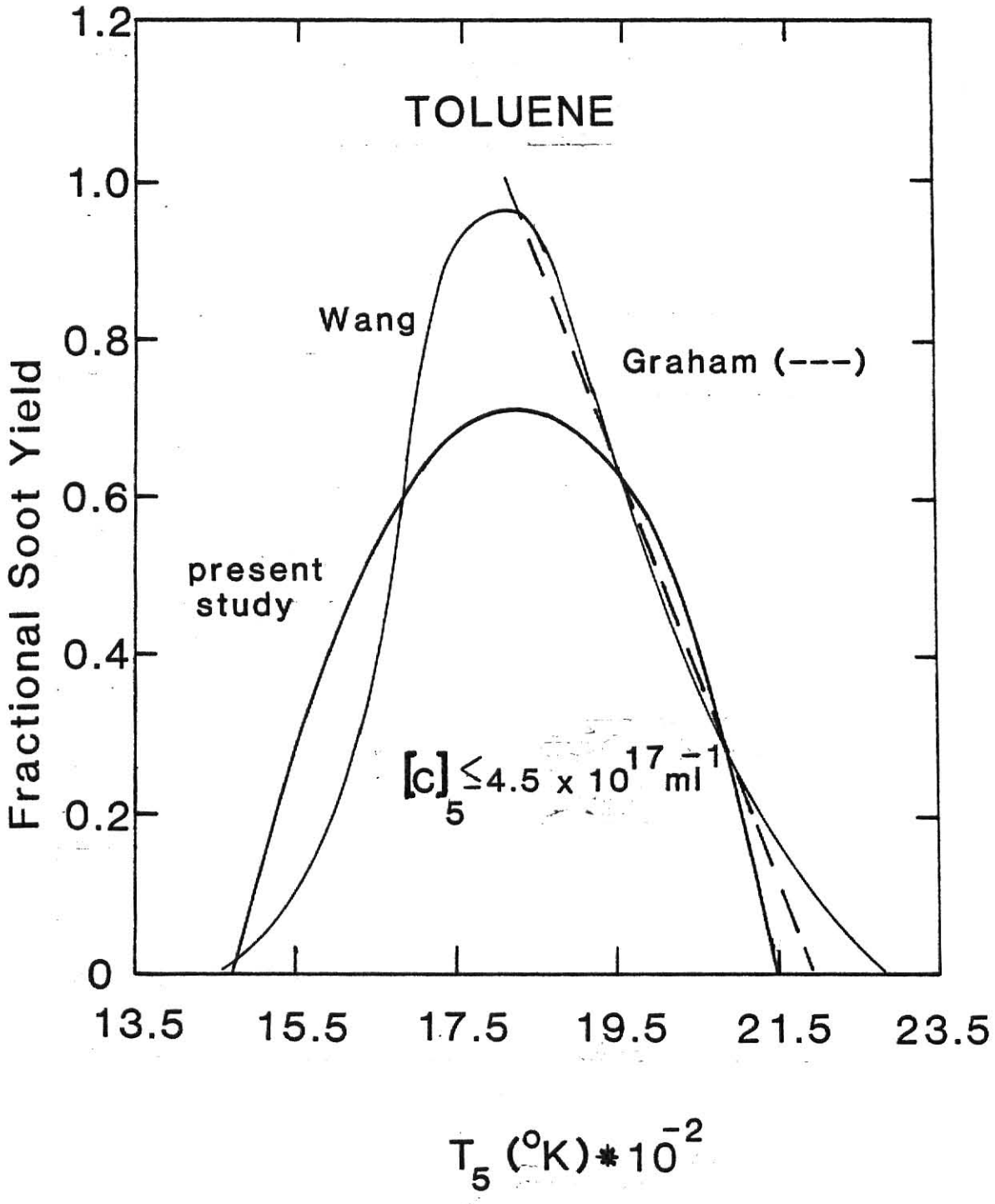

Fig. 4-3. Comparison of soot yields versus temperature from toluene, as determined optically by Wang, et al.[33], Graham, et al.[13], and this study.

indicates that ring fragmentation is becoming more prevalent. As might be expected, the amount of benzene decreases with increasing temperature, but note that it does not drop to zero even at temperatures as hot as 2100 K. This means that either less than 100 percent the decomposition is occurring at this point, or some fragments are reforming to stable benzene as a reaction product. From mass spectrographic analysis of gaseous products from isotopically labeled benzene pyrolysis, Vaughn[32] showed this latter process to occur, although the reformed benzene was always less than 5 percent of the original benzene.

4.4 Reaction Kinetics

The formation of a mature soot particle during hydrocarbon oxidation or pyrolysis is believed to occur in three, possibly distinct phases: 1) nucleation, where solid particles arise from large gas phase molcules that have reached a critical size; 2) surface growth, involving the attachment of gas phase species to the surface of the particle and their incorporation into the particulate phase; and 3) coagulation of the smaller particles. Once nucleation occurs, surface growth adds to the volume of each particle while the total number of particles in the reaction zone remains unchanged. The gas phase species responsible for this growth are necessarily products of the pyrolysis, and most likely include a number of hydrocarbons. Since, as mentioned in Chapter 1, the C/H ratio increases from 1 to about 8 as a soot particle matures, one might suspect these additional molecules to be highly unsaturated or aromatic in nature. Coagulation is the process whereby spherical

particles collide and fuse together to give a larger spherical particle. During this process, the particle number density decreases while the soot volume fraction, f_v, is constant. Typically, it is found that particles collide in this manner until their diameters reach a few tens of nanometers, beyond which chain formation results.[23] If, after nucleation, pure coagulation is occurring, the rate of decrease in particle number could be easily calculated from collision theory. Since laser transmission traces in this study show that f_v is not constant over the reaction time, surface reactions, in which the volume of the solid phase increases, must also be taking place. Consequently, extinction rate data from this experiment may be used to describe the particle growth process as a whole, between surface growth and coagulation.

The rate of increase in extinction was determined for all benzene shocks, and these values used to find the activation energy for soot particle growth. As reported in Section 3.3, this value was found to be 21.8 kcal/mole assuming a first order reaction with respect to benzene concentration, or 17.0 kcal/mole assuming second order. When rate data are plotted, the value of n which yields the best linear fit is the order for the reaction. Although the fit to the data in Figs. 3-7 and 3-8 is not good, under the limited analysis performed here, the particle growth process is better described by first order kinetics. It is interesting to note from Fig. 3-9 that for the highest concentration studied, the process(es) is characterized by a very low activation

energy, indicative of either free radical reactions or a physically-controlled growth process. This difference in behavior compared to the results at lower concentration, especially when noting the marked difference in soot yields, suggests that post-nucleation growth may be quite complex.

Further complicating the characterization of this process is the fact that only data collected below temperatures of 1750 K (for $[C]_5 < 5 \times 10^{17}$ ml^{-1}) could be used, since soot yields began to level off and decrease above this temperature. This behavior further suggests the existence of more than one growth mechanism. If growth species could be divided up into two groups: those of large and small molecular weight (eg., ringed and fragmented hydrocarbons), one can postulate that surface addition of the large molecules, which are preserved at lower temperatures, results in more rapidly growing particles. At temperatures above 1750 K, where extensive fragmentation increasingly leaves behind small gas phase molecules, the accumulation of mass via surface reaction may proceed much more slowly, and thus decreasing yield below this temperaure is the outcome. This theory is further substantiated when one considers the soot yields of this study compared with those of Vaughn (Fig. 4-2). Remembering that Vaughn determined yields long after shock heating, the fact that soot yields compare well for both studies for $T_5 < 1800$ K implies that soot formation and thus surface growth, must have been complete in 2.5 msec. At temperatures greater than 1800 K, Vaughn found that more soot was produced than was detected after 2.5 msec by this study. If surface reactions proceed more slowly at these temperatures due to the prevalence of smaller gas-phase radicals, then a great deal of soot may be formed in the cooling period.

The nucleation process is most closely related to the induction time, which is extracted from optical traces. These values may be used to calculate an overall activation energy for the nucleation process (see Section 3.3). In addition, qualitative analysis may be performed on the graphs shown in Figs. 3-10 thru 3-12.

As shown in Fig. 3-10, the dwell time varies little with initial benzene concentration over the range studied ($0.0012 \leq f_m \leq 0.0130$). A fractional-order dependence appears justified from comparing zero, one-half, and first order reaction linear fits. Correlation coefficients, as listed in Section 3.3, for lines through these data are highest for n=0 and n=½. Fussey, et al.[8] in a study of induction times from shock-induced acetylene pyrolysis, obtained a fractional reaction order of 0.41 by this iterative process. Such an analysis was not conducted as part of this work; however, it is clear that for benzene, the nucleation process appears to be of order $n \leq ½$. Because of the similarity of these results with those of Fussey for acetylene, it seems plausible to suggest that a comparable mechanism is involved in soot nucleation from both fuels. In fact, an activation energy of 32.7 kcal/mole may be calculated from his data (C_2H_2 mole fraction of 0.02), which is near that calculated below for benzene with $f_m = 0.013$.

Assuming a zero order process, an activation energy of 27.6 kcal/mole was obtained. When analyzing each data group individually for $n = ½$, activation energies of 26.9, 26.9, and 32.1 kcal/mole were obtained for $[C]_5 = 2.75$, 4.93, and 23.1×10^{17} ml^{-1}, respectively. Had more data been taken at the highest concentration, perhaps a value nearer 27 kcal/mole would have resulted.

Another important result from the induction time analysis, aside from the apparent low reaction order, is the monotonic behavior of the data over the temperature range, as shown in Figs. 3-10 thru 3-12. In contradiction to the maximum observed in the yield of soot, such behavior suggests that a single mechanism is involved in the nucleation of soot. In results presented previously, multiple growth mechanisms were postulated to be present in post-nucleation particle growth. It may be concluded, as Palmer and Cullis[21] suggested, that reactions leading to soot nucleation are different than those involved in subsequent growth.

4.5 The Soot Particulate

The soot which formed during benzene pyrolysis was filtered from product gases and examined under a trasmission electron microscope. Enlarged micrographs of soot agglomerates at varying magnification are presented in Figs. 3-13 through 3-17. Variance of the measured particle diameters with temperature, reaction dwell time, and initial benzene concentration are plotted in Figs. 3-18 to 3-20.

From Figs. 3-13 to 3-15, one can see that the collected particles are roughly spherical in shape, and tend to assemble in chains or clusters. The three-dimensional nature of the agglomerates is exemplified by the areas of increased opacity caused by particles stacking in the vertical plane. There are few groupings of less than 50 particles. In most cases, individual particles can be distinguished, suggesting that chain formation occurs after particle growth is complete. Were this not case, chains of particles would appear smeared

together from interstitial surface growth. The ability to differentiate particles allowed size measurements to be performed.

There were two shock experiments from which soot was collected that yielded particles which were undifferentiable. The filamentous, coral-like structure of this soot is seen in Fig. 3-16. One could postulate that chaining of immature particles followed by continued surface growth (as mentioned above) would yield such a result. Conditions necessary for the formation of this type of soot could not be acertained because of the inability to deliberately produce it; however, the chaining process would have had to proceed during a period where a substantial concentration of gas phase hydrocarbons critical to surface growth still existed.

Particle size results obtained under varying conditions are summarized in Table 3-1. An overall average particle diameter of 18.6 nm compares well with sizes reported in the literature.[3,32] A typical standard deviation associated with each measurement is about ± 15 percent. The narrower size distribution of ± 5 percent reported by Vaughn[32] was rarely observed for soot from these experiments. The breadth of the size distribtuion may be related to the time interval between the first and last nucleation, if the description of crystal nucleation by Dunning[6] is applicable in the present case.

Early in the process of nucleation, molecules of some hydrocarbon X are present in a solvent (argon, in this case) with an infinite solubility. As the numbers of X increase, the solution becomes supersaturated with respect to X and clusters containing various numbers of

X arise. These clusters or embryos build up until they may be considered as minute crystals. Certain embryos having a critical size will have a solubility equal to the concentration, so that those which are smaller have a higher solubility, and will thus dissolve; those larger will tend to grow. Once an embryo reaches, by fluctuations, this critical size, it can add another molecule of X and proceed to grow relatively freely into a macroscopic crystal. Such critical embryos are called "nuclei." The rate of nucleation will be greatest at the time which nuclei are first formed, and will decrease rapidly. Not only will the first-born particles be the most numerous, but at all times they will also be the largest crystals, since they have been exposed to growth conditions longest.[6]

The standard deviation associated with each particle diameter presented in Table 3-1 may be reflective of the time frame over which the nucleation process occurred. To make an inference such as this, one must assume that either a limiting number of species are available for surface addition so that late-nucleating embryos will experience famine, or that a rarefaction fan causes a quick end to surface growth.

The response of particle size to temperature is shown in Fig. 3-18 for a dwell time of 2.5 msec and a carbon atom concentration of 4.93×10^{17} ml^{-1} ($f_m \simeq 0.0025$). The particle diameters increased from 19 to 20 nm over a temperature range of 1500 to 2300 K. If one recalls how soot yield varied with temperature, it is seen from this figure (if the highest point is ignored) that particle size may depend on temperature

in a similar fashion. Additional data are necessary to ascertain to what extent the yields are influenced by particle size.

Particle size variance with reaction dwell time is shown in Fig. 3-19 for carbon atom concentrations of 4.93×10^{17} ml^{-1} (at 1690 and 1860 K) and 2.31×10^{18} ml^{-1} (at 1730 K). It is evident from the two sets of data that the particle size does not increase with dwell time (it inexplicably appears to decrease at the higher concentration). This means that soot particles reach their limiting size even at very short reaction times. Thus, growth processes, and in some cases nucleation, are occurring after passage of the rarefaction fan in the cooling period. Recall from Fig. 3-5 that soot yield decreases with decreasing dwell time. Since the particles are not smaller at these short times, reduced yields demand that fewer mature particles were formed. This infers that either few molecular embryos actually nucleate, or that coagulation of young particles reduces their number.

As can be seen from Fig. 3-20, particle size appears to increase with the initial benzene concentration. The two points on this plot result from averaging particle sizes over all dwell times and temperatures for the two concentrations tested. When considering the soot yield results for these concentrations at moderate temperatures (approx. 1750 K), the fact that the lower concentration exhibited higher yields after 2.5 msec indicates that more particles were produced (relative to the number of benzene molecules initially present) than at the higher concentration.

5.0 SUMMARY

Soot produced from the shock-induced pyrolysis of benzene/argon mixtures was observed optically in real time. Fractional soot yields and reaction kinetic parameters were determined from these data over a range of conditions. Sampling of the post-shock gas mixture allowed gas chromatographic analysis of stable gases and electron microscopic measurement of the filtered soot. From the analyses, several conclusions regarding soot formation from aromatic hydrocarbons were drawn.

The soot yield from benzene pyrolysis was seen to be considerably less than 100 percent over the concentration range ($0.0012 \leq f_m \leq 0.0130$) and temperature range (1450 to 2400 K) studied, contrary to earlier optical studies of soot formation.[13,33] At carbon atom concentrations less than 5×10^{17} ml^{-1} (behind the reflected shock wave), yields increased from below detectable limits at 1500 K to near 50% at 1800 K, and then decreased to zero at temperatures above 2100 K. At temperatures greater than 2100 K, the reactant mixture richest in aromatic content produced a greater fractional soot yield; at cooler temperatures, low concentrations yielded higher conversions. At the highest concentration tested (2.31×10^{18} ml^{-1}), the soot yield increased continuously with temperature. Soot yields from another aromatic compound, toluene, were compared to those from benzene. The qualitative behavior with temperature was similar, but the peak yield from toluene was higher with a fractional conversion of about 70%. No soot was observed in shocks of 2.5 msec dwell time below about 1450 K.

As might be expected, soot yield was seen to decrease with diminishing residence time behind the reflected shock; however, particle size remained relatively constant with this parameter. Thus, shortening of the dwell time results in fewer, not smaller particles, since the mass loading changes, but the particle diameter does not. It is important to note that measureable soot was formed even at dwell times shorter than 0.1 msec, indicating that particle nucleation and growth processes continue during the quench.

From induction time measurements, results regarding soot nucleation were obtained. Particle nucleation was seen to be a low order chemical process ($n \leq \frac{1}{2}$) with respect to benzene concentration, with an activation energy of about 27 kcal/mole. The rate of nucleation was observed to increase monotonically with temperature over the range studied; thus, the process was not hindered, and was possibly aided, by extensive ring fragmentation.

Particle growth analysis was performed on the rates of increase of extinction. These rates were observed to increase with temperature to about 1750 K, and beyond that point decreased. An activation energy for particle growth below this temperature was found to be 21.8 kcal/mole for a first order reaction and carbon atom concentrations less than 5×10^{17} ml^{-1}. At a higher concentration (2.31×10^{18} ml^{-1}), a very low activation energy was calculated (< 1 kcal/mole), indicating that free radical reactions or physical processes are responsible for particle growth.

Gas analysis was performed on two reaction products, acetylene and benzene, and their appearance with temperature plotted. Benzene is seen

to diminish as a reaction product with temperature due to the advancement of ring fragmentation and addition of these smaller hydrocarbons to rings yielding larger aromatic compounds. From a study utilizing isotopic labeling of the benzene, Vaughn determined that some of the product benzene results from reformation of ring fragments. Acetylene yields increased with temperature from 1500 K and approached 45% of the initial benzene concentration (on a mass basis) at 2000 K.

Soot particles filtered from the product stream were measured from micrographs produced by a transmission electron microscope. The particle diameters ranged from 13 to 25 nm. Particle size as a function of temperature, dwell time, and initial benzene concentration was studied, and it was concluded that, in general, size varies little with these parameters (additional data would have been helpful in a more precise characterization).

When considering the results as a whole, it was concluded that particle nucleation, involving probably a single mechanism of low reaction order, is a simpler and distinctly different process from particle growth. Considerable evidence exists which supports the theory that particle surface growth occurs more slowly at temperatures above 1800 K than below this temperature. In the absence of definitive data, it may be assumed that higher concentrations of intact ring growth species at low temperatures and their comparative absence at higher temperatures is responsible for this behavior. Excessive ring fragmentation appears to be more detrimental to high rates of surface growth than to nucleation.

If alternate fuels are to become a major energy source without undue environmental degradation, more knowledge of the soot formation

from aromatic hydrocarbons is necessary. Infrared analysis of in situ gas species may reveal the identity of gas phase reaction intermediates which lead to large soot precursor molecules. Fourier transform infrared analysis may allow investigation of gas phase reaction species present during particle growth by removing the blackbody radiative emission that heretofore has frustrated infrared analysis of particle-laden gases. The continuation of particle size measurements and product gas analysis similar to, but more extensive than that presented in this work, would also contribute significally to our understanding of the soot formation process

6.0 LITERATURE CITED

1. J.D. Bittner and J.B. Howard,"Role of Aromatics in Soot Formation," Progress in Astronautics and Aeronautics 62, 335(1978).
2. J.D. Bittner and J.B. Howard, Eighteenth Symposium (International) on Combustion (The Combustion Institute, Pittsburg, in press).
3. P.A. Bonczyk, "Measurement of Particle Size by In-Situ Laser-Optical Methods: A Critical Evaluation Applied to Fuel-Pyrolized Carbon," Gas Turbine and Fuels Technology,edited by E.K. Bostress (ASME, New York, 1977).
4. G.W. Breipohl, M.S. Thesis, Kansas State University, 1979.
5. W.H. Dalzell and A.F. Sarofim, "Optical Constants of Soot and Their Application to Heat Flux Calculations," Transactions of the ASME Journal of Heat Transfer 91, 100(1969).
6. W.J. Dunning, "Ripening and Ageing Processes in Precipitates," Particle Growth in Suspensions, Proc. Soc. Chem. Ind., p. 3(1972).
7. F.E. Ferguson, J. Chem. Phys. 23, 2085(1955).
8. D.E. Fussey, A.J. Gasling, and D. Lampard, "A Shock Tube Study of Induction Times in the Formation of Carbon Particles by the Pyrolysis of the C_2 Hydrocarbons," Combustion and Flame 32, 181-192(1978).
9. A.G. Gaydon, Spectroscopy and Combustion Theory, 2nd Ed.(Chapman and Hall, London, 1948).
10. A.G. Gaydon and I.R. Hurle, The Shock Tube in High Temperature Chemical Physics (Reinhold, New York, 1963).
11. H.S. Glick, W. Squire, and A. Hertzberg, Fifth Symposium (International) on Combustion (Reinhold, New York, 1955), p.393.
12. D.M. Golden, "Pyrolysis and Oxidation of Aromatic Compounds," Progress in Astronautics and Aeronautics 62, 233(1978).
13. S.C. Graham, J.B. Homer, and J.L.J. Rosenfeld, "The Formation and Coagulation of Soot Aerosols Generated by the Pyrolysis of Aromatic Hydrocarbons," Proc. R. Soc. Lond. A.344, 259-285(1975).
14. W.J. Hooker, "Shock Tube Studies of Acetylene Decomposition," Seventh Symposium (International) on Combustion (Buttersworth, London, 1959), pp. 949-952.
15. M. Kerker, The Scattering of Light and Other Electromagnetic Radiation (Academic Press, N.Y., 1969), pp. 121-2.

16. G.F. Knoll, Radiation Detection and Measurement (John Wiley and Sons, N.Y., 1979), p. 619.
17. J. Lahaye, G. Prado, and J.B. Donnet, Carbon (Pergamon Press, London, 1974), Vol. 12, p. 27.
18. S.C. Lee and C.L. Tien, "Optical Constants of Soot in Hydrocarbon Flames," a manuscript for the Eighteenth Symposium (International) on Combustion (The Combustion Institute, Pittsburg, in press).
19. J.P. Longwell, "Alternate Fuels and Combustion Problems," Progress in Astronautics and Aeronautics 62, 3(1978).
20. P.J. Pagni and S. Bard, "Particulate Volume Fractions in Diffusion Flames," Seventeenth Symposium (International) on Combustion (The Combustion Institute, Pittsburg, 1979), pp. 1017-1027.
21. H.B. Palmer and C.F. Cullis, "The Formation of Carbon from Gases," Chem. and Phys. of Carbon, Vol. 1, 1965.
22. G. Porter, Fourth Symposium (International) on Combustion (The Williams and Wilkens Co., Baltimore, 1953), p. 248.
23. G. Prado and B.S. Haynes, "Soot and PAH Formation in Coal Combustion," Pulverized Coal Combustion: Pollutant Formation and Control, edited by A.F. Sarofim, G.B. Martin, W.S. Laneir, and T.W. Lester, U.S. Government Printing Office, in press.
24. D.B. Scully and R.A. Davies, "Carbon Formation from Aromatic Hydrocarbons," Comb. and Flame 9, 185(1965).
25. W.R. Seeker, M.S. Thesis, Kansas State University, 1976.
26. W.R. Seeker, Ph.D. Dissertation, Kansas State University, 1979.
27. R.D. Smith, Comb. and Flame 35, 179(1979).
28. J.C. Street and A. Thomas, "Soot Formation in Premixed Flames," Fuel 34, 4(1955).
29. A. Streitwieser and C.H. Heathcock, Introduction to Organic Chemistry (Macmillan, N.Y., 1976), p. 569.
30. V.R. Stull and G.N. Plass, "Emissivity of Dispersed Carbon Particles," J. Opt. Soc. Am. 50, No. 2, 121(1959).
31. S. Szydlowski, M.S. Thesis, Kansas State University, 1980.
32. S. Vaughn, Ph.D. Dissertation, Kansas State University, 1980.

33. T. Wang, R.A. Matula, and R.C. Farmer, "Soot Formation from Toluene," 1980 Spring (Central States Section) Combustion Meeting, The Combustion Institute.

34. B.L. Wersborg, Ph.D. Dissertation, Massachusetts Institute of Tech., 1972.

Appendix A. The End Plug

After the completion of several benzene shocks, erratic data indicated that some change in the basic experimental setup was needed. The major difference between the initial setup and that reportedly used by others was the distance between the optical windows and the end wall which terminated the reaction zone (Wang, et al.[33] reported a separation distance of 0.8cm). It became evident that the 8.9 cm separation distance from which soot formation was observed in this experiment was too large. During a typical experiment, the reactant mixture experiences an increase in pressure and temperature which reduces the reactant gas volume to approximately 15% of its original value, compressing it to the last 7-8 cm of the experimental section. Prior to installation of an end plug, only soot that happened to drift into the observation path from this compressed volume attenuated the laser beam.

By securing a 7.0 cm long stainless steel plug on the end flange of the shock tube, the observation point was relocated to within 2.0 cm of the terminus, making the effective length of the experimental section 42.4 cm. A 0.32 cm hole was bored through the plug to facilitate product sampling. Additionally, an O-ring was placed around the plug's perimeter which acted to seal the reaction zone to a volume upstream from the plug face. This ring also aided in uniform shock wave reflection from this face, which was of slightly smaller diameter than the inside of the tube.

The overall effect of the plug's insertion on the laser trace is is shown in Fig. A-1. The top transmission trace shows the erratic

behavior before the plug's use; the bottom trace displays the well behaved behavior. All subsequent shock experiments, and all data reported in this thesis, were recorded with this plug in place.

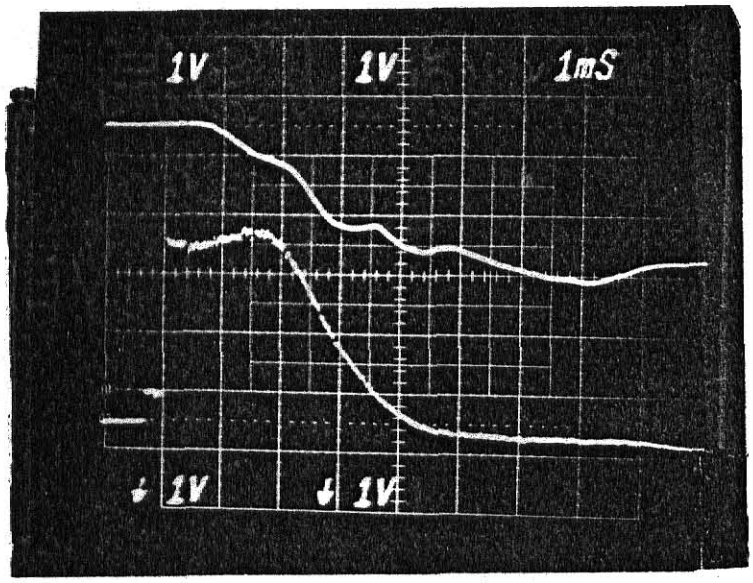

(a)

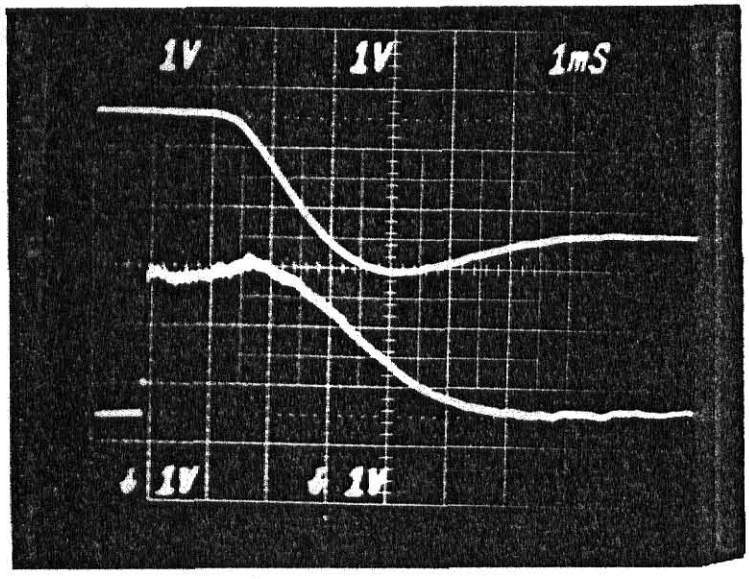

(b)

Fig. A-1. Comparison of laser transmission traces (a)before and (b) after addition of the 7.0 cm end plug.

Appendix B. The Low-pass Filtering Circuit

In electrical circuits, the term "R-C shaping" refers to the use of passive resistor-capacitor networks to carry out the desired alterations in pulse shape. The RC (as opposed to CR) integrating circuit used in this experiment acted as a filter in the higher frequency domain, allowing, ideally all low frequency signals to pass unaltered. If the time constant τ ($\tau = R*C$) is chosen to be sufficiently large. The pulse amplitude may be expressed as[16]

$$E_{out} \simeq \frac{1}{\tau}\int E_{in}\,dt \quad , \qquad (B.1)$$

where E is the potential in volts and t is time; hence, the name "integrator." In the opposite extreme of small time constant, $E_{in} \simeq E_{out}$, and the waveform is passed without change. It was necessary in this experiment to choose a time constant which allowed integration (and thus smoothing) of the noise which was present in the signal, but still allow the low frequency laser transmission output to pass unaltered. By experimenting with differing values of resistance at a fixed capacitance, a time constant of 6.8×10^{-5} sec was found to produce the best overall response. The laser trace was not totally unaltered, however. The response to a square wave input was checked by placing a beam chopper in front of the photomultiplier tube and observing the resulting output. This output, with and without the RC filter, is shown in Fig. B-1.

The minimum response time is about 0.5 msec/V with the circuit in place. This is faster than the minimum response time required for almost all shock experiments. The shortest time was slightly greater than 1.0 msec/V (see Section 4.2 for discussion of an exception). Additionally, experiments run under identical conditions with and without the circuit yielded transmission traces which were nearly identical. The only difference was a greater signal to noise ratio from the filtering circuit. Thus, it was assumed that use of this RC filtering circuit allowed a faithful representation to be made of the temporal response of the laser beam to soot production.

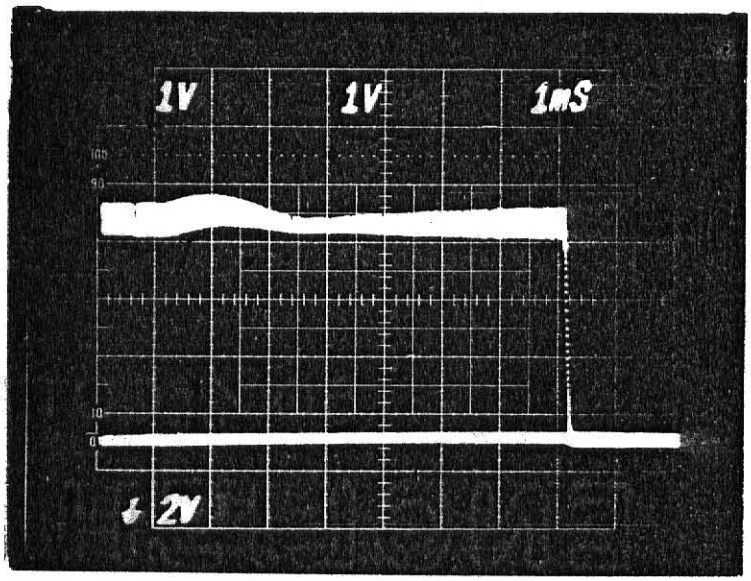

(a)

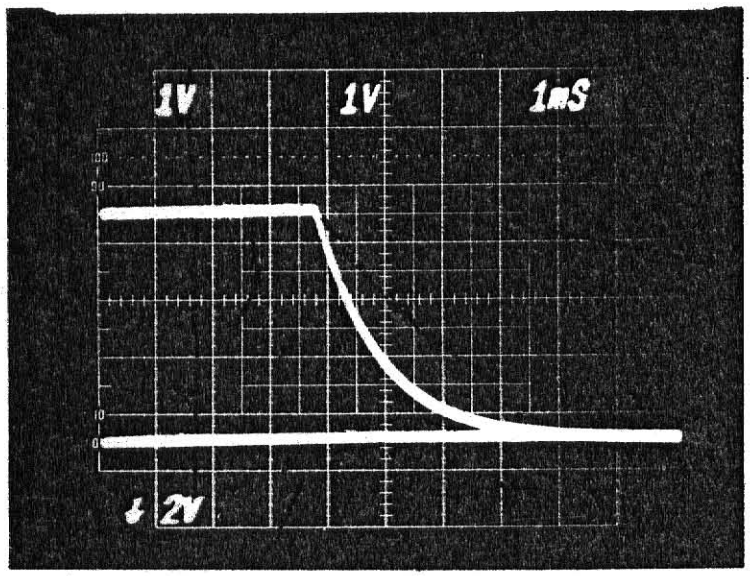

(b)

Fig. B-1. Response of laser detection system to step voltage change (a) before and (b) after addition of RC filtering circuit; $\tau = 6.8 \times 10(-5)$ sec.

Appendix C. Photomultiplier Tube Linearity

An RCA IP28 photomultiplier tube (PMT) was used to convert the transmitted laser light intensity into voltage pulses which could be recorded by the oscilloscope. It was of great importance that the response of this detector be linear with laser intensity. Assurance that this linearity existed was gained by placing a series of neutral density filters in the beam path and recording the voltage output from the oscilloscope. A plot of PMT response versus relative light intensity is shown in Fig. C-1. The data are well correlated by a straight line. The response of this tube was assumed to be linear throughout the testing.

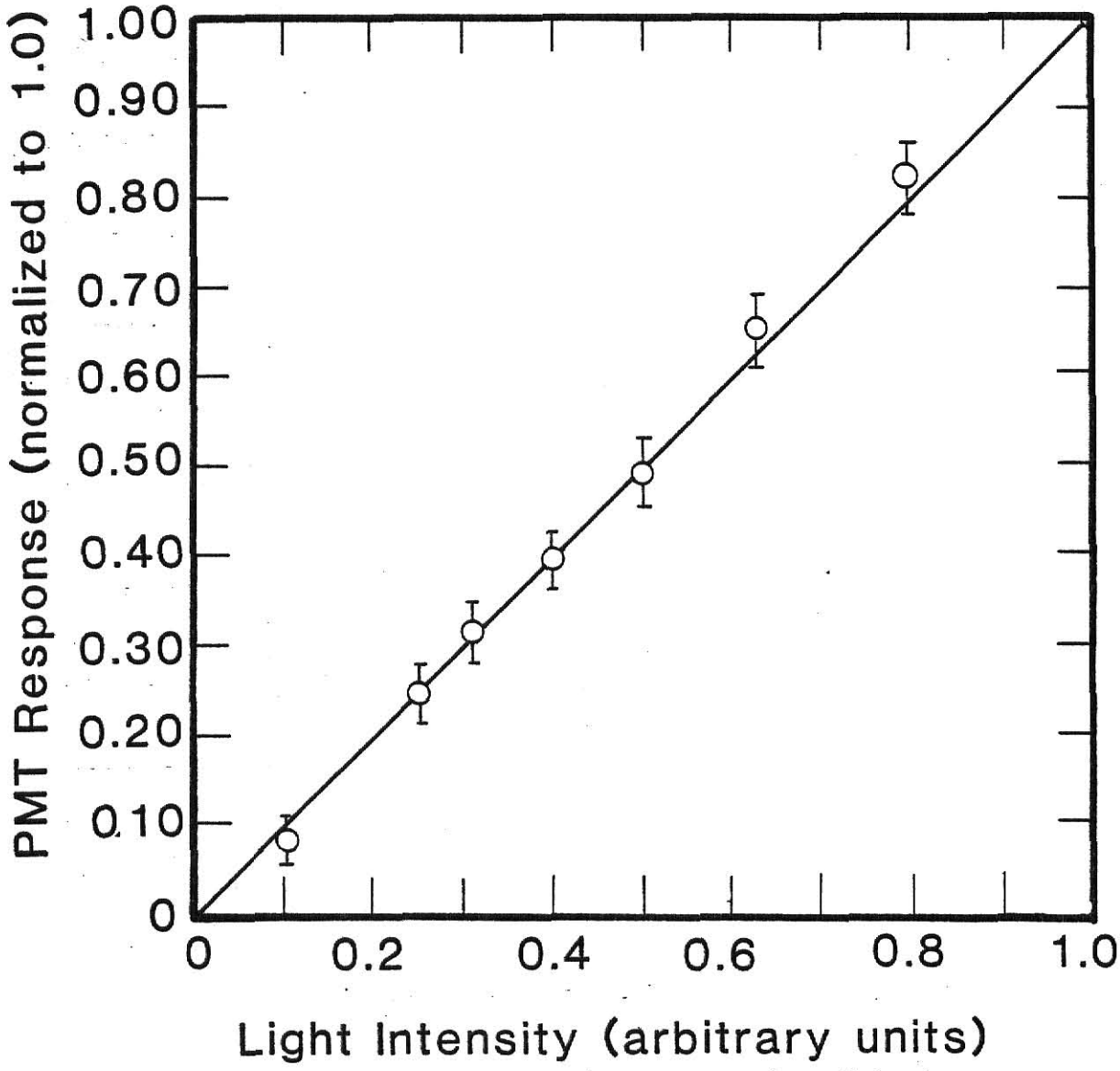

Fig. C-1. Photomultiplier response as a function of relative light intensity.

Appendix D. Toluene Pyrolysis Data

Pyrolysis experiments were performed with toluene/argon mixtures in addition to those performed with benzene/argon. Soot yields were calculated from the toluene data for comparison with those from benzene, but further analyses were not conducted. Presented in Table D-1 are data from the toluene pyrolysis experiments.

Table D-1 Individual Toluene Shock Data

RUN	T_5(K)	$p(C_6H_6)$(atm)[a]	SOOT YIELD(%)	Δt_i(msec)	$-dI/dt$(msec^{-1})	$f_m\left(\frac{\text{moles toluene}}{\text{mole argon}}\right)$
112	1529	0.0135	24.8	1.4	0.25	0.0017
113	1489	0.0122	25.7	1.3	0.22	"
114	1559	0.0126	45.7	1.0	0.29	"
115	1554	0.0126	30.7	1.4	0.30	"
116	1441	0.0132	1.9	2.2	0.04	"
117	1678	0.0140	71.9	0.7	0.37	"
124	1645	0.0130	79.4	0.6	0.35	"
125	1839	0.0149	71.2	0.5	0.34	"
126	1837	0.0146	84.4	0.35	0.33	"
130	1794	0.0151	63.3	0.5	0.30	0.0019
131	1820	0.0154	59.5	0.4	0.28	"
132	1582	0.0119	54.7	0.3	0.25	"
133	2047	0.0162	36.3	0.3	0.20	"
134	2137	0.0164	14.6	0.2	0.10	"
135	1832	0.0140	62.5	0.5	0.30	"
136	2062	0.0169	16.7	0.2	0.10	"
137	1844	0.0147	58.2	0.6	0.33	"
138	1977	0.0163	53.1	0.2	0.24	"
139	1826	0.0144	65.7	0.5	0.29	"
140	1977	0.0160	52.7	0.15	0.25	"
141	2014	0.0161	37.1	0.2	0.20	"
142	1936	0.0152	61.0	0.3	0.25	"

Table D-1 Individual Toluene Shock Data (cont.)

RUN	T_5(K)	$p(C_6H_6)$(atm)[a]	SOOT YIELD(%)	Δt_i(msec)	$-dI/dt$(msec^{-1})	$f_m\left(\frac{\text{moles toluene}}{\text{mole argon}}\right)$
143	1967	0.0156	60.1	0.2	0.25	0.0019
144	1800	0.0136	78.6	0.65	0.32	"
102	1508	0.0284	41.0	0.8	0.40	0.0037
103	1637	0.0321	31.3	0.8	0.43	"
104	1519	0.0280	12.0	1.4	0.26	"
105	1705	0.0310	53.0	0.5	0.46	"
106	1521	0.0256	20.0	1.35	0.35	"
107	1563	0.0270	20.2	1.4	0.38	"
108	1739	0.0308	55.2	0.4	0.46	"
109	1665	0.0289	46.8	0.65	0.46	"
110	1694	0.0298	54.1	0.6	0.46	"
111	1696	0.0286	55.0	0.6	0.46	"
119	1585	0.0241	51.4	0.8	0.43	0.0032
120	1467	0.0205	8.4	1.45	0.20	"
121	1522	0.0208	17.0	1.5	0.30	"
122	1741	0.0251	65.8	0.5	0.45	"
127	1803	0.0257	90.1	0.3	0.47	"
128	1939	0.0264	93.9	0.15	0.55	"
129	1793	0.0243	85.4	0.3	0.50	"
145	1841	0.0270	51.5	0.2	0.40	0.0034
146	1960	0.0290	63.6	0.15	0.44	"
147	2008	0.0300	63.9	0.1	0.44	"

Table D-1 Individual Toluene Shock Data (cont.)

RUN	T_5(K)	$p(C_6H_6)$(atm)[a]	SOOT YIELD(%)	Δt_i(msec)	$-dI/dt(msec^{-1})$	$f_m\left(\frac{\text{moles toluene}}{\text{mole argon}}\right)$
148	1798	0.0249	66.9	0.4	0.42	0.0034
149	1998	0.0298	64.0	0.15	0.46	"
150	1931	0.0273	68.5	0.15	0.44	"
151	1962	0.0269	69.6	0.2	0.44	"
152	2025	0.0281	69.7	0.13	0.44	"
153	2041	0.0272	46.9	0.1	0.38	"
154	2175	0.0284	43.0	0.05	0.31	"
155	2149	0.0277	46.3	0.05	0.34	"
156	2554	0.0283	22.7	0.05	0.22	"

[a]Partial pressure behind the reflected shock.

AN OPTICAL STUDY OF SOOT FORMATION FROM SHOCK-INDUCED BENZENE PYROLYSIS

by

GREG NELSON

B.S., Kansas State University, 1979

AN ABSTRACT OF A MASTER'S THESIS

submitted in partial fulfillment of the

requirements for the degree

MASTER OF SCIENCE

Department of Nuclear Engineering

KANSAS STATE UNIVERSITY
Manhattan, Kansas

1981

ABSTRACT

Soot formation from benzene pyrolysis in a single pulse shock tube has been studied in real time optically and after the fact with electron microscopy. Reaction conditions were varied over a temperature range of 1450-2400 K, with initial benzene concentrations from 0.12 to 1.3 mole percent in argon, and reaction dwell times of < 0.1 to 2.5 msec, at an average pressure of 845 ± 144 kPa. The beam from a He-Ne laser was passed through windows bounding the reaction zone, and its transmitted intensity over time measured. From this transmission trace, which was displayed on an oscilloscope, the intensity at t = 2.5 msec, the induction time, and the rate of increase in extinction were measured. From the transmitted intensity at 2.5 msec, soot yields were determined, as a mass fraction of the initial benzene concentration, over the temperature range. At carbon atom concentrations less than 5×10^{17} ml^{-1} (behind the reflected shock wave), yields increased from below detectable limits at 1500 K to near 50% at 1800 K, and then decreased to zero at temperatures above 2100 K. At a higher concentration (2.31×10^{18} ml^{-1}), the soot yield increased continuously with temperature. Soot yields from a similar aromatic compound, toluene, were compared to those from benzene. Overall trends with temperature were similar, but the peak yield from toluene was higher with a fractional conversion of about 70%. From the induction time and rate of increase in extinction data, activation energies for soot nucleation and particle growth were calculated as $\sim$ 27.0 and 21.8 kcal/mole, respectively. Nucleation was concluded to be a low order kinetic process ($n \leq \frac{1}{2}$) whose rate increased continuously with temperature despite increasing

aromatic ring fragmentation. On the other hand, the particle growth rate increased continuously up to a temperature of 1800 K, and thereafter decreased. It is concluded, therefore, that the primary impact of ring fragmentation is not on the nucleation of soot, but rather on the surface growth. Surface growth was estimated to be a first order kinetic process with respect to benzene concentration, with much of the growth occurring during the quench, especially at temperatures greater than 1800 K. Soot particles were removed from product gases by filtration and measured under a transmission electron microscope. Particle diameter was found to be relatively insensitive to changes of temperature, dwell time, and initial reactant concentration.